INVESTIGATING THE INFLUENCE OF MICROENCAPSULATED HEALING AGENTS ON THE PROPERTIES OF EPOXY THERMOSETS

THESIS

Submitted to the Delhi Technological University

for the award of the degree of

DOCTOR OF PHILOSOPHY

By

MANORAMA TRIPATHI

DEPARTMENT OF APPLIED CHEMISTRY AND POLYMER TECHNOLOGY
DELHI TECHNOLOGICAL UNIVERSITY
BAWANA ROAD, DELHI-110042

MARCH, 2017

INVESTIGATING THE INFLUENCE OF MICROENCAPSULATED HEALING AGENTS ON THE PROPERTIES OF EPOXY THERMOSETS

By

MANORAMA TRIPATHI

Department of Applied Chemistry and Polymer Technology

Submitted

in fulfilment of the requirements of the degree of Doctor of Philosophy

to the

DEPARTMENT OF APPLIED CHEMISTRY AND POLYMER TECHNOLOGY

DELHI TECHNOLOGICAL UNIVERSITY

BAWANA ROAD, DELHI-110042

MARCH, 2017

Dedicated
To
My family

CERTIFICATE

This is to certify that the thesis entitled **"Investigating the influence of microencapsulated healing agents on the properties of epoxy thermosets"** submitted by **Ms. Manorama Tripathi** to **Delhi Technological University**, for the award of the degree of "Doctor of Philosophy" is a record of bonafide work carried out by her. Ms Manorama Tripathi has worked under our guidance and supervision and has fulfilled the requirements for the submission of this thesis, which to our knowledge has reached requisite standards.

The results contained in this thesis are original and have not been submitted to any other university or institute for the award of any degree or diploma.

Dr. P. K. Roy

Scientist 'F'
Centre for Fire, Explosive and
Environment Safety (CFEES)
Defence Research and Development
Organization (DRDO), Delhi-110054

Prof. D. Kumar

Professor
Department of Applied Chemistry
and Polymer Technology
Delhi Technological University (DTU)
Bawana Road, Delhi-110042

Dr. Archna Rani

Head of Department
Department of Applied Chemistry and
Polymer Technology
Delhi Technological University (DTU)
Bawana Road, Delhi-110042

I

ACKNOWLEDGEMENT

ABSTRACT

The primary motivation behind the present research work is to study the effect of inclusion of healant loaded microcapsules on specific properties (thermal, structural and mechanical) of a representative epoxy thermoset. In addition, we also explore alternate chemistry for introducing self healing functionality in epoxy composites. Two distinct healing systems have been investigated, namely cycloaliphatic epoxy and unsaturated polyester. The healants were encapsulated in urea-formaldehyde microcapsules by adopting an in-situ dispersion polymerization route and in polystyrene shell through solvent evaporation process. The effect of operating parameters particularly stirring speed on the particle size distribution has been studied. Under optimal conditions, the core content of the epoxy loaded microcapsuleswas found to be $65 \pm 4\%$for microcapsules prepared by dispersion polymerization route and $38 \pm 2\%$for microcapsules prepared using solvent evaporation route.

It is to be noted that the healing efficiency is strongly influenced by the internal microstructure of the microcapsule and we also developed an analytical model for predicting the amount of healant released in the event of microcapsule rupture. In microcapsules possessing "reservoir" type microstructure, the healant exists as a single droplet, where the entire content is expected to be released upon rupture. On the other hand, in monolithic microcapsules, the healant is dispersed in the form of discrete micro-droplets, and only the healant available within the cracked microcapsule is expected to be released and cause healing. Our model predicted that significantly lower amounts of healant is released in monolithic microspheres in comparison to reservoir microcapsules, especially when the micro-droplet dimensions and core content, both are low.

Triethylenetetramine (TETA) hardener was encapsulated by adopting two methods, namely interfacial polymerization and physical entrapment technique. The effects of experimental parameters, namely reaction temperature (50-75°C), stirring speed (400-700 rpm) and epoxy: amine concentration ratio (10:1.2-10:4.3) on the microcapsule properties was investigated. A polymeric surfactant was used to stabilize the suspension in order to modulate the particle size distribution of the resultant microcapsules. Highest encapsulation efficiencies resulted when the reaction medium was maintained at 70°C under a stirring speed of 600 rpm, while maintaining an epoxy: amine ratio of 10:3.2. The microcapsule dimensions and core content could be tailored, following the interfacial polymerisation route. Under optimal conditions, spherical microcapsules with 100 % yield and 12% core content were obtained.

Physical entrapment approach was also explored for the immobilisation of amine hardener in mesoporous silica. For this purpose, mesoporous silica (SBA-15) was synthesised using polymer-templated technique and employed as a substrate for immobilization. Vacuum infiltration of TETA led to its entrapment within the porous structure of SBA-15 with loadings as high as 5g/g, which could be attributed to hydrogen bonding and acid–base interactions.

The curing kinetics of self-healing epoxy compositions was investigated by non-isothermal differential scanning calorimetric (DSC) studies. Epoxy loaded microcapsules and immobilised amine was dispersed into epoxy resin, and cured using TETA. DSC studies revealed the autocatalytic nature of epoxy curing, which remained unaltered due to addition of the fillers responsible for introducing self healing functionality. The kinetic parameters of the curing process were determined using both Friedman and Kissinger–Akahira–Sunose (KAS) method. The activation

energy at different degree of conversion (E_α) was found to decrease with increasing degree of cure (α). Although urea-formaldehyde possess secondary amine functionalities, which have the potential to react with the epoxy groups, no significant differences in the curing kinetics of the base resin were observed. Kinetic parameters were used to predict the curing behaviour of compositions at higher heating rates using KAS method. As expected, the onset curing temperature (T_{onset}) and peak exotherm temperature (T_{peak}) of epoxy shifted towards higher temperatures with increased heating rate; however introduction of fillers do not affect these characteristic temperatures significantly. Also, the overall order of reaction does not vary significantly. The results suggest that although 2° amino groups are available with the urea-formaldehyde (UF) resin, these do not directly participate in the curing reaction, as the primary amino groups in TETA are more easily accessible.

To evaluate the effect of self healing additives on the mechanical properties and healing efficiency, epoxy composites containing UF and PS microcapsules (5-30%, w/w) were prepared by room temperature curing and their mechanical behaviour and healing efficiency was studied under both quasi-static and dynamic loadings. The tensile strength, modulus and impact resistance of the matrix was found to decrease with increasing amount of microcapsule in the formulation, the detrimental effect being less pronounced for polystyrene microcapsules due to its monolithic internal microstructure. Morphological investigations on the cracked surface revealed features like crack pinning, crack bowing, microcracking and crack path deflection, which were used to explain the toughened nature of microcapsule containing epoxy composites.

Healing efficiency was quantified in terms of the ratio of impact strength before and after healing. For the purpose of validation of the developed analytical model, composites were prepared using epoxy encapsulated microcapsules with varied internal structures. Ni and Cu-imidazole complexes were prepared for use as latent hardeners for epoxy. Both the imidazole-metal complexes could effectively cure the epoxy released from within the microcapsules in the event of damage followed by thermal treatment. In line with our predictions, the extent of healing was much lower in the case of samples containing monolithic microcapsules. At 20% w/w microcapsule loadings, healing efficiencies close to 60% was observed upon introduction of reservoir type microcapsules, while under similar loadings, only 10% healing could be evidenced in the presence of monolithic microcapsules.

For reservoir type microcapsules, complete healing (efficiency ~ $100\pm2\%$) could be effected at 30% microcapsule loading, in the presence of metal imidazole complexes. In comparison, the complete healing was evidenced at relatively lower microcapsule loading (20%, w/w) when amine immobilised SBA-15 was used.

The potential of encapsulated unsaturated polyester resin (USP) towards introduction of healing functionality was also explored. USP was encapsulated in urea-formaldehyde shell and polystyrene shell by dispersion polymerization and solvent evaporation technique respectively both resulting in the formation of free flowing microcapsules. Calorimetric studies confirmed the chemical activity of the encapsulated USP, which spontaneously polymerised in the presence of a free radical initiator, 2,2'-Azobis(2-methylpropionitrile) (AIBN), at temperature as low as 80°C. Temperature triggered healing of epoxy-microcapsule composites was performed at 110° C and healing efficiency was quantified as the ratio of impact strength of healed and virgin specimens. The same was found to increase with increasing amount of

microcapsule in the formulation and reached a maximum (100 ± 2%) at 20% (w/w) loading. Fractographic analysis of the surface revealed the flow pattern of chemically active polyester resin from the ruptured microcapsules, which subsequently cured in the presence of AIBN available within the matrix.

CONTENTS

LIST OF FIGURES

CHAPTER I

CHAPTER II

APPENDIX B

LIST OF TABLES

APPENDIX A

APPENDIX B

CHAPTER I

INTRODUCTION

1. Introduction

The requirement of high performance polymeric materials, particularly in challenging applications, has been a driving force for development of materials with enhanced mechanical properties and increased life times. One of the possible routes for lifetime extension is to design means to mitigate the failure routes. In brittle polymers, e.g., epoxy, failure primarily occurs through micro-crack initiation followed by its propagation. The ability to detect and repair these micro-cracks at the initial stages can go a long way in extending the life time of the component. For this purpose, methodologies need to be adopted which can arrest propagation of crack at the initial stages to avert catastrophic failure, thereby increasing the lifetime and scope of these materials.

The scope of manual intervention towards repair of crack in polymeric materials has been extensively investigated[1-5]. Initial studies on thermoplastics like poly(methylmethacrylate) (PMMA) and polystyrene (PS) revealed that by promoting chain entanglement, crack healing could be effectively achieved. This type of manual healing requires chain mobility that can be achieved by raising the temperature of the polymer above its glass transition temperature (T_g) or by using solubilizing agents[5-8]. Although these techniques are rather successful in laboratory scale studies, their scope is limited to applications, where it is possible to detect damage for subsequent manual intervention.

With the need for autonomic repair thus evident, current research has focused on developing complete self- healing systems. The most common methodology towards

designing of autonomic systems involves encapsulation of an active healing agent and then introduction of these encapsulated healing agents into a composite material. Capsule based healing system was first reported by White and co-workers[9]. As per this system (Figure 1.1), when a crack progresses through the material, the healant loaded containments are ruptured. Capillary action drives out the liquid healant into the crack where it reacts in the presence of a catalyst/ initiator/curing agent and solidifies to bridge the crack plane thereby causing healing.

Matrix

Microcapsules   **Catalyst or encapsulated curing agent**
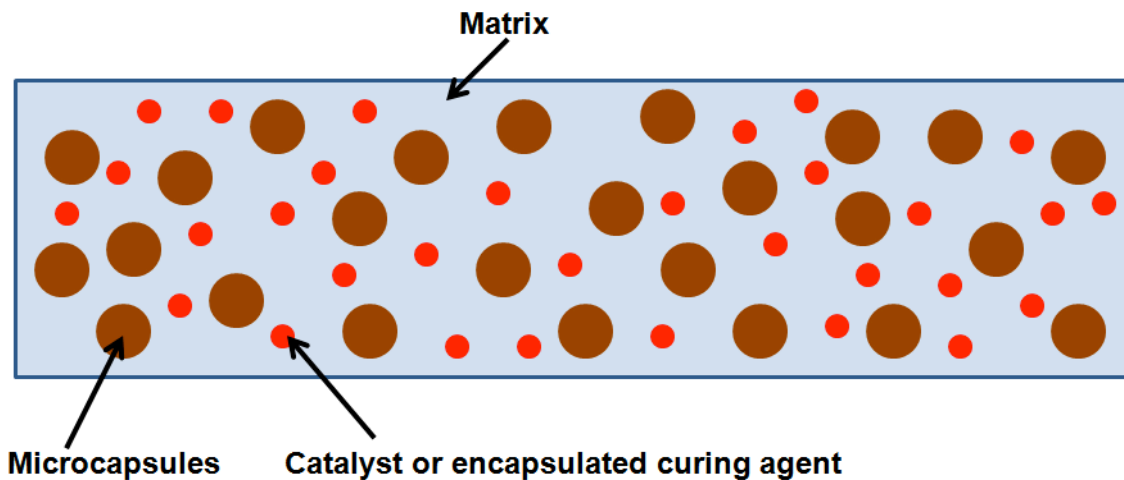
Figure 1.1: Capsule-based self-healing system

Depending on the requirement of manual intervention, self-healing methodology can be classified as non-autonomic healing and autonomic, which are described as follows:

Non-autonomic healing: As the name suggests, here the healing functionality is introduced into the material, but the realisation of the same mandate additional factors. This definition differentiates this system from the previously discussed approaches e.g.,

solvent welding, which require manual application of solvent into the crack plane.

Autonomic healing: This type of healing system is fully self-contained and does not mandate any manual intervention.

Both these systems are explained in detail in the following section.

1.1.   Non-autonomic healing system

Expeditious development in the field of self-healing has led to some intuitive and interesting chemisty which although are not completely autonomic, do add to the portfolio of strategies that can be used towards designing smart responsive materials. This sub-class of materials possess the inherent ability of undergoing healing, usually through a rearrangement reaction occuring over extended time periods under specific conditions (temperature, pH, UV light etc.). In these materials, self-healing of damaged site is triggered via thermally reversible reactions, UV reversible reactions, or molecular diffusion and entanglement, which have been discussed separately in the following subsections.

1.1.1. Thermally reversible healing

This class of healing material is capable of undergoing repair through thermally reversible bonds. Incorporation of healant vessels or catalyst is not needed for this class of composites. The healing property of this class of composites can be attributed to Diels-Alder reaction (between a diene and a dienophile) which is a thermally reversible reaction[10]. A celebrated example of this class of material is based on furan (diene) and maleimide (dienophile) derivatives, where the reversibility of the process is achieved via

the retro-Diels-Alder reaction (Figure 1.2). It is to be noted that the bond formed in furan/maleimide-derived polymers (via Diels-Alder reaction) undergoes disruption at elevated temperatures, and reconnects upon cooling, thereby rendering the process impractical for room temperature application[10-13].
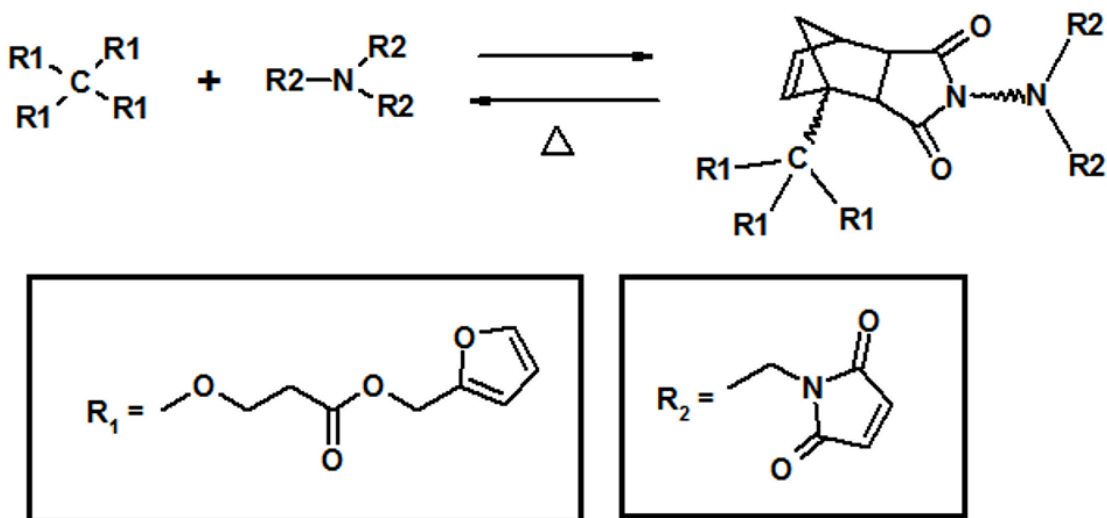
Figure 1.2: Chemical structures of a thermally reversible self healing system[11]

While the thermally reversible systems exhibit great potential for healing, the scale up synthesis of these monomers do not appear to be economically viable at present, thus outweighing the benefit of healing for industrial applications.

1.1.2. UV-initiated healing

Conceptually, this healing system is very similar to the thermally-reversible system discussed above, the only difference being the application of UV instead of heat for attainment of bond reformation at the damaged site. One of the suitable chemistry is the [2+2] cycloaddition of cinnamoyl groups[14]. The photo-cycloaddition of cinnamoyl

groups results in formation of a cyclobutane structure and its disruption to original cinnamoyl structure has been reported to occur in PMMA upon crack propagation (Figure 1.3). The self healing property was visualised in the form of regain of flexural properties of the sample. This type of healing system is very quick and does not require any catalyst, initiator or heat treatment. It is to be noted that although, this system is promissing for applications in films or coatings where the cracked surface is exposed to light, however it is unlikely to heal internal cracks in thicker substrates.
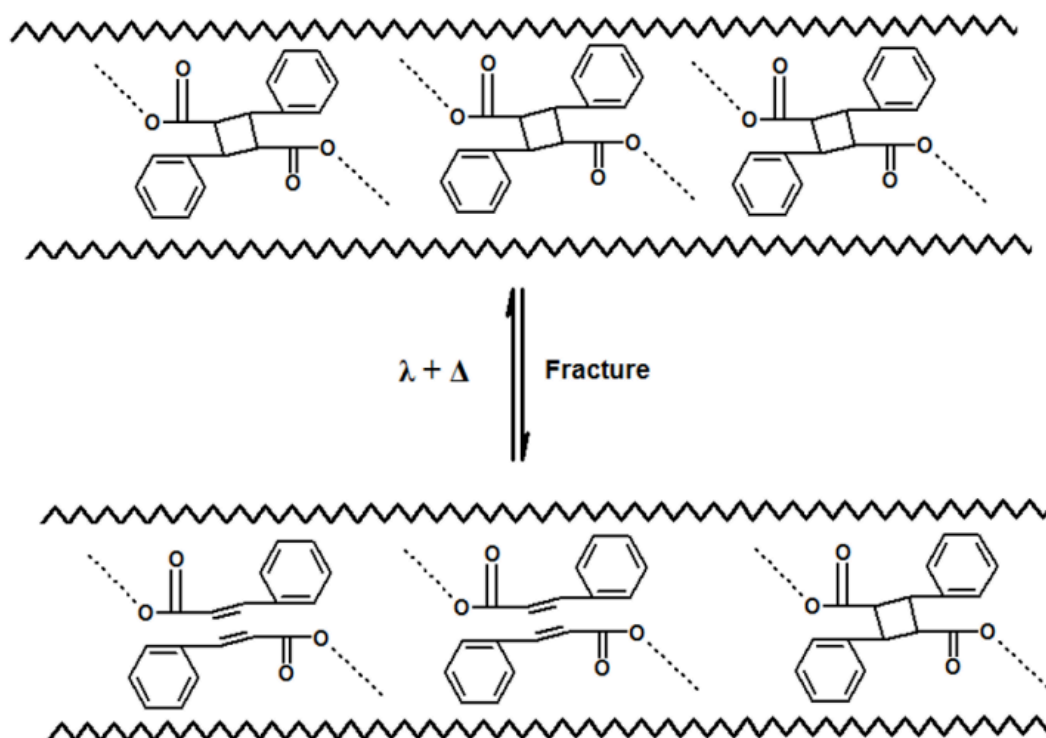
Figure 1.3: Mechanism of photo induced healing in PMMA[14]

1.1.3. Healing by thermoplastic additives

This class of self healing polymers is based on crack filling additives or thermoplastic-thermoset polymer solid solution (Figure 1.4). Upon being heated, these

fillers melt and move into the crack by capillary action, and subsequently solidify resulting into healing. This was first reported by Zako and Tanako in 1999[15], where 40% (w/v) epoxy particles (diameter ~105μm) were dispersed in a epoxy based fiber reinforced composite. Another example is the dispersion of a thermoplastic resin like poly(bisphenol-A-co-epichlorohydrin) into a (diglycidyl ether of bisphenol A) based polymer matrix[16,17]. It is to be noted that the selection of the thermoplastic is very important in this class of healing system, with the requirement of thermoplastic having a solubility parameter as close to the matrix resin as possible to result in a single phase post resin curing.
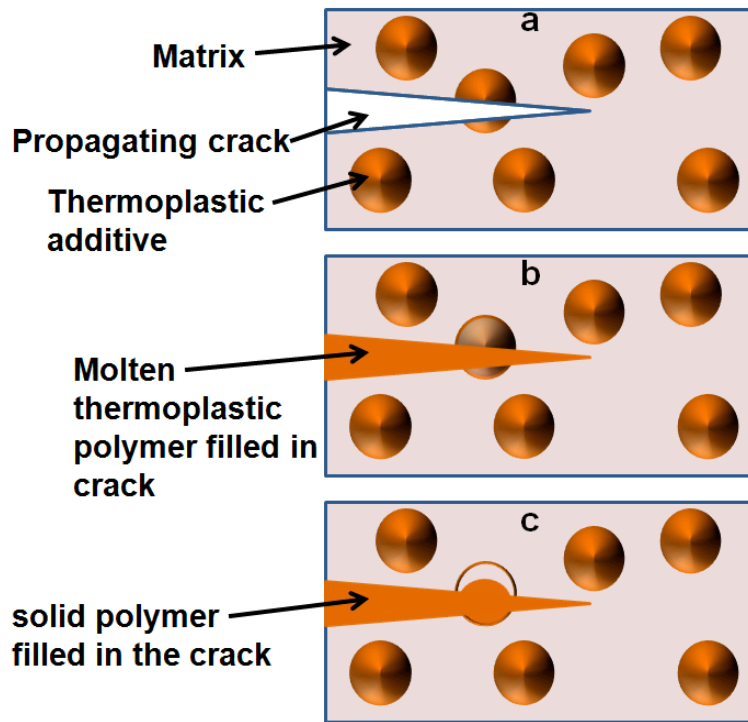
Figure 1.4: Pictorial representation of healing by thermoplastic additives a)

crack initiation, b) crack filling and c) crack termination[15]

1.1.4. Healing by chain rearrangement

Molecular level chain rearrangement is another method for achieving healing in thermosetting resin, which can be effected at room temperature or elevated temperatures. The rearrangement occurring at room temperature occurs via inter-diffusion of dangling chains. A representative example of this class is epoxy based system prepared from diglycidyl ether of bisphenol-A (DGEBA), benzyl dimethylamine (BDMA) and nadic methyl anhydride (NMA): a system which has been shown to heal repeatedly temperature greater than 150°C[18]. Another example is based on polyurethane prepared from a polyester-diol, trifunctional polyisocyanate and a dibutyl-tin-dilaurate catalyst[19].

1.2. Autonomic healing system

As mentioned previously, this healing system does not mandate any manual intervention. The basic principle is rather simple. The healant is loaded within microcontainers and dispersed within the matrix during the processing stage. The propagating crack ruptures these microcontainers, leading to the release of the healant within the crack through capillary action. When the healant comes in contact with the catalyst, it undergoes polymerization and arrests the growth of crack.

For designing a truly self-healing system, all the components, namely the healing agent, catalyst, containment wall and the healing chemistry have to be judiciously chosen. A short summary of the desirable characteristics is shown in Table 1.1

Table 1.1: Desirable characteristics of components for extrinsic self-healing system

Healing Agent	Catalyst/curing agent	Containment Shell	Healing Chemistry
Should possess low viscosity to flow into the crack plane	Should dissolve in the liquid healing agent	Should be chemically compatible with the liquid healing agent	Should not be governed by stoichiometry
Must be stable and possess long shelf life	Should be stable in the matrix	Should have thermal stability for wide range of temperature for broad range of application	
Reaction kinetics should be fast to ensure healing within a realistic time frame			

Based upon the underlying healing concept, the materials undergoing autonomic healing can further be sub-classified as: Single-capsule system, dual-capsule system, hollow glass tube or glass fiber system and microvascular or fiber network-based system.

1.2.1. Single-capsule system

As the name suggests, this methodology requires the introduction of healant loaded microcapsule and a chemical trigger (an initiator or a catalyst) in the matrix to effect healing. The basic concept is presented in Figure 1.5. It can be observed that as the propagating crack ruptures the microcapsule, the encapsulated healant is released into the crack by capillary action. Initiation of polymerisation of the healant starts upon its contact with the embedded initiator or catalyst, resulting in the formation of a solid,

which bridges the crack plane.
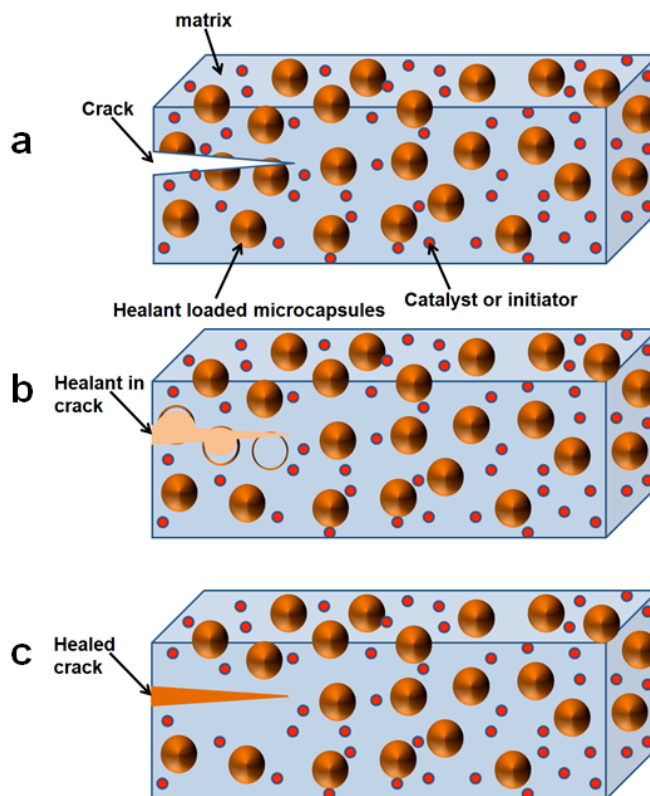
Figure 1.5: Pictorial representation of single capsule based system a) crack initiation,

b) healant flow within crack plane c) crack termination

The capsule based systems can be further classified on the healing chemistry involved, which is usually based on monomers undergoing ring opening metathesis reaction or induced by solvent.

1.2.1.1.   Ring opening metathesis

Perhaps the most celebrated example of this type of autonomic healing system is that of dicyclopentadiene (DCPD) healant loaded microcapsules and a suitable catalyst, both of which are dispersed within the matrix. Dicyclopentadiene undergoes ring opening

metathesis reaction in the presence of Grubbs' catalyst, leading to the formation of a cross-linked polymer and thus bridging the crack plane effectively (Figure 1.6).
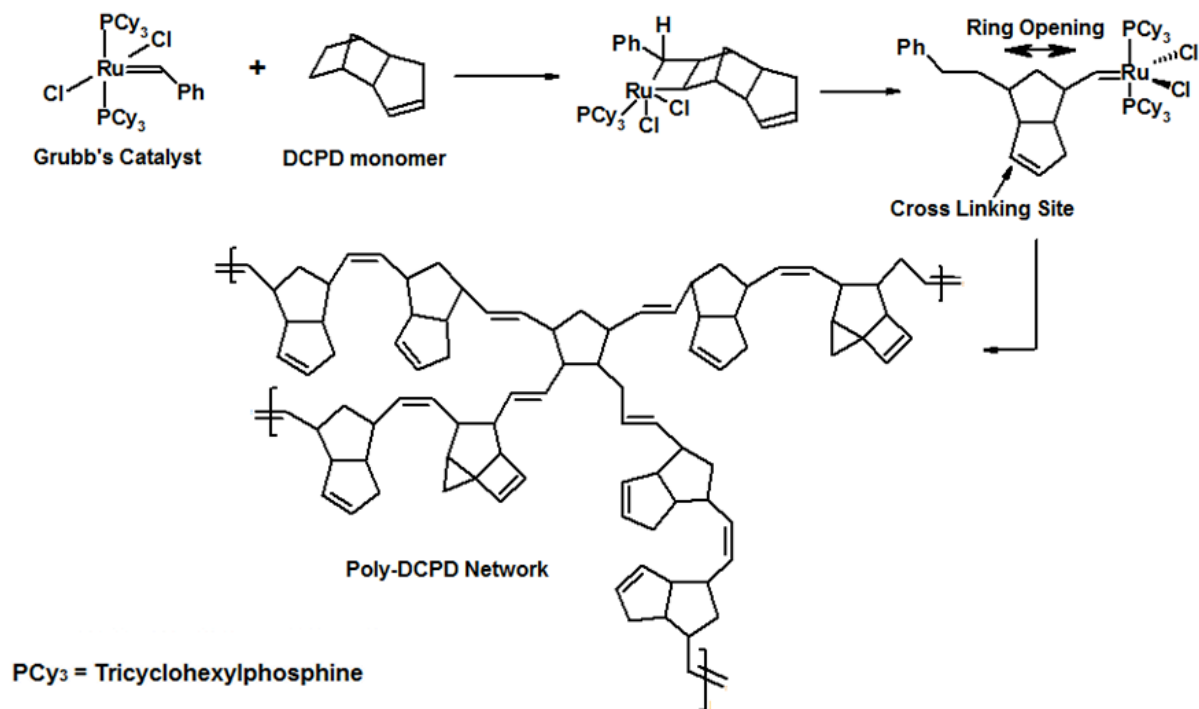
Figure 1.6: ROMP of DCPD with first generation Grubbs' catalyst[20]

The selection of DCPD as a suitable healing agent was done in view of its low viscosity, long shelf life, low cost, wide availability, and ability to undergo rapid polymerization at room temperature upon contact with an appropriate catalyst[21]. DCPD exists as two isomers: *exo*-DCPD and *endo* DCPD, the structures being presented in Figure 1.7. Commercially available DCPD contains 95% *endo*-DCPD but *exo*-DCPD has been found to be more reactive towards ring opening reaction[22]. The major drawback of using the more reactive *exo*-DCPD is its rapid polymerisation and thus inadequate time to solubilise the catalyst completely. The insufficient availability of catalyst leads to a low degree of cure which in turn results into low healing efficiency[23]. Another alternate

healing agent monomer containing reactive diene is ethylidenenorbornene (ENB) (Figure

1.7). It reacts much faster than DCPD, but a major drawback of this healing agent is that

the polymer formed after polymerization is linear and hence as compared to poly-DCPD

has inferior mechanical properties. Blend of the two monomers (DCPD and ENB) has

also been used as healing agent[24]. The system polymerized faster while maintaining the

mechanical properties.

endo-DCP   **exo-DCP**   **ethylidene norbornene**

Figure 1.7: Monomers capable of undergoing ROMP, showing potential as

healing agent

It is to be noted that the Ruthenium based Grubbs' catalyst, required for initiating

ROMP, is highly susceptible to degradation. Upon exposure to air and moisture for

extended time period, the first generation Grubbs' catalyst is deactivated. The reactivity

also decreases in the presence of diethylenetriamine (DETA), a common curing agent for

epoxy matrix[25]. Several attempts have been made in terms of coating the catalyst with

wax to get a homogeneous distribution and extend the lifetime of the catalyst[26,27].

Subsequently, more efficient next generation Grubbs' catalysts have also been developed

(Figure 1.8)[28]. Second generation catalysts have higher reactivity, higher thermal stability

and improved chemical stability against curing agent or initiator for matrix.
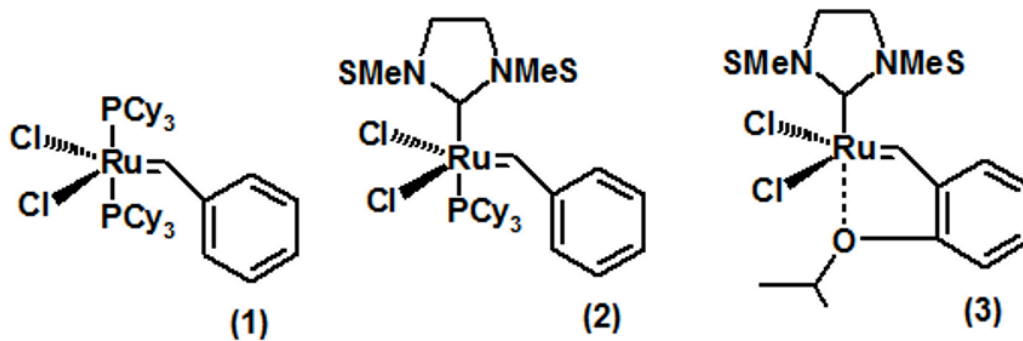
Figure 1.8: Grubbs'catalyst for ROMP 1) Grubbs' catalyst, 1ˢᵗ generation; 2) Grubbs' catalyst, 2ⁿᵈ generation and 3) Hoveyeda- Grubbs' catalyst, 2ⁿᵈ generation

1.2.1.2.   Solvent-induced self healing

As the name suggests, here a suitable solvent is encapsulated within the containment structure and in turn incorporated in the polymeric matrix prior to use in the proposed application, as depicted in Figure 1.9. During crack propagation, the microcapsule is ruptured leading to release of the solvent into the crack plane. Once in the crack plane, the solvent diffuses within the epoxy matrix to elute out the unreacted epoxy resin as well as unreacted amines, which subsequently react to repair the crack. Preliminary tests were performed, where the solvent was injected manually to determine the most suitable solvent system for epoxy healing[29]. On the basis of the study, solvents which unveiled the highest healing efficiencies included dimethylformamide (DMF), nitrobenzene, dimethylacetamide (DMA), *N*-methyl pyrrolidone (NMP), and dimethyl

sulfoxide (DMSO). When studied for both extremes of the polarity range with cyclohexane, hexanes, formamide and water, no indication of healing ability was observed which in turn demonstrated the ineffectiveness towards recovery of mechanical properties. An important advancement in the solvent-induced healing system was the understanding that microencapsulation of a mixture of an epoxy resin as a healing agent and a solvent could result into more effective healing[30].
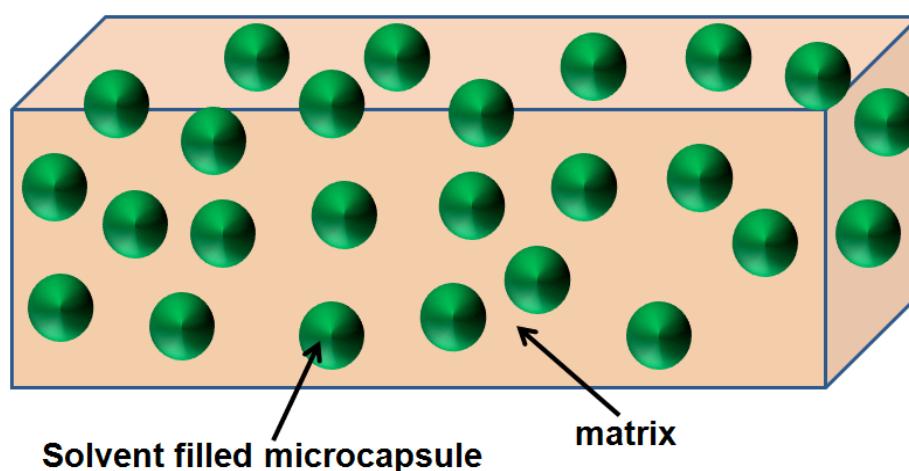
Figure 1.9: Pictorial representation of single capsule solvent based healing system

1.2.2. Dual-capsule system

While single-capsule system (DCPD and Grubbs' catalyst) has been extensively studied, other methods have to be investigated due to the lower stability and high cost of the Grubbs' catalyst. In the dual capsule system, healant and the curing agent are separately encapsulated and dispersed within the polymeric matrix, as shown in Figure 1.10. Dual-capsule systems became a necessity when it was attempted to explore alternate self-healing systems. Typical examples of dual capsule system are based on polydimethylsiloxane (PDMS) and epoxy chemistry. In the PDMS based system, the

liquid siloxane is homogeneously dispersed in the matrix as phase separated droplets. The suitable catalyst for siloxane is encapsulated and then embedded into the matrix, along with the phase-separated healing agent[31-33]. Another advantage is that, the condensation reaction is efficiently catalysed by organotin compounds, which are relatively cost effective and stable upon exposure to air and moisture, which was a major drawback of Grubbs' catalyst[34]. Another alternative approach to dual capsule approach is systems containing encapsulated epoxy as healing agent. The healing process of this system would yield the same material that encompasses the matrix and hence ensuring recovery of the initial mechanical properties and good adhesion between the healed surface and the matrix[35-38].
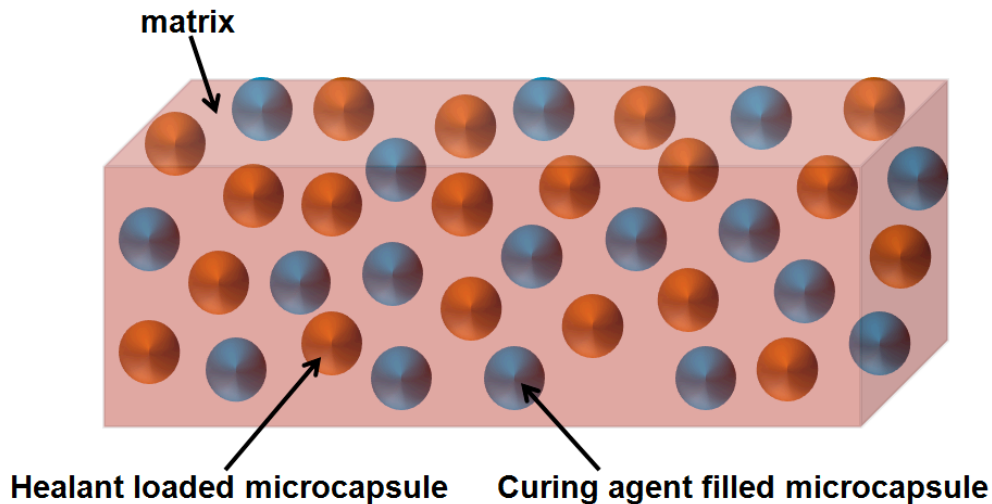
Figure 1.10: Pictorial representation of dual-capsule based system

1.2.2.1. Microencapsulation of healants

Microencapsulation can be defined as a process through which very small particles (diameter 1- 1000 μm) of a solid or droplets of liquid are surrounded with a film

14

of polymer. Microcapsules have a unique characteristic of protecting the core material, hence reducing undesirable reaction with external reactants. The microcapsules have been extensively used in a large number of industries including pharmaceutical[39-47] food[48-53], agriculture[54-59] and lately in the field of microcapsule based self-healing[9,60-64]. Commercial microcapsules have a diameter between 3 to 800 μm and exhibit a core content of anywhere between 10 to 90%. For the purpose of healant encapsulation, the following methods are commonly employed.

Interfacial Polymerisation: In Interfacial polymerisation, the two reactants meet at an interface and react rapidly to form thin flexible films under proper conditions. A solution of core material and one of the reactant required for shell formation is emulsified and separately an aqueous solution containing the co-reactant for shell formation is added. Polymer walls formed as a result of condensation reaction form immediately at the interface of the dispersed droplets of core material.

Dispersion Polymerisation Method: Dispersion polymerisation belongs to the sub-class of precipitation type of polymerisation process. A polymeric surfactant or stabilizer is essentially required for stabilization of the heterogeneous reaction medium. The choice of the solvent for the reaction medium should be such that it is a good solvent for the initiator and monomer, but non-solvent for the polymer formed. As the polymerization proceeds, polymer particles are formed thus creating an inhomogeneous solution. These particles form the locus of polymerisation, with monomer being added to the particle throughout the reaction. It differs slightly from the precipitation polymerisation process, where the continuous phase (solvent) is the main locus of polymerisation. Examples of

this type of encapsulation method include melamine-formaldehyde (MF) and urea-formaldehyde (UF) systems.

Solvent evaporation: All the processes of solvent evaporation technique are performed in a liquid continuous phase. The polymeric coating material is dissolved in a volatile solvent, which is immiscible with the continuous phase. The core material is dissolved in the coating polymer solution and the mixture is then dispersed in the continuous phase with agitation to obtain the desired size microcapsule. The solvent for the polymer is then allowed to evaporate by heating (if necessary). Since the core material is dissolved in the coating material solution, a monolithic microcapsule is formed. After the evaporation of the solvent for the polymer, the temperature of the mixture is reduced to room temperature and the resulting microcapsules are filtered and washed for subsequent use.

For successful encapsulation by solvent evaporation process, the solvent should fulfill the following criteria:

- It should dissolve the shell polymer
- It should be immiscible with the continuous phase
- It should have a low boiling point and high volatility.

In addition, it is preferable to use solvents with low toxicity. Chloroform (vapour pressure 212 mbar, boiling point 61°C, water solubility 8 g/L) has been extensively studied, but due to its low vapour pressure and high toxicity, methylene chloride (vapour pressure 453 mbar, boiling point 39.7°C, water solubility 20 g/L) appears to be a better choice. As compared to other solvents, the high vapour pressure (453 mbar) of methylene chloride promises a high solvent evaporation rate, which in turn reduces the duration of

formation of microcapsules. It is to be noted that the physical properties of prepared microcapsules are strongly dependant on the nature of materials (sell material, core material and solvent) and the operating parameters used for its preparation.

1.2.2.2. Internal microstructure of microcapsules

Morphologically, two general structures can be envisaged for a microcapsule: A reservoir-type system with a well-defined core (regular or irregular shapes) surrounded by a solid shell. The core, in the context of self-healing is necessarily a liquid and the surrounding shell is usually a fragile solid. The cross-sectional view of the reservoir type microcapsule is depicted in Figure 1.11
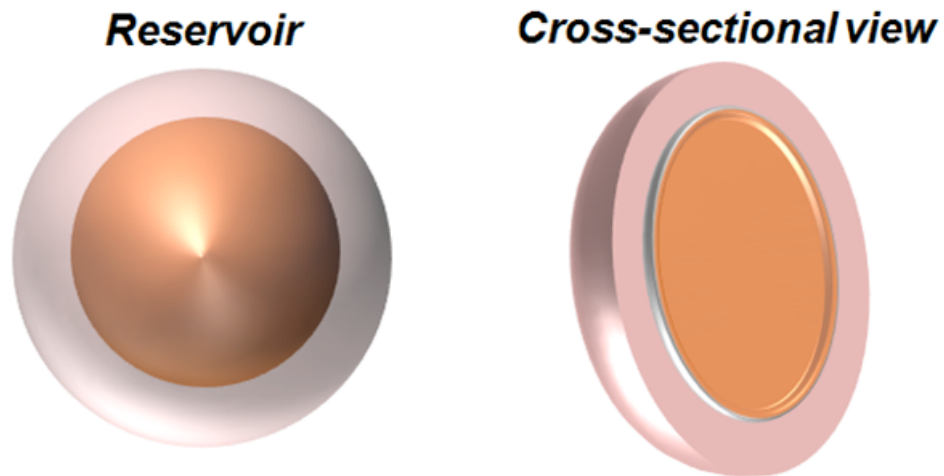
Figure 1.11: Pictorial representation of reservoir type cross section

Alternatively, in the monolithic morphology the entire structure constitutes a continuous phase in which the core is distributed throughout the matrix, at either the macroscopic or molecular (dissolution) level. The cross-sectional view of this type of microcapsules is shown in Figure 1.12.
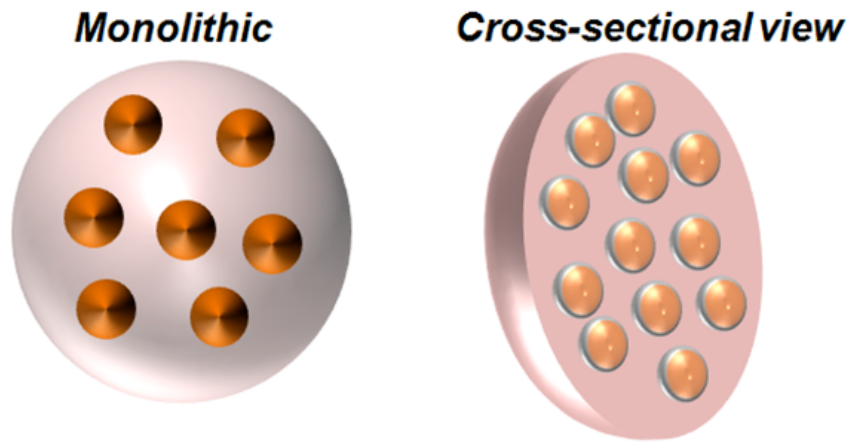
Figure 1.12: Pictorial representation of monolith type cross section

Interestingly, the methodology adopted for the preparation of microcapsule plays a strong role in defining its internal morphology, with the dispersion polymerization route leading to the formation of a single drop of healant surrounded by shell wall, commonly referred to a "reservoir" type structure. Solvent evaporation route results into the formation of a monolithic type of internal microstructure, where the microdroplets of healants are dispersed within the shell homogenously.

1.2.3. Hollow glass tube based system

In this approach, the healant is filled in hollow glass tubes and embedded in the polymeric matrix during the curing stage. Upon crack propagation, rupture of the healing agent loaded glass tubes lead to the release of the monomer, which undergoes polymerization to cause healing (Figure 1.13 and 1.14). It is to be noted that this concept was initially applied to cementitious materials[65] and subsequently extended to polymeric material[66-71]. Here, the resin is introduced in the hollow glass tubes through the open ends via capillary action or through vacuum assistance and are subsequently sealed. The major

issue associated with this technique lies in filling and release of the healant, which is difficult in view of the small diameter of the tubes or fibers used[72,73]. A number of different healants have been reported for this concept:

Single-part adhesive: The hollow fibers contain a single kind of resin which can undergo polymerisation upon exposure to air. e.g., cyanoacrylate[66,74,75].
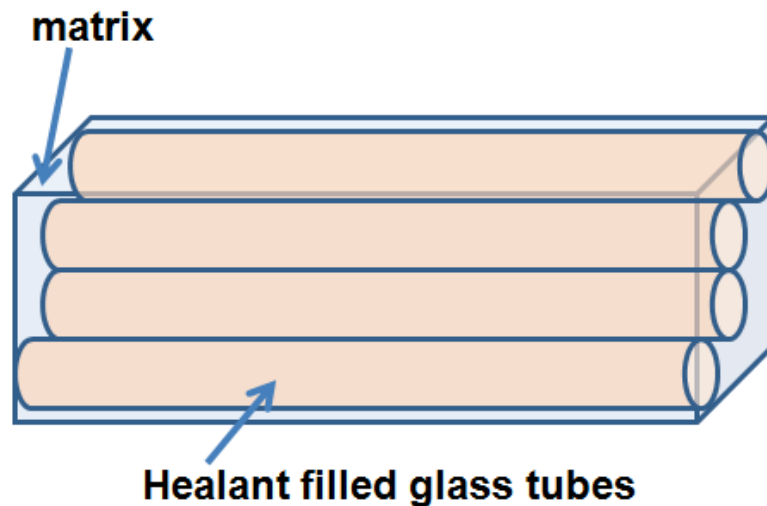
Figure 1.13: Pictorial presentation of hollow fibers or tubes based system

containing one part adhesive

Two-part adhesive: Here, the two part adhesive (e.g., resin and hardener) is filled into neighboring hollow tubes or one component is filled into the hollow tubes and the other is compartmentalised in another type of containment vessel[67,70].
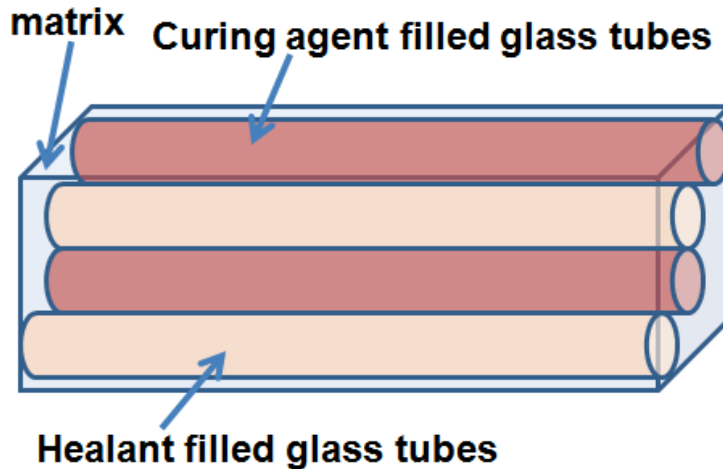
Figure 1.14: Hollow fibers or tubes based system with two-part adhesive

1.2.4. Three-dimensional micro-vascular networks

This method is practically an extension of the 2D channels, with the additional advantage of supplying larger volumes of healant. In this system, a series of healant-filled interlinked channels are connected to an external, rechargeable liquid pump, pictorially the concept being presented in Figure 1.15. The basic healing concept is mechanistically most close to biomimetic self-healing system, as the interconnected channels are similar to the vascular systems of animals and plants.

Initial self-healing work based on the vascular system contained DCPD into the microvascular network and Grubbs' catalyst embedded in the epoxy matrix[61]. Another healing chemistry reported is a two-part system, where both the liquid epoxy resin and the amine hardener flow through segregated vascular networks[76]. It is to be noted that the complexity of design conditions for connecting channels of storage vessels require extremely sophisticated fabrication techniques, which is presently unavailable and is in its nascent stage.

20
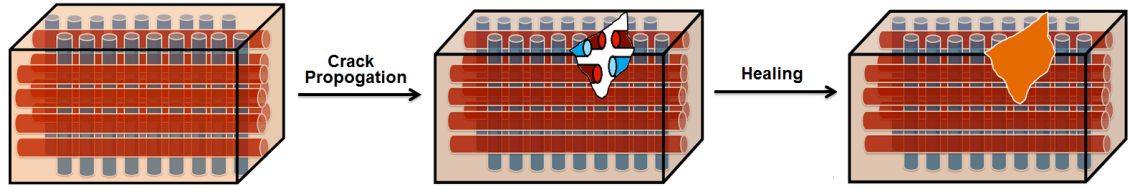
Figure 1.15: Microvascular network based self-healing system

1.3. Healing Efficiency

Healing of any material refers to the recovery of properties, usually in terms of regain of tensile strength, fracture toughness, impact strength and surface smoothness. Therefore, self healing efficiency can be estimated as the ratio of property being monitored, before healing to that post-healing. A list of material properties which have been used for quantification of self-healing efficiency is presented in Table 1.2.

Table 1.2: Material properties for evaluation of healing efficiency

Property	Calculation	Remarks
Fracture Toughness	$\eta = \dfrac{K_{IC}^{Healed}}{K_{IC}^{Virgin}} \times 100$	K_{IC} = Fracture toughness
Strength	$\eta = \dfrac{\sigma_{Healed}}{\sigma_{virgin}} \times 100$	σ = Tensile, Impact, Compressive, Tear, Flexural
Stiffness	$\eta = \dfrac{E_{Healed}}{E_{virgin}} \times 100$	E = Young's Modulus
Strain energy	$\eta = \dfrac{U_{Healed}/A_{Healed}}{U_{virgin}/A_{virgin}} \times 100$	U = Strain Energy A = Surface area created by fracture

1.3.1. Healing efficiency by fracture toughness measurement

Under quasi-static conditions, the most established protocol for measuring the healing efficiency is to monitor the recovery of fracture toughness[9,77]. It is essential to measure the length of the crack both before and after healing for sample geometries like compact tension (CT), single-edge notch tension (SENT) and single-edge notch bend (SENB). However, tapered double-cantilever beam (TDCB) geometry (Figure 1.16) being crack length independent is a most widely used method for fracture toughness measurement in self-healing composites. In this method the fracture toughness is related to the peak load at failure (P_c) by a simple geometric coefficient. Therefore, under quasi-static conditions, the healing efficiency (η) for TDCB geometry can be estimated by both the fracture toughness (K_{IC}) and the peak load at failure (P_c) using equation 1.1.

$$\eta = \frac{K_{IC_{Healed}}}{K_{IC_{virgin}}} = \frac{P_{C_{Healed}}}{P_{C_{virgin}}} \dots\dots\dots\dots\dots\dots\dots\dots\dots\dots\dots\dots\dots\dots1.1$$
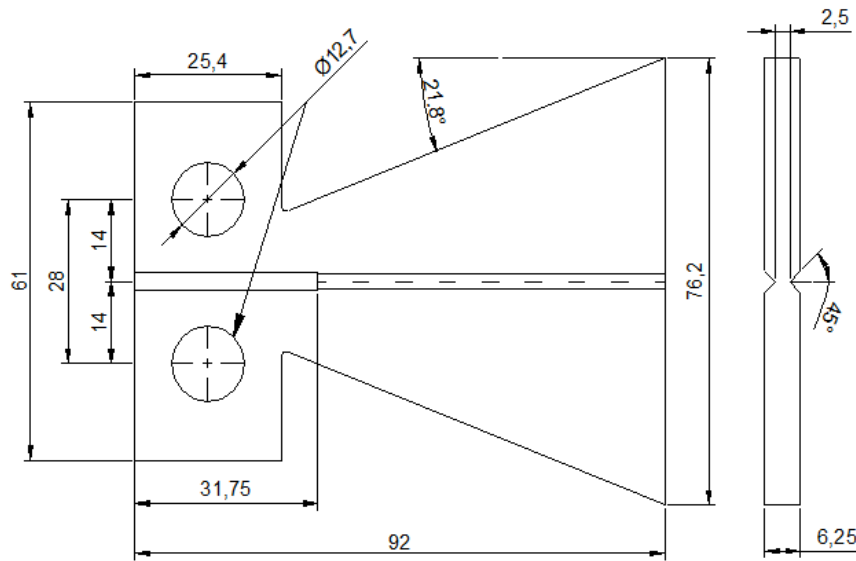
***Figure 1.16: Schematic of TDCB geometry (all dimensions in mm)**[77]*

1.3.2. Self-healing efficiency by fatigue measurement

This method is relatively complex than monotonic fracture, as it is dependant on additional factors like applied stress, loading frequency, kinetics of healing and employed rest periods[78]. The self-healing efficiency of the system to retard fatigue crack growth is assessed under cyclic loading as the fatigue life-extension as per equation 1.2.

$$\eta = \frac{N_{Healed} - N_{Control}}{N_{Control}} \dots\dots\dots\dots\dots\dots\dots\dots\dots\dots\dots\dots\dots\dots\dots\dots\dots\dots\dots 1.2$$

where

N_{healed}= number of cycles to failure for a healing sample
$N_{control}$= number of cycles to failure for a similar non-healing sample

1.3.3. Self-healing efficiency by impact strength measurement

Self-healing efficiency has also been estimated from impact testing, where it is calculated as the ratio of impact strength of the sample after healing to that of the virgin sample[79]. For this purpose, the specimen is subjected to impact tests and the broken parts are placed next to each other for sufficient durations to allow healing. The healed specimen is re-subjected to impact loading and impact strength is again measured. The healing efficiency can then be determined by equation 1.3:

$$\eta = \frac{\sigma_{Healed}}{\sigma_{virgin}} \dots\dots\dots\dots\dots\dots\dots\dots\dots\dots\dots\dots\dots\dots\dots\dots\dots\dots\dots\dots 1.3$$

where

σ_{Healed} = impact strength of healed sample

σ_{virgin} = impact strength of virgin sample

1.4. Deterioration in material properties due to inclusion of microcapsules

For practical application of self-healing materials, it is critical to understand how the self-healing fillers affect the virgin properties of matrix polymer which they are intended to heal. Self-healing, being an applied field, the effect of the inclusion of fillers on the virgin properties of matrix is of great importance, but this information appears to be lacking in the literature. Most of the literature reports that in case of microcapsule-based self-healing mechanisms, increasing the loading of healant-filled microcapsules toughens the composite matrix significantly, when compared to the virgin polymer matrix, till a critical loading. After this loading further increase in microcapsule loading decreases toughness. This toughening can be attributed to sub-surface microcracking at fracture surfaces[60]. Literature reporting the effect of introduction of microcapsules on other neat properties like strength, modulus are inadequet, but studies do suggest that inclusion of microcapsules have deleterious effect on modulus[36] and strength[80] which is quite expected in view of their hollow nature. Thus, it is to be noted that although most of the literature deal with enhancement in the self healing efficiency of the composite, the introduction of self-healing additives into the polymeric resin results in substantial deterioration in properties of the matrix. To the best of our knowledge, no systematic empirical investigations have been performed to quantify the effect of microcapsules on the

mechanical, thermal, structural and curing behaviour of the resulting compositions, and this instigated us to take up the present study.

1.5. Aim of the work

The main aim of this research work is to establish the effect of inclusion of healant-loaded microcapsules on the thermal, structural and mechanical properties of epoxy thermoset.

Another goal of this work is to investigate alternate systems capable of bestowing self-healing functionality to epoxy resin, besides dicyclopentadiene (DCPD) and quantify the effect of inclusion of these additives on the various properties of the base resin. We also aim to explore the potential of physical and chemical methodologies for encapsulation of two different resins (i.e., epoxy and unsaturated polyester) in different shell walls (polystyrene and urea-formaldehyde).

More specifically, the objective of this research includes:

- Encapsulation of different healing agents, namely epoxy and unsaturated polyester resin resin in different shell walls (urea-formaldehyde and polystyrene) to form microcapsules.
- Comparison of different methods of encapsulation: solvent evaporation and dispersion polymerization for resin encapsulation
- Exploration of the potential of interfacial methods and physical entrapment technique towards encapsulation of amine based hardener (for epoxy curing).

- Investigation of the effect of inclusion of microcapsules on the thermal, curing behaviour and mechanical response of a representative cycloaliphatic epoxy resin

- Quantification of the healing efficiency of the developed compositions.

1.6.   Plan of Work

The experimental work has been divided into the following sections to achieve the above objective

I.   Preparation and characterization of different healant loaded microcapsules

  a. Cycloaliphatic epoxy

  b. Triethylenetetramine hardener

  c. Unsaturated polyester

II.   Study the effect of inclusion of microcapsules on the thermal, structural and mechanical properties of epoxy

III.   Curing of epoxy in the presence of the developed microcapsules

IV.   To prepare epoxy composites containing microcapsules (of varying loadings) and determine their impact strength before and after healing to quantify the healing efficiency.

1.7. Thesis organization

In the present thesis, we have prepared, characterized and evaluated self-healing epoxy composites, where the healing functionality is bestowed through the inclusion of healant-containing microcapsules. This work is organized into six chapters, most

of which are manuscripts that have either been published, or have been communicated to peer reviewed international journals.

Chapter I gives an introduction that summarizes a brief background of the self-healing polymers and composites. It also gives an insight of types of self-healing polymers and specific self-healing methodologies. Self-healing polymer composites based on encapsulated healants is discussed more elaborately.

Chapter II presents encapsulation of liquid epoxy resin as healing agent in different shell materials like polystyrene and urea-formaldehyde. This work is proposed to serve as tool for the optimization of encapsulation reaction using different shell wall materials as well as different encapsulation methodologies, i.e., solvent evaporation and dispersion polymerization. This chapter also discusses an analytical model, which quantifies the amount of healant released in the crack plane in the event of rupture of microcapsules with varied internal microstructure.

Chapter III discusses different techniques, particularly interfacial encapsulation and physical adsorption towards encapsulation of amine hardener for epoxy microcapsules.

Chapter IV discusses the effect of inclusion of self-healing additives on the curing kinetics of the epoxy resin.

Chapter V describes the investigation results of inclusion of microcapsules on mechanical properties of composite matrix (epoxy). The validation of the developed model through healing experiments is also detailed in this chapter.

Chapter VI summarizes the conclusions drawn from this thesis and provides suggestions for future work.

Appendix 'A' discusses the applicability of a novel healing chemistry hitherto unreported, i.e., unsaturated polyester towards introducing self-healing in epoxy resin.

The detailed calculations for determination of epoxy equivalent and Hoys solubility parameter are presented in Appendix 'B'

MICROENCAPSULATED

CYCLOALIPHATIC EPOXY

FOR SELF HEALING

APPLICATIONS

2.1. Introduction

The most common approach towards introduction of extrinsic self healing functionality to polymers relies on inclusion of healant loaded microcontainers in the polymeric formulation prior to curing. In this context, the most successful are binary systems, in which the two components, i.e., the resin and hardener, meet in the crack plane (formed as a result of propagating crack) and react to trigger off the healing process. Several microcapsule based systems have been described in the literature such as DCPD/Grubbs'catalyst[9,81], ENB/ Grubbs' catalyst[82,83], DCPD/tungsten hexachloride[84], PDMS/dimethyldineodecanoate tin catalyst[33], PDMS/Pt catalyst[31], epoxy/mercaptan[36] and epoxy/boron trifluoridediethyletherate $((C_2H_5)_2O.BF_3)$[85], to name a few.

An extremely attractive binary combination is based on microencapsulated epoxy and its amine hardener. Studies on the preparation of microcapsules encapsulating epoxy resin have been extensively reported[62,86-91]. The method of encapsulation defines the internal microstructure of the microcapsule, which in turn affects the self healing efficiency. Conventionally, healant encapsulated microcapsules are prepared using dispersion polymerization route wherein the hydrophobic healant remains encapsulated within a spherical fragile shell leading to formation of a "reservoir" type internal microstructure.

Another relatively less complex methodology, which almost routinely employed for the encapsulation of drugs for pharmaceutical applications, is "solvent evaporation"[92]. Interestingly, the use of this process for healant encapsulation has not been popular in the past, but has garnered a lot of attention lately[93-97]. Solvent evaporation results into the formation of a monolithic structure, where the microdroplets of healants are dispersed

within the shell homogenously.

In this chapter, we report the results of our studies dealing with the encapsulation of epoxy by two methodologies (i.e., dispersion polymerization and solvent evaporation) in two different shell wall materials, i.e., urea-formaldehyde and polystyrene. The effect of operating parameters on the microcapsule size has been discussed and the chemical activity of the system has been demonstrated. We also discuss a model for predicting the amount of healant, which is released in the crack plane in the event of microcapsule rupture. The predictions have been validated with experimental studies, presented in Chapter V, where healant encapsulated microcapsules, with varied microstructure along with suitable catalysts were included in the formulation to obtain healable compositions. The healing efficiency has been quantified in terms of the ratio of impact strength both before and after healing.

2.1.1. Thermosetting epoxy resins

Polyepoxide, commonly referred to as "epoxy" is a thermosetting polymer formed as a result of reaction between an epoxide "resin" with polyamine "hardener". The cross linked resin network has a number of advantageous properties which include high tensile strength, magnificent chemical and corrosion resistance and excellent dimensional stability[98,99]. As a result, these materials are being extensively used for applications such as adhesives for structural applications, reinforced particles and matrix for composites[100-102]. Depending upon the end application, commercial epoxy resins can comprised of aromatic, aliphatic or cycloaliphatic backbones.

The cycloaliphatic epoxides contain one or more cycloaliphatic rings in the molecules to which the oxirane ring is fused. They are prepared from Tischenko condensation of tetrahydrobenzaldehydefollowed by epoxydation of resulting olefin with peracids[103]. The general synthesis scheme of cycloaliphatic resin is presented below.
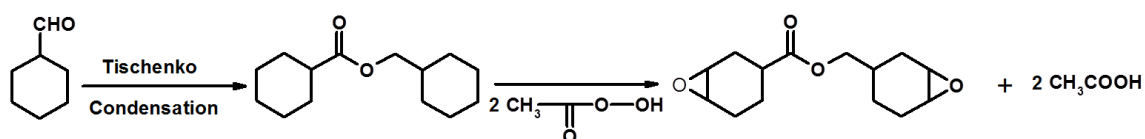
Scheme 2.1: Synthesis scheme of cycloaliphatic epoxy

This class of epoxides displays low viscosity, higher temperature resistance and better electrical properties at higher temperatures. Another advantage of this class of resin is the complete absence of chlorine since no epichlorohydrin is used in the manufacturing process.

2.1.2. Curing agents for epoxy: The oxirane ring of epoxy can react with various compounds, especially those that have active hydrogen atoms such as alcohols, amines, and carboxylic acids, to mention a few. Treatment of epoxy resins with these agents results in formation of cross linked three dimensional networks which are insoluble and infusible. The selection of curing agents is dependant on the processing methods, curing conditions and physical and chemical properties, which are desired. Epoxy resins can be cured with either catalytic or co-reactive curing agents which function as initiators for epoxy ring- opening homopolymerization.

2.1.2.1. Amine curing agents: Among chemicals which have the potential to act as epoxy curing agents, primary and secondary amines are commonly used. The active hydrogen of the primary amine reacts with the epoxy group to form secondary amine,

which further reacts with the other epoxy group and undergo curing. The resulting polymer is heavily cross linked, rigid and mechanically strong. A reaction scheme representing the reaction between the primary amine functionality of TETA with epoxy group is shown in Scheme 2.2.
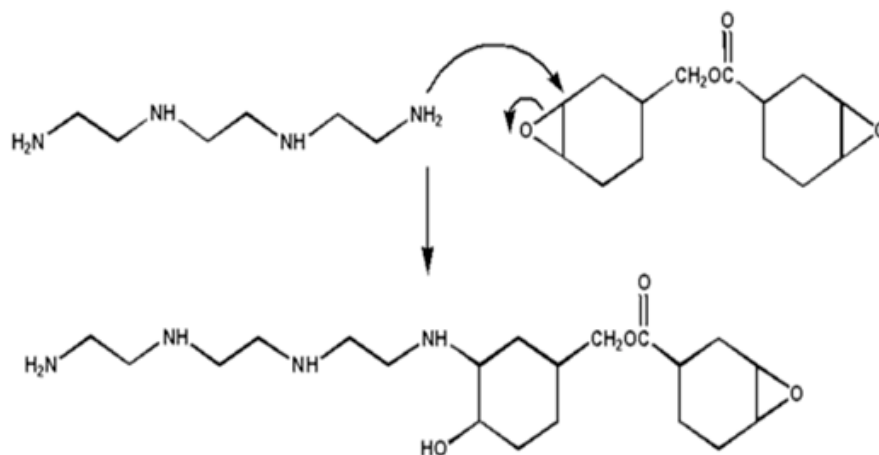
Scheme 2.2: Reaction scheme of primary amine of TETA with epoxy group

This process, also referred to as "curing", can be controlled through proper selection of temperature, type of hardener and resin, and resin to hardener ratio. The curing is an exothermic process which can take time ranging from few minutes to hours for completion. Some epoxy formulations require heating during the curing process, while others demand time and ambient temperatures.

2.2. Experimental

2.2.1. Materials

Aliphatic Epoxy resin (Araldite CY 230; epoxy equivalent 200eq g^{-1}), and TETA based hardener (HY 951; amine content 24 eq kg^{-1}) was received from Ciba Geigy and used as received. Urea, formalin (37% formaldehyde in water), sodium hydroxide,

resorcinol, ammonium chloride, dichloromethane, polyvinyl alcohol (PVA) (M_w ~14,000) was obtained from CDH. Sodium lauryl sulphate, styrene, potassium persulphate, sodium metabisulphite and ethyl acetate were of 'AR' grade, E. Merck. Poly(ethylene-alt-maleic anhydride) (EMA) (M_w ~100,000-500,000) was purchased from Sigma Aldrich. Double distilled water was used throughout the course of experimental work.

2.2.2. Preparation of polystyrene

Polystyrene was prepared by emulsion polymerisation as per the procedure reported previously[104].A monomer premix containing water (4g), sodium lauryl sulphate (2g) and styrene (20g) was prepared with a high-speed stirrer. An aqueous solution of redox initiator (potassium persulphate and sodium metabisulphite) was separately prepared. The reaction was performed under inert atmosphere. 10% of the monomer premix along with 25 mL of distilled water was taken in a reaction vessel and the temperature was raised to 60°C, after which initiator solution (1ml) was added. After seed formation, the rest of the monomer was metered in for 1h. After complete addition of monomer, the reaction was continued at 80°C for 4h. The emulsion was precipitated using an electrolyte, and a soxhlet extraction was performed for duration of 12h. The intrinsic viscosity of polystyrene in toluene was ~105ml/g (34°C), which was used to evaluate the viscosity average molecular weight of the polymer (3.19×10^5 g/mol).

2.2.3. Microencapsulation of epoxy in polystyrene shells

Cycloaliphatic epoxy was microencapsulated in polystyrene shell by solvent evaporation method using the process reported in the literature[105], a schematic of which

is presented in Figure 2.1. Predetermined amount of epoxy and polystyrene was dissolved in dichloromethane (30 ml), which was then introduced to 50 ml of 2.5% (w/w) aqueous solution of PVA under stirring at room temperature resulting into oil in water (o/w) emulsion. The mixture was then transferred into 150 ml aqueous PVA solution under continuous agitation. The stirring rate was varied from 350-550 rpm to investigate its effect on the particle dimensions. After evaporation of the solvent, the reaction mixture was allowed to cool, and the epoxy microencapsulated polystyrene capsules were filtered and washed many times with water followed by drying under vacuum.
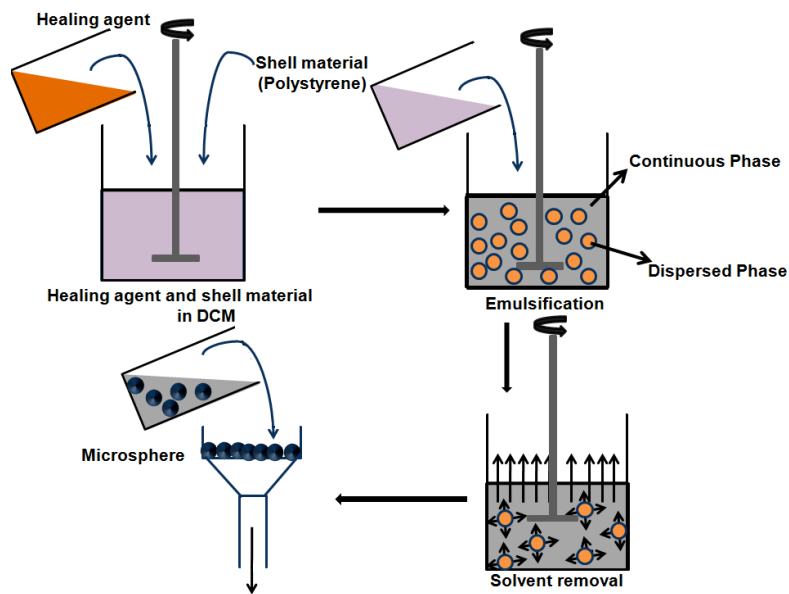
Figure 2.1: Schematic of preparation of healing agent encapsulated polystyrene microcapsules

2.2.4. Microencapsulation of epoxy in urea-formaldehyde shells

Epoxy encapsulated microcapsules were prepared by a dispersion polymerization route as per the methodology described in the literature[106]. For this, 25 ml EMA solution

(2.5 %, w/v) was mixed with 100 mL distilled water by stirring at room temperature (~ 350 rpm) using a magnetic stirrer (IKA RCT, Staufen Germany). To this solution, shell forming materials (2.5 g urea, 0.25 g ammonium chloride and 0.25 g resorcinol) were added. After complete dissolution, the pH was brought to 3.2 ± 0.2 with aqueous sodium hydroxide solution (1% w/v). Subsequently, ~ 60 ml of the healing agent solution (Epoxy: ethyl acetate:: 1:1 w/w) was introduced over a period of 20 min under stirring. Thereafter, requisite amount (6.33 g) of formalin was introduced and the rection mixture was heated to 50-55°C, while varying the stirring speed (250-450 rpm). The reaction was allowed to proceed for 4 h, followed by filtration of the microcapsules and air drying for 24 h, which led to the formation of free-flowing powder. Urea and formaldehyde was separately reacted in the absence of epoxy, which led to the precipitation of a white powder comprising only of the shell wall material, i.e.,urea-formaldehyde resin. The methodology adopted and the reaction along with the structure of the polymer is presented in Figure 2.2.
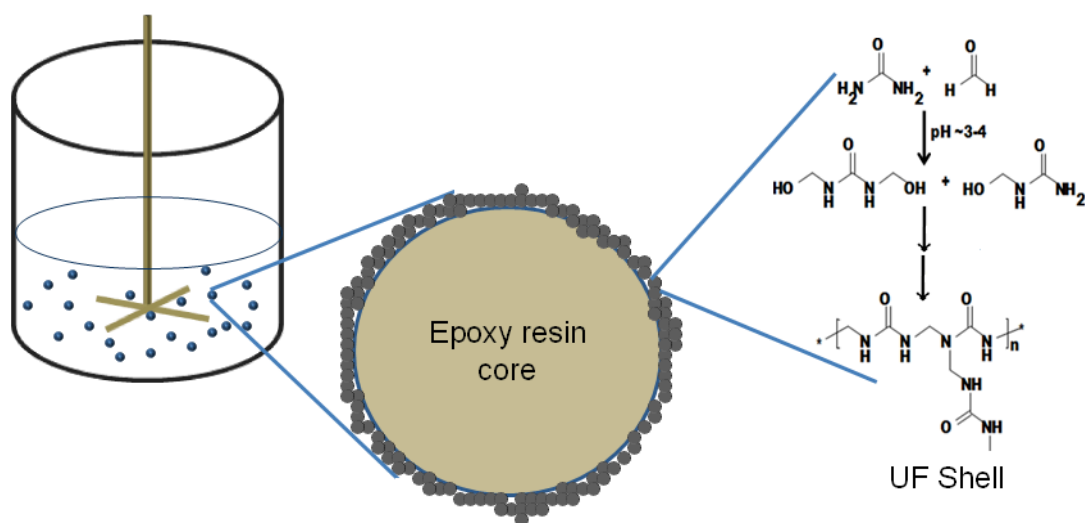
Figure 2.2: Schematic of formation of healing agent encapsulated urea-formaldehyde (UF) microcapsules

The extent of encapsulation in the microcapsules was estimated by solvent (acetone) extraction technique as per the reported procedure[107]. For this, a precisely weighed amount of microcapsules (M_{mc}) was crushed to release the encapsulated healing agent. The resulting powder was then washed with acetone, filtered, dried, and weighed (M_{shell}). The core content was determined gravimetrically as the ratio of encapsulated mass of epoxy ($M_{mc}-M_{shell}$) to the initial mass of the microcapsules (M_{mc}) as given in equation 2.1.

$$\text{Core content} = \frac{M_{mc} - M_{shell}}{M_{mc}} \dots\dots\dots\dots\dots\dots\dots\dots\dots\dots\dots\dots\dots\dots\dots 2.1$$

2.3. Characterization

The morphological studies of epoxy encapsulated microcapsule were performed using a scanning electron microscope (Zeiss EVO MA15) under an acceleration voltage of 1 kV. Samples were placed on aluminium stubs and sputter-coated with gold (10 nm) by a sputter coater (Quorum SC7620) operating at 10-12 mA for 120 s. Average microcapsule size with standard deviations were determined by using ImageJ software. Optical images of dispersed epoxy micro-droplets were captured by using an optical microscope (MOTIC B3-223PL). Structural characterization of microcapsules was performed using a Thermo scientific FTIR (NICOLET 8700) analyser which is equipped with an Attenuated Total Reflectance (ATR) crystal accessory. The FTIR spectra were recorded in the wavelength range 600- 4000cm^{-1}. The thermal degradation behaviour of the epoxy filled microcapsules was studied using Perkin Elmer Diamond STG-DTA in the temperature range 50-600°C at a heating rate of 10°C/min under N_2 atmosphere. For each experiment, a sample mass of 5.0 ± 0.5 mg was used. For calorimetric studies a

Differential Scanning Calorimeter (TA instruments Q 20) was used. Dynamic DSC scans were performed under flowing N_2 (50 mL/min) to minimize oxidative degradation of the sample. For each experiment, requisite amount of samples (10 ±2 mg) were sealed in aluminum pans, and then heated from 50 to 200°C at 10°C /min. Before the experiments, the temperature and enthalpy of the instrument was calibrated using standard indium and zinc. The instrument regained thermal equilibrium was within 1 min of sample insertion, and the exothermic reaction was considered to be complete when the signal levelled off to the baseline. For the quantification of heat of curing, the area under the exothermic curve was estimated.

2.4. Results and Discussion

2.4.1. Preparation of polystyrene

The prepared polystyrene was found to exhibit an onset decomposition temperature (T_{onset}) of 400 °C and a T_g of 98°C. The TG-DTG and DSC trace is shownin Figure 2.3. The viscosity average molecular weight of the polymer was determined to be 3.19 x 10^5 g/mol from intrinsic viscosity measurements in toluene at 34°C ([η] ~105ml/g).
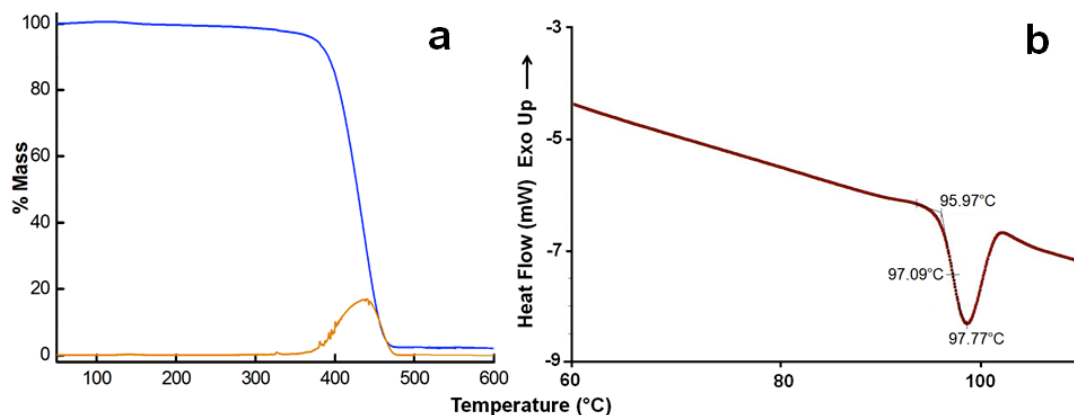
Figure 2.3: a) TG-DTG and b) DSC traces of polystyrene

37

2.4.2. Encapsulation of epoxy through solvent evaporation

For encapsulation of water-insoluble materials, including drugs and healants, the celebrated "oil-in-water (o/w) method" is undoubtedly the most popular. The major steps involved, include dissolution of the healant along with the polymer in an organic solvent, extortion of the solvent into the continuous phase, followed by solvent evaporation from the continuous phase: a process, which transforms the dispersed droplets into solid particles over a period of time. It is important to choose a solvent with high vapour pressure, which is capable of dissolving the shell material completely, in addition of being poorly soluble in the continuous phase. It is to be noted that the presence of gaseous bubbles can disturb the stability of the dispersed drops, therefore the temperature was maintained at 35 °C under atmospheric pressures for the purpose of microencapsulation.

Proper stabilization of the emulsionis an absolute necessity for the success of this process.In the absence of stabilizer, the instability of the water-epoxy dispersion leads to the coalescence of the epoxy droplets. The effect of stabilizer concentration on the stability of epoxy-water emulsion is shown in Figure 2.4. It can be observed that the droplet size decreased with increasing concentration of PVA and a properly stabilized emulsion could be obtained at surfactant concentrations >2% w/w.
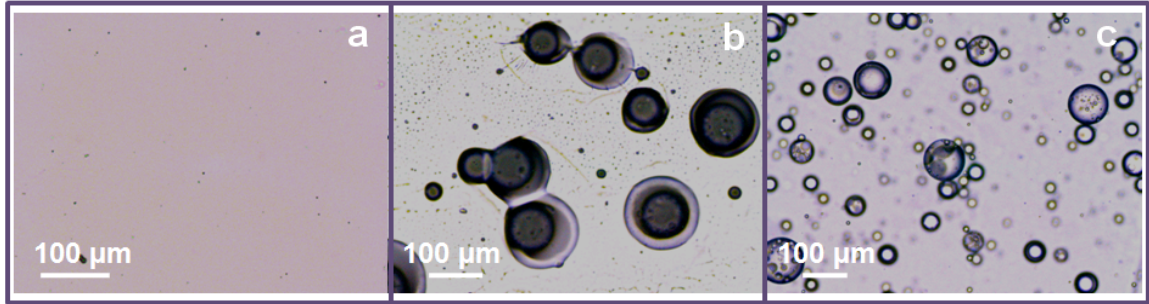
Figure 2.4: Effect of the concentration of stabilizer on the stability of epoxy-water emulsion a) nil, b) 1% and c) 2%

Post-stabilisation of the emulsion, the solvent is allowed to evaporate under controlled conditions, so as to obtain solid microspheres with the liquid resin encapsulated within. Due to the interaction of the two concurrent mass flows, the course of solvent removal takes place in three distinct stages. Representative contours of solvent evaporation rates, concentration of solvent in the continuous phase and the decrease in solvent mass with respect to time is presented in Figure. 2.5. The aliquot appearance was captured at periodic intervals through optical imaging by removing samples, followed by quenching in water 15°C.
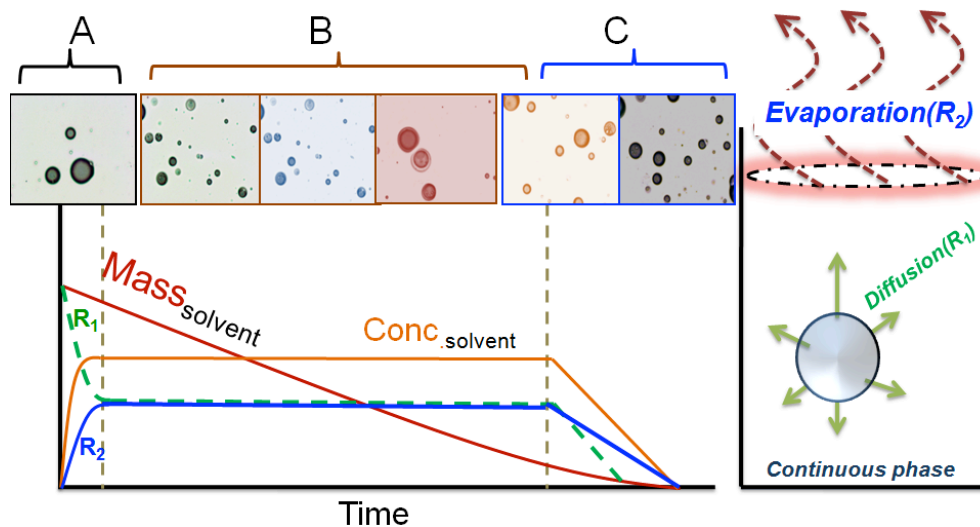
Figure 2.5: Characteristic contours as a function of time

Stage A: In the initial stages of the process, the diffusion rate of solvent from the dispersed phase to the continuous phase (R_1) is higher than the solvent evaporation rate from continuous phase to air (R_2). As a result, the concentration level of solvent in continuous phase (C_s) goes on increasing and reaches its maxima (solubility of dichloromethane in water at 30°C = 15.8 g/L).

Stage B: The loss of solvent due to evaporation at the continuous phase-air interface, is compensated through the diffusion of solvent into the continuous phase which results in a practically constant plateau region where the concentration of solvent in the continuous phase maintains a constant value (C_S). The time span of this stage is dependant on the starting amounts of the continuous phase and of the dispersed phase.

Stage C: The ability of the solvent to diffuse in the dispersed phase decreases with an increase in polymer concentration ($R_1 < R_2$), as a consequence of which C_S decreases: a period which marks the transition from stage B to C. Complete solidification of the dispersed droplet takes place during this step.

2.4.2.1. Effect of stirring speed on encapsulation of epoxy in polystyrene shells

Solvent evaporation process was successfully used for the encapsulation of epoxy resin in polystyrene shells. Several experimental factors affect the microcapsule dimensions, including stirring speed, reaction temperature, surfactant concentration, reactor geometry, interfacial tension, hydrodynamics and viscosity of the media. The influence of increasing stirring rate on the micropcapsule dimensions was investigated and representative SEM images along with the average size of the microcapsules produced by varying the stirring speed, keeping all other conditions constant is shown in

Figure 2.6. The yield of the microcapsules, as determined by gravimetric analysis, was found to be $72 \pm 5\%$. Analysis of the SEM micrographs reveals that the synthesized microcapsules were poly-dispersed and spherical in shape with no inter-capsule bonding. In addition, microcapsules appear to exhibit a smooth texture with some sub-micron debris on their shell.
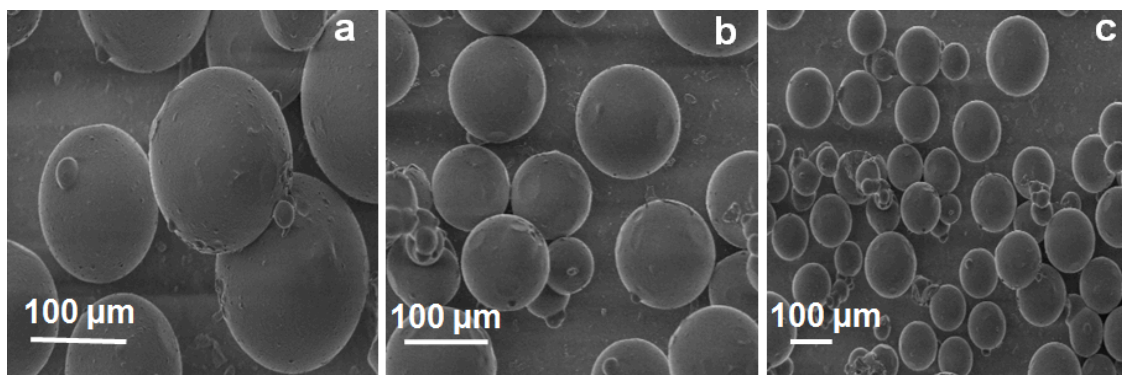
Figure 2.6: SEM micrographs of epoxy encapsulated polystyrene microcapsules prepared under different stirring speeds a) 350, b) 450, c) 550 rpm

The associated particle size distribution of epoxy encapsulated polystyrene microcapsules is shown in Figure 2.7. The rate of agitation decides the equilibrium between interfacial tension and shear forces of the discrete oil microdroplets[108]. At low agitation rates, larger suspended droplets are formed as the interfacial tension dominates over shear forces. As the agitation speed is increased, these further shear to form smaller droplets, the dimensions of which depend upon the reaction conditions prevalent[109].
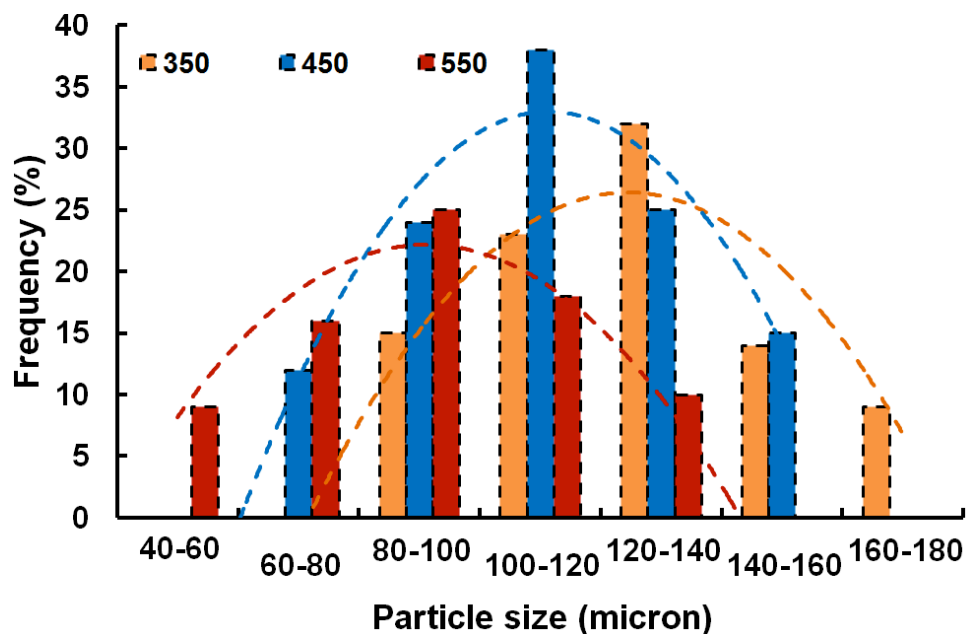
Figure 2.7: Effect of agitation speed on the particle size distribution of epoxy

encapsulated polystyrene microcapsules

The core content of the microcapsules, as estimated by gravimetric analysis, was found to be 38 ± 2%.

2.4.2.2. Thermal properties

The TG traces of epoxy encapsulated polystyrene microcapsules are presented in Figure 2.8. For comparison purposes, the TG traces of neat epoxy resin and polystyrene are also included. The thermal degradation profile of epoxy resin clearly shows two-steps: the first occurring at ~ 150-225°C followed by another at ~ 225-325°C. Polystyrene exhibits a single step degradation at 300-400 °C, with the major thermal degradation products being a mixture of unsaturated saturated compounds, particularly styrene.

The first step (~300-400°C) in the decomposition profile of microcapsules occurs due to the degradation of polystyrene shell, which is followed by the decomposition of the core healant, i.e., epoxy resin at ~ 400-550°C.
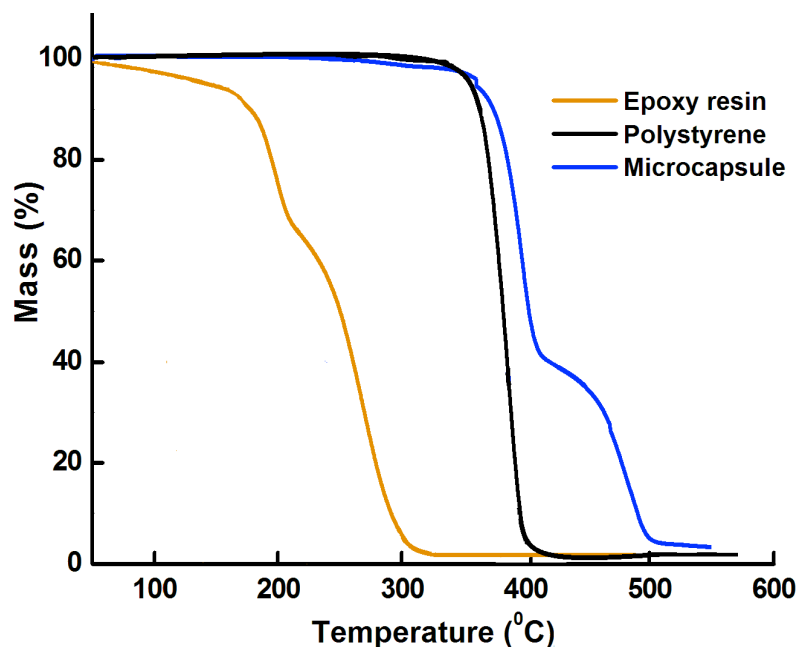
Figure 2.8: TG traces of epoxy resin, microcapsules and polystyrene

2.4.2.3. Structural properties

FTIR spectra of epoxy encapsulated PS microcapsules, epoxy resin and polystyrene shell is shown in Figure 2.9. Epoxy resin exhibits absorption at 3610-3339 cm^{-1} (v O-H str.), 2873-2964 cm^{-1} (v C-H(al) str.), 1250 cm^{-1} and 1027 cm^{-1} (v C-O-C str.), 910 cm^{-1} (v epoxy ring str.). The poystyrene shell shows absorption at 3026 cm^{-1} (v C-H(ar) str.), 2922 cm^{-1} (v C-H (al) str), 1625-1475 cm^{-1} (v C=C(ar) str.) and 900-650 cm^{-1} (v C-H(ar) deform). The epoxy encapsulated polystyrene microcapsules also exhibit absorptions similar to that of polystyrene shell which confirms the encapsulation of epoxy in polystyrene shell.

43
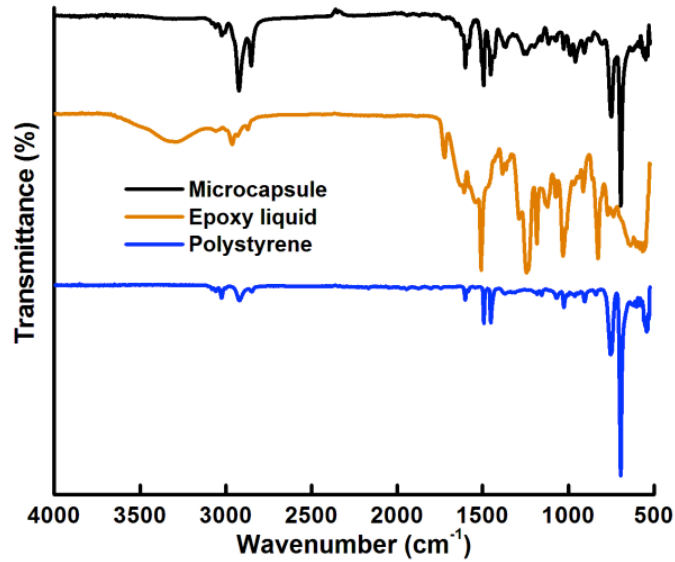
Figure 2.9: FTIR of microcapsules, epoxy liquid and polystyrene

2.4.3. Epoxy encapsulation by dispersion polymerisation

SEM image of epoxy encapsulated urea-formaldehyde (UF) microcapsules is presented in Figure 2.10a, and a representative broken microcapsule is also presented Figure 2.10b. It is to be noted that dispersion polymerisation route adopted for the preparation of microcapsules lead to the formation of microcapsules with 'reservoir' type internal structure.
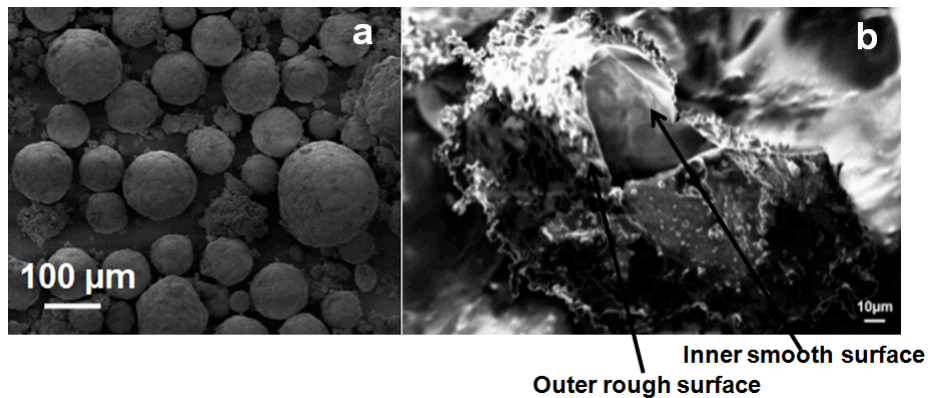
Figure 2.10: SEM image of a) microcapsules b) broken microcapsule

44

It can be seen that, the microcapsule shell has a rough porous morphology on the outer surface while a smooth inner surface. The mentioned feature of shell wall is attributed to the reactions occurring during dispersion polymerization. Urea and formaldehyde react in the aqueous phase and forms a low molecular weight pre-polymer, which with increase in the molecular weight tends to deposit on the epoxy–water interface. Ultimately, the urea-formaldehyde becomes highly cross-linked, forming the microcapsule shell[110]. The prepolymer subsequently precipitates out of the aqueous reaction media as the molecular weight increases[111]. Thus it is believed that the smooth non-porous microcapsule wall is the result of the accumulation of low molecular weight pre-polymer at the epoxy–water interface. As the polymerization of urea-formaldehyde pre-polymer in the aqueous solution progresses, urea-formaldehyde nanoparticles are formed which subsequentally gets deposited on the capsule surface resulting in the rough, porous outer layer of the UF shell[112]. The roughness of outer surface can be attributed to a number of factors, resulting from the interplay of the fluid-determined shear forces and shell-induced elastic forces[113].

2.4.3.1. Effect of stirring speed on encapsulation of epoxy in urea-formaldehyde shells

The effect of agitation speed on the morphology of microcapsules is depicted in Figure 2.11. It can be seen that the prepared microcapsules are polydispersed and spherical in shape with rough outer texture. Our studies revealed that microspheres of dimensions ~190 ± 49 μm and core content of 65 ± 4 % could be obtained, while maintaining stirring speed at 250 rpm. The thickness of shell wall of the microcapsule was determined to be 3.5 ± 1.2μm.
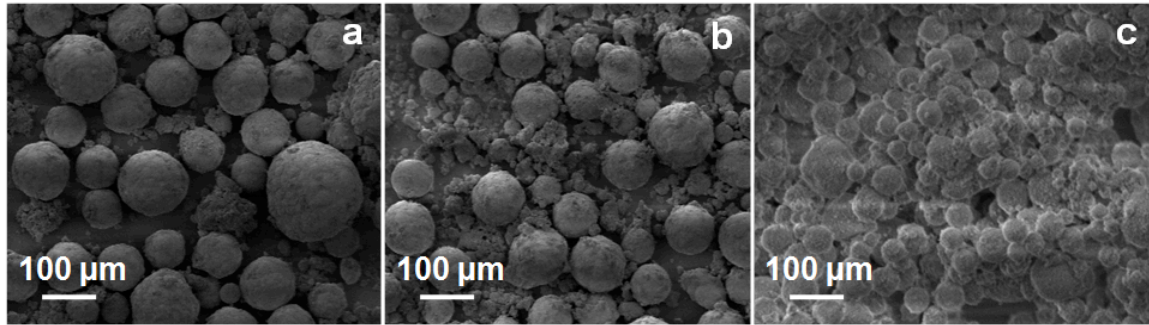
Figure 2.11: Effect of increasing stirring speed on microcapsule size a) 250 rpm,

b) 350 rpm and c) 450 rpm

The average particle size distribution of the microcapsules is illustrated in Figure 2.12. The distribution was found to shift to lower dimensions with increasing mixing speed.
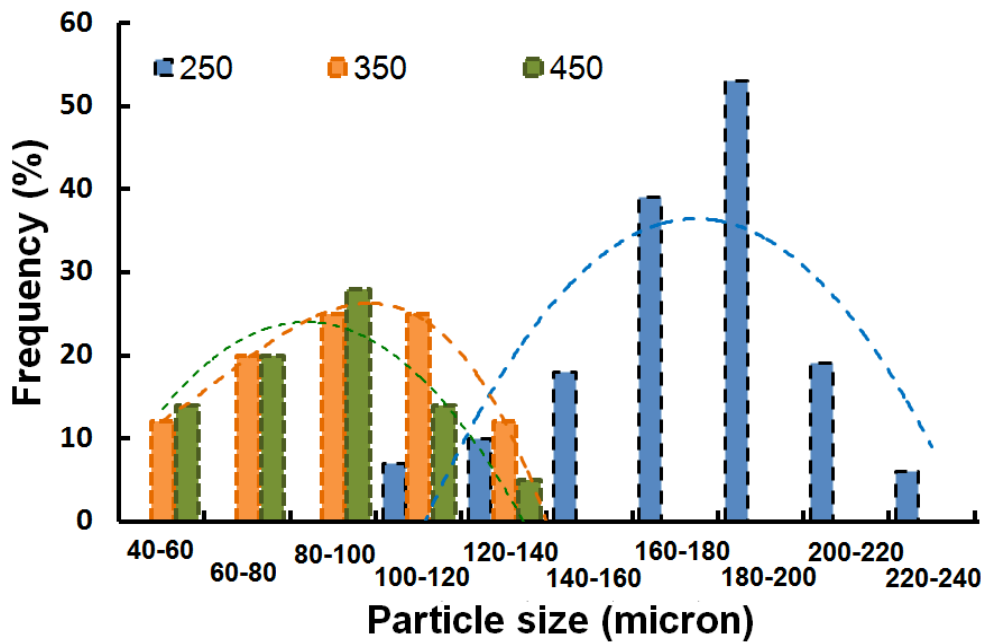
Figure 2.12: Effect of agitation speed on the particle size distribution of epoxy

encapsulated urea-formaldehyde microcapsules

2.4.3.2 Thermal properties

The TG traces of epoxy encapsulated UF microcapsules, neat epoxy resin and urea-formaldehyde shell are shown in Figure 2.13. It is clearly indicated from the TG traces of epoxy resin that it exhibits a two-step thermal degradation process one between 150-225°C and another between 225-325°C. The urea-formaldehyde shell undergoes initial weight loss (T < 150 °C) due to water loss, and the subsequent loss between 250-300°C can be attributed to degradation of shell wall. At T > 400°C, pyrolytic degradation of the three-dimensional framework reportedly occur leading to the evolution of ammonia and formaldehyde[114]. In comparison, the UF microcapsules exhibit a weight loss at ~200°C, which is associated with loss of formaldehyde and the subsequent mass loss at 300-390°C occur due to pyrolytic degradation of the crosslinked network.
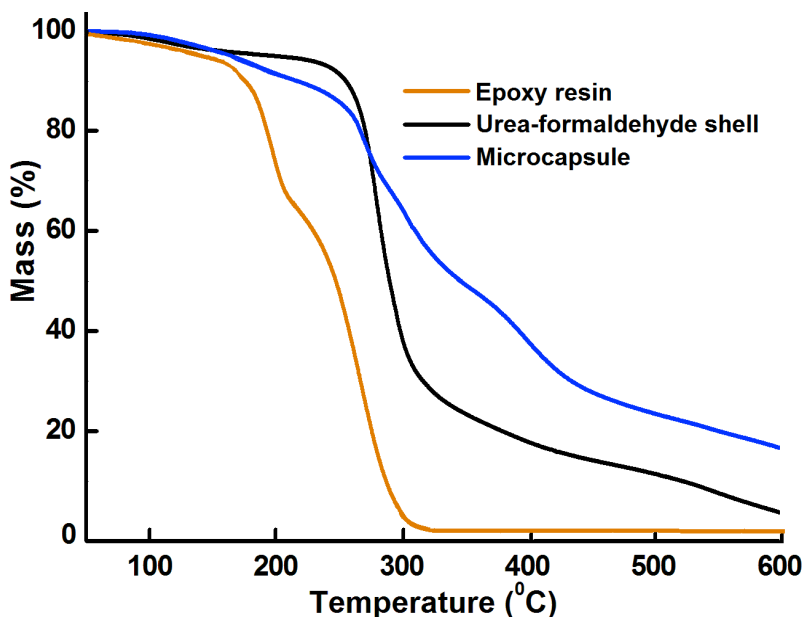
Figure 2.13: TG traces of epoxy resin, microcapsules and urea-formaldehyde shell

2.4.3.3. Structural properties

FTIR spectra of epoxy encapsulated urea-formaldehyde microcapsules are presented in Figure 2.14. UF microcapsules exhibit characteristic broad absorption band around 3350 cm^{-1} which arises from the overlapping absorptions due to hydroxyl, imino and amino functionalities. Other characteristic absorptions include 2962 cm^{-1}(v C-H(al) str), 1461 cm^{-1}and 1361 cm^{-1} (v C–H bend), 1255 and 1181 cm^{-1} (v C-N(al) str), 1649 cm^{-1}(v NH-CO-NH str) and 1034 cm^{-1}(v C–O–C str)[114]. For comparison purpose, the FTIR spectra of epoxy resin and urea-formaldehyde shell is also presented.
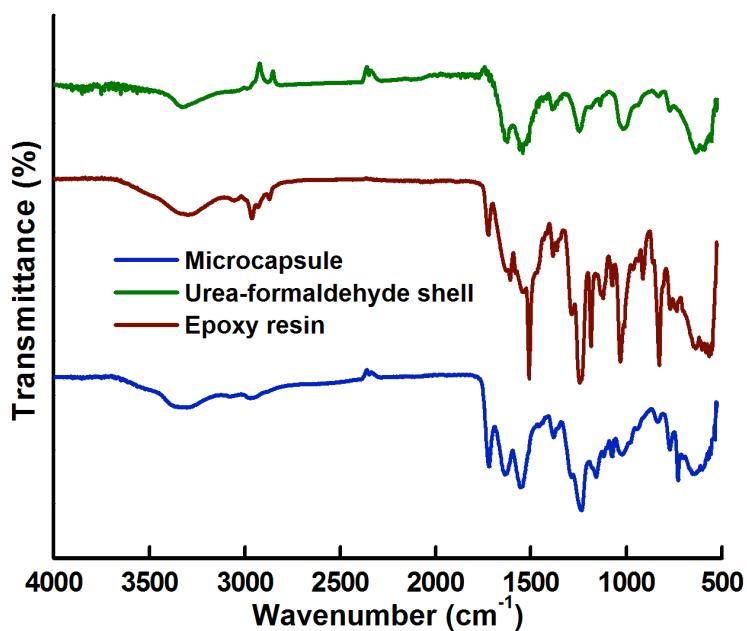
Figure 2.14: FTIR of microcapsules, epoxy liquid and urea-formaldehyde shell

2.4.4. Chemical reactivity of encapsulated epoxy

The chemical reactivity of the encapsulated epoxy was asseessed through calorimetric studies. For this purpose, the microcapsules were crushed and transferred to a DSC pan. After addition of stoichiometric amount of the hardener, the mixture was

subjected to programmed temperature scan from 50 to 200°C. For comparison purpose, the DSC scan was also performed on crushed microcapsules in the absence of amine and the traces are included in Figure 2.15.
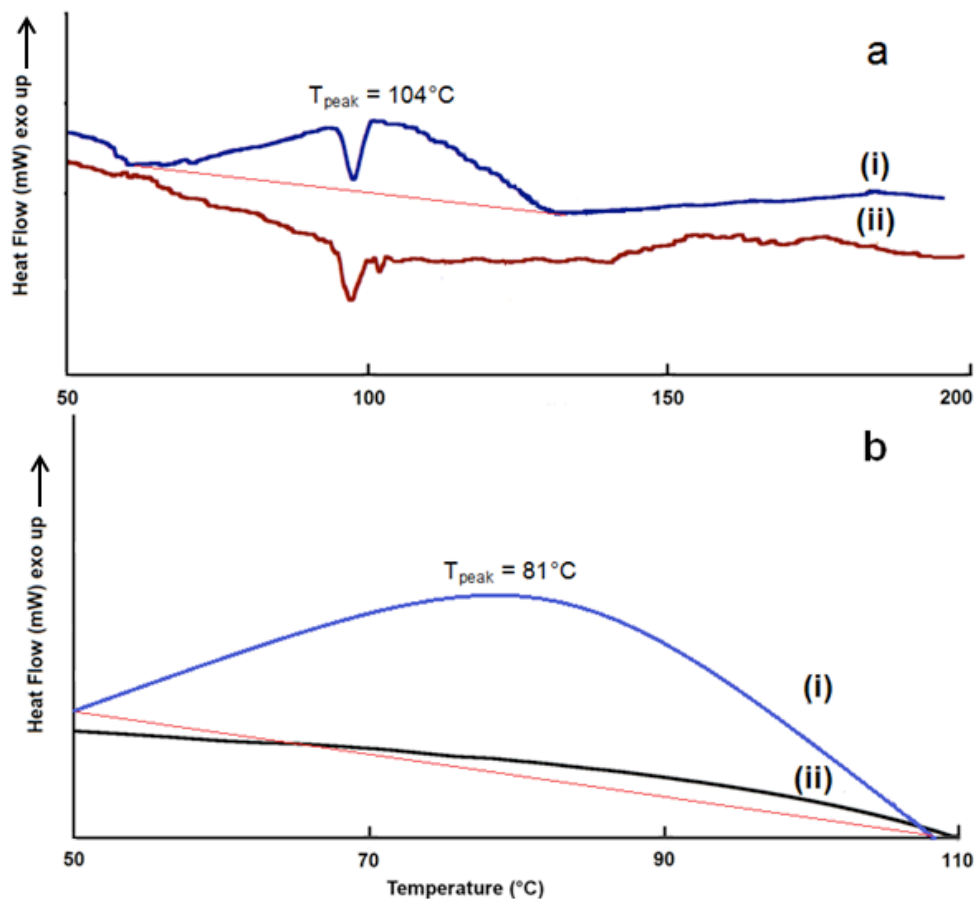
Figure 2.15: DSC trace associated with the curing behaviour of microencapsulated epoxy in the presence of amine hardener a) PS shell and b) UF shell. Line (i) and (ii) show the profile obtained in the presence and absence of amine hardener respectively

It can be observed from the DSC traces that, irrespective of shell wall (UF or PS), the released epoxy undergoes crosslinking, which is indicated by the curing exotherm confirming its chemical activity even after encapsulation. An interesting feature is

observed at ~95°C, in the case of polystyrene microcapsules, which can be associated with the glass transition phenomenon of the shell material, i.e., polystyrene. It can be assumed that around this temperature, the PS shell looses its mechanical strength and the high temperature leads to the bursting of the microcapsule releasing its contents, thereby leading to the observed endotherm. No such feature is observed in the case of UF microcapsules, where the onset of the exotherm is at much lower temperatures. It can be seen that in the case of UF microcapsules the curing reaction initiated at temperature as low as 50 ºC, with T_{peak} at 81ºC while for PS microcapsules it initiates at 70ºC, with T_{peak} at 104ºC. In the absence of amine hardener (Fig 3.8 (i)), the curing exotherm was not evidenced in the temperature range studied.

2.4.5. Internal morphology of microcapsule

Microcapsules can exhibit different internal morphologies, which can be broadly categorised as "reservoir" type or "monolith" type. The cross-sectional view of the plane formed as a result of rupture of microcapsules with different internal microstructure is presented in Figure 2.16. Representative surface of fractured samples are also included in this figure, where "reservoir" and "monolithic" morphology can be clearly observed. It is clear that rupturing of microcapsules with "reservoir" type morphology lead to the release of the entire mass of healant into the crack. In comparison, only a fraction of the healant, which is released from the micro-droplets on the cross-sectional crack plane, is available in the case of monolithic microcapsules. It can hence be presumed that self-healing compositions containing reservoir type microcapsules will be more efficient as compared to those containing monolithic microcapsules.
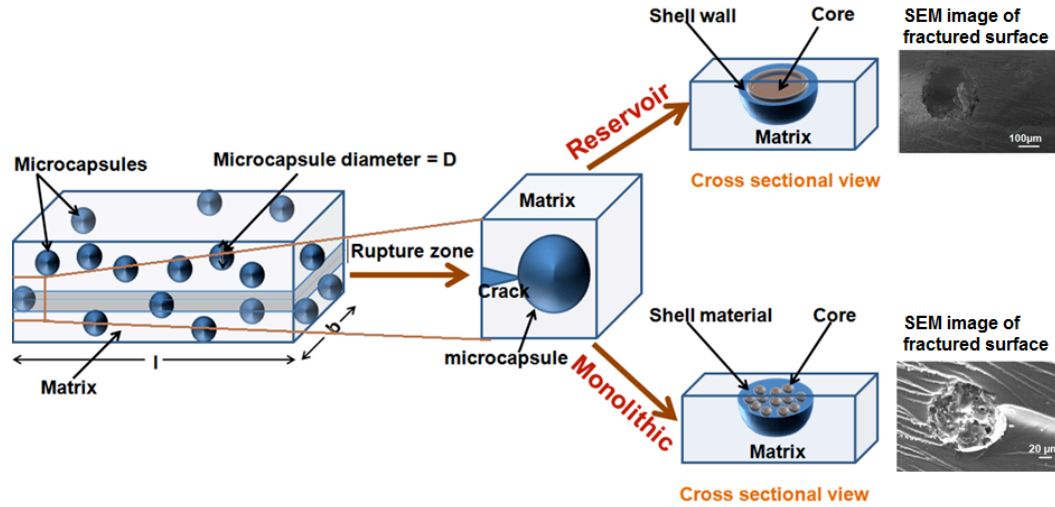
Figure 2.16: Pictorial representation of reservoir type and monolith type microcapsule

A theoretical model does exist to determine the amount of healant released in the event of rupture of "reservoir" type microcapsules[115], however the predictions cannot be extrapolated to that of monolithic microcapsules. Hence, it was considered of interest to develop a model for monolithic microcapsules and compare both the models to arrive at the most suitable morphology for healing purposes. The same is discussed in the following section.

2.4.6. Healant release from microcapsules with "monolithic" microstructure

For the sake of calculation, it is assumed that the healant is homogeneously dispersed as microdroplets within the monolithic microsphere, with each micro-droplet separated from the other by the matrix. A single microcapsule is assumed to be composed of cubic spaces each of length (L) containing a single microdroplet (Figure 2.17)[92]. The micro-droplets are assumed to be perfectly spherical (diameter, D_d) with the distance between two droplets being L_{drop}. The core content ($core_{mic}\%$, v/v), is related to the droplet diameter (D_d) and cubic edge length (L) as:

$$Core_{mic} = \frac{\left(\frac{\pi}{6}\right)D_d^{\,3}}{L^3}$$ 2.2

The distance between two microdroplets $(L - D_d)$ can hence be estimated as

$$L_{drop} = D_d\left[\left(\frac{\pi}{6 \times core_{mic}}\right)^{1/3} - 1\right]$$ 2.3
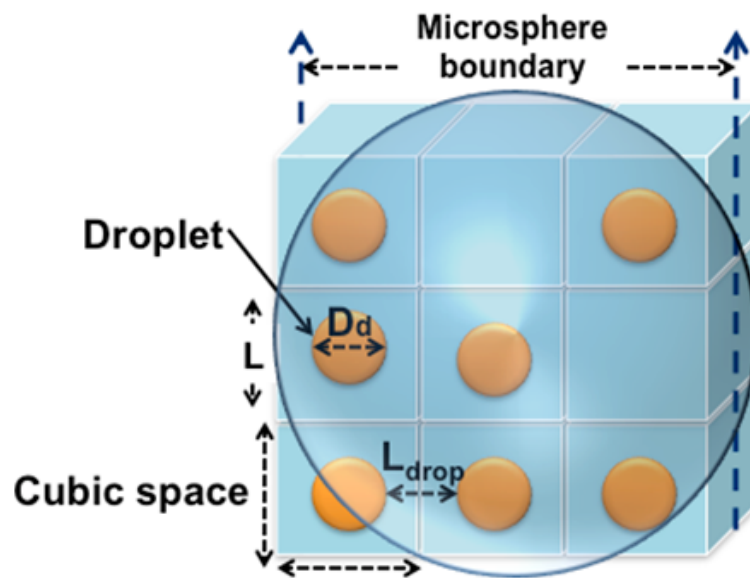
Figure 2.17: Model for estimating distance between droplets within a microcapsule

The effect of increasing core content on the distance between two adjacent droplets is also illustrated in Figure 2.18. As can be observed from the figure, at core content ~50 %, irrespective of the dimensions of the dispersed microdroplets, the microcapsules essentially exhibit "reservoir" type morphology, as the distance between two adjacent droplets reduces to zero.

52
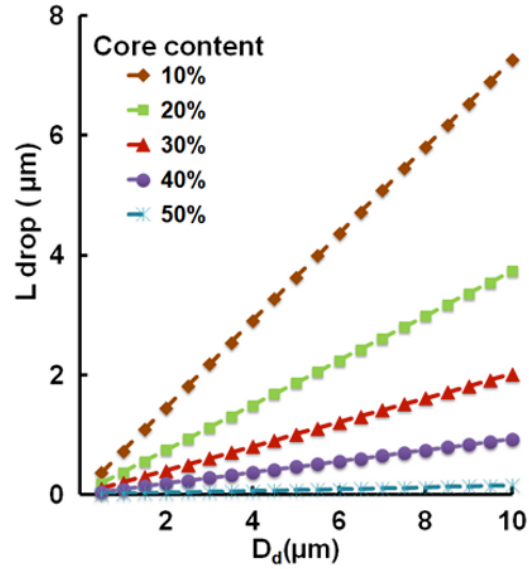
Figure 2.18: Variation of distance between microdroplets (L_{drop}) with core content

The effect of increasing microdroplet dimensions on the distance between drops (L_{drop}) is presented in Figure 2.19. It is interesting to observe that as the dimension of the microdroplet increases, the distance between the droplets also tend to increase, which appears to be contrary to the common perception.
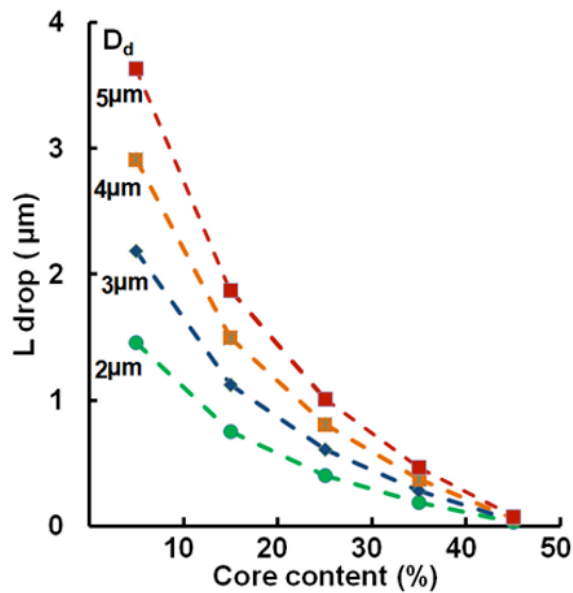
Figure 2.19: Variation of distance between microdroplets (L_{drop}) with microdroplet diameter

For the sake of ease of visualisation, a pictorial representation of how the microdroplets coalescence leading to the increase in L_{drop} is shown in Figure 2.20. It can be seen that although the number of droplets are same in number, the distance between the droplets will be much larger when the micro-droplets coalesce.
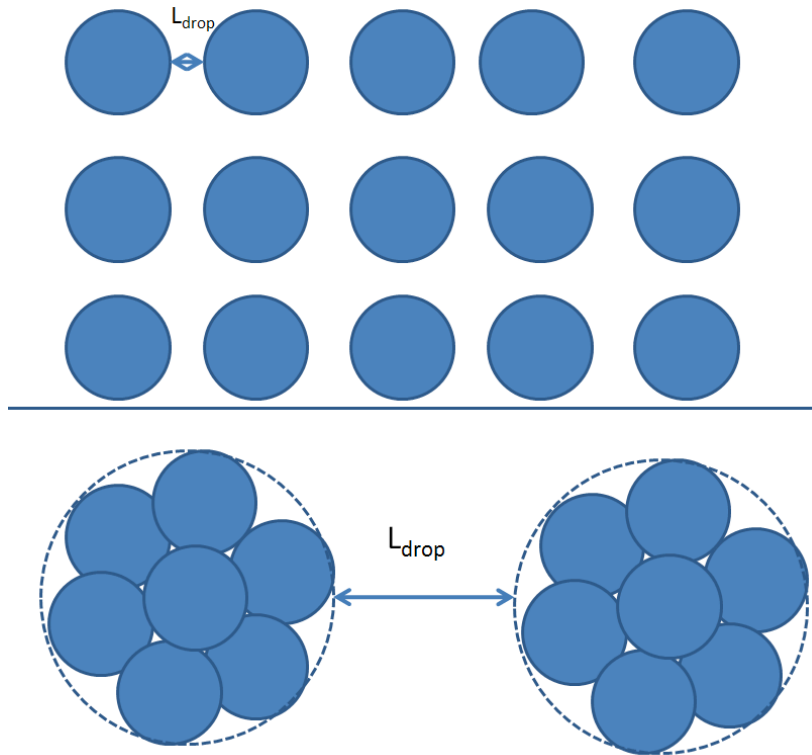
Figure 2.20: Pictorial representation of coalescence of microdroplets

For the purpose of determining the amount of healant released in the event of rupture of a microcapsule, a 2D cross-section of both monolithic and reservoir type microcapsule is considered, as illustrated in Figure 2.21.
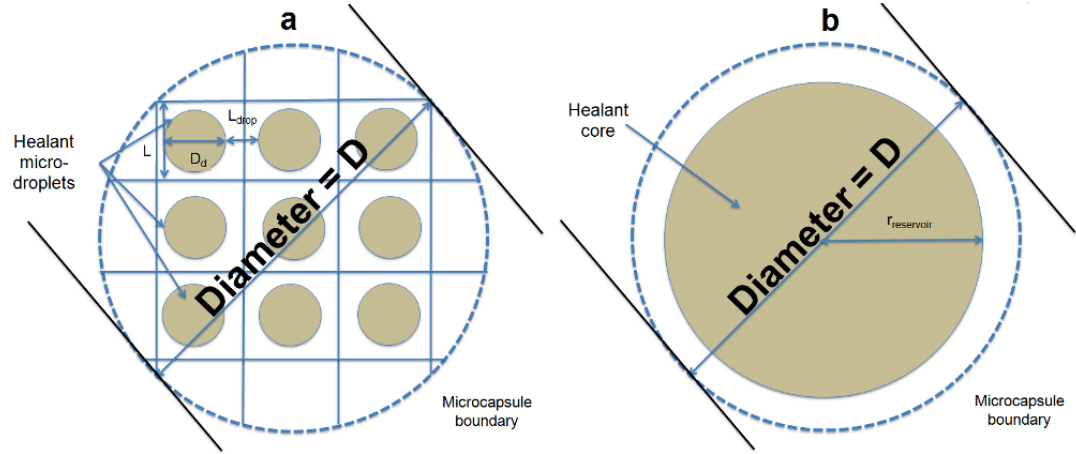
Figure 2.21: Cross sectional plane of a) monolithic and b) reservoir

microcapsule

The number of micro-droplets in a single microcapsule (N) can be estimated as

$$\frac{\pi r^2}{(L_{drop}+D_d)^2}$$

The volume of liquid entrapped in a single micro-droplet $(V_d) = \frac{4}{3}\pi r_d{}^3$

The total volume of liquid released in the event of rupture of monolithic microcapsule can be estimated as

$$V_{monolith} = N \times \frac{4}{3}\pi r_d{}^3$$

Detailed calculations for two microcapsule dimensions (D= 150μm and 200μm) are presented in Table 2.1 and 2.2 respectively.

Table 2.1: Amount of healant delivered in the event of rupture of "monolith" type microcapsule (D= 150μm).The fraction of liquid released (monolith/ reservoir) is also presented

D_d (μm)	L_{drop} (μm)	$D_d + L_{drop}$ (μm)	Area (μm^2)	(N)	V_h (μm^3)	$V_{monolith}$ (μm^3)	$F_{mon/res}$ (%)
1	0.09	1.09	1.19	14792	0.52	7740.99	1.10
2	0.19	2.19	4.78	3698	4.19	15481.98	2.19
3	0.28	3.28	10.75	1644	14.13	23222.97	3.29
4	0.37	4.37	19.11	924	33.49	30963.95	4.38
5	0.46	5.46	29.85	592	65.42	38704.94	5.48
6	0.56	6.56	42.99	411	113.04	46445.93	6.57
7	0.65	7.65	58.51	302	179.50	54186.92	7.67
8	0.74	8.74	76.42	231	267.95	61927.91	8.77
9	0.83	9.83	96.72	183	381.51	69668.90	9.86
10	0.93	10.93	119.41	148	523.33	77409.89	10.96
11	1.02	12.02	144.48	122	696.56	85150.87	12.05
12	1.11	13.11	171.95	103	904.32	92891.86	13.15
13	1.21	14.21	201.80	88	1149.76	100632.85	14.24
14	1.30	15.30	234.04	75	1436.03	108373.84	15.34
15	1.39	16.39	268.67	66	1766.25	116114.83	16.44
16	1.48	17.48	305.68	58	2143.57	123855.82	17.53
17	1.58	18.58	345.09	51	2571.14	131596.81	18.63
18	1.67	19.67	386.88	46	3052.08	139337.79	19.72
19	1.76	20.76	431.06	41	3589.54	147078.78	20.82
20	1.85	21.85	477.63	37	4186.67	154819.77	21.91
21	1.95	22.95	526.59	34	4846.59	162560.76	23.01
22	2.04	24.04	577.94	31	5572.45	170301.75	24.10
23	2.13	25.13	631.67	28	6367.40	178042.74	25.20
24	2.23	26.23	687.79	26	7234.56	185783.72	26.30
25	2.32	27.32	746.30	24	8177.08	193524.71	27.39
26	2.41	28.41	807.20	22	9198.11	201265.70	28.49
27	2.50	29.50	870.49	20	10300.77	209006.69	39.44
28	2.60	30.60	936.16	19	11488.21	216747.68	40.91
29	2.69	31.69	1004.22	18	12763.58	224488.67	42.37
30	2.78	32.78	1074.67	16	14130.00	232229.66	43.83
31	2.87	33.87	1147.51	15	15590.62	239970.64	45.29
32	2.97	34.97	1222.74	14	17148.59	247711.63	46.75
33	3.06	36.06	1300.36	14	18807.03	255452.62	48.21
34	3.15	37.15	1380.36	13	20569.09	263193.61	49.67
35	3.25	38.25	1462.75	12	22437.92	270934.60	51.13
36	3.34	39.34	1547.53	11	24416.64	278675.59	52.59
37	3.43	40.43	1634.70	11	26508.40	286416.58	54.05

Table 2.2: Amount of healant delivered in the event of rupture of "monolith" type microcapsule (D= 200μm).The fraction of liquid released (monolith/ reservoir) is also presented

D_d (μm)	L_{drop} (μm)	$D_d + L_{drop}$ (μm)	Area (μm²)	(N)	V_h (μm³)	$V_{monolith}$ (μm³)	$F_{mon/res}$ (%)
1	0.09	1.09	1.19	26296.35	0.52	13761.76	0.82
2	0.19	2.19	4.78	6574.09	4.19	27523.51	1.64
3	0.28	3.28	10.75	2921.82	14.13	41285.27	2.47
4	0.37	4.37	19.11	1643.52	33.49	55047.03	3.29
5	0.46	5.46	29.85	1051.85	65.42	68808.79	4.11
6	0.56	6.56	42.99	730.45	113.04	82570.54	4.93
7	0.65	7.65	58.51	536.66	179.50	96332.30	5.75
8	0.74	8.74	76.42	410.88	267.95	110094.06	6.57
9	0.83	9.83	96.72	324.65	381.51	123855.82	7.40
10	0.93	10.93	119.41	262.96	523.33	137617.57	8.22
11	1.02	12.02	144.48	217.33	696.56	151379.33	9.04
12	1.11	13.11	171.95	182.61	904.32	165141.09	9.86
13	1.21	14.21	201.80	155.60	1149.76	178902.85	10.68
14	1.30	15.30	234.04	134.17	1436.03	192664.60	11.50
15	1.39	16.39	268.67	116.87	1766.25	206426.36	12.33
16	1.48	17.48	305.68	102.72	2143.57	220188.12	13.15
17	1.58	18.58	345.09	90.99	2571.14	233949.88	13.97
18	1.67	19.67	386.88	81.16	3052.08	247711.63	14.79
19	1.76	20.76	431.06	72.84	3589.54	261473.39	15.61
20	1.85	21.85	477.63	65.74	4186.67	275235.15	16.44
21	1.95	22.95	526.59	59.63	4846.59	288996.91	17.26
22	2.04	24.04	577.94	54.33	5572.45	302758.66	18.08
23	2.13	25.13	631.67	49.71	6367.40	316520.42	18.90
24	2.23	26.23	687.79	45.65	7234.56	330282.18	19.72
25	2.32	27.32	746.30	42.07	8177.08	344043.93	20.54
26	2.41	28.41	807.20	38.90	9198.11	357805.69	21.37
27	2.50	29.50	870.49	36.07	10300.77	371567.45	22.19
28	2.60	30.60	936.16	33.54	11488.21	385329.21	23.01
29	2.69	31.69	1004.22	31.27	12763.58	399090.96	23.83
30	2.78	32.78	1074.67	29.22	14130.00	412852.72	24.65
31	2.87	33.87	1147.51	27.36	15590.62	426614.48	25.47
32	2.97	34.97	1222.74	25.68	17148.59	440376.24	26.30
33	3.06	36.06	1300.36	24.15	18807.03	454137.99	27.12
34	3.15	37.15	1380.36	22.75	20569.09	467899.75	27.94
35	3.25	38.25	1462.75	21.47	22437.92	481661.51	28.76
36	3.34	39.34	1547.53	20.29	24416.64	495423.27	29.58
37	3.43	40.43	1634.70	19.21	26508.40	509185.02	30.41

Where

N = Number of droplets present in the hemispherical cross-section

V_h = *Volume of healant released from each droplet of diameter D_d*

$V_{monolith}$ = *Total liquid released in the event of microcapsule rupture*

$F_{mon/res}$ = *Fraction of liquid released (monolith: reservoir)*

In comparison, the total volume of liquid released in the event of rupture of microcapsule with comparable core contents, but possessing "reservoir" type microstructure, is $V_{reservoir} = \frac{4}{3}\pi r_{reservoir}^{3}$, where the radius of the healant reservoir ($r_{reservoir}$) is related to the diameter of the microcapsule (D) by $r_{reservoir} = \frac{D}{2}(core\ content)^{1/3}$. It is obvious that for lower core contents, $V_{monolith}$ is much lesser than $V_{reservoir}$.

2.4.7. Healant delivery into the crack plane

A well accepted model for predicting the amount of healant delivered in the event of microcapsule rupture exists in the literature[115]. It is assumed that all the microcapsules in the crack plane undergo rupture, releasing the entire content encapsulated within, which unfortunately restricts the predictions to that of microcapsule with "reservoir" type microstructure. A pictorial of the scenario described is depicted in Figure 2.22.
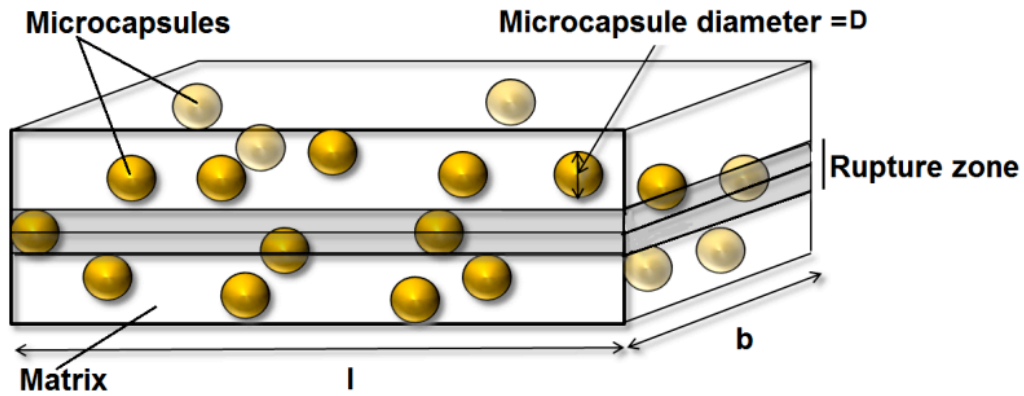
Figure 2.22: Pictorial representation of a cuboidal sample containing microcapsules. Microcapsules lying within the shaded region are expected to rupture leading to the release of healant

According to this model, the total quantity of healant delivered per unit crack area (m) is directly proportional to both the microcapsule mass fraction as well as microcapsule diameter. It is presumed that the microcapsules in the crack plane that are intersected during the crack propagation will rupture and release the contents encapsulated within. The number of such ruptured capsules (n) can be estimated as,

$$n = p \times N \dots\dots\dots\dots\dots\dots\dots\dots\dots\dots\dots\dots\dots\dots\dots\dots\dots\dots\dots\dots\dots\dots\dots\dots\dots2.4$$

where,

N= number of capsules in the sample

p = probability of the microcapsule centre lying in the rupture zone associated with a single microcapsule diameter (D).

Assuming random distribution of the microcapsules possessing thin shell wall, (shell wall <2% of the microcapsule diameter), the probability (p) can be estimated as,

$$p = \frac{\rho_s AD}{M_s} \dots\dots\dots\dots\dots\dots\dots\dots\dots\dots\dots\dots\dots\dots\dots\dots\dots\dots\dots\dots 2.5$$

where

ρ_s= sample density,

A = area of crack (l x b),

D= microcapsule diameter,

M_s = sample mass.

The total number of capsules in the sample depends on the microcapsule loading as follows

$$N = \frac{\phi M_s}{m_c} \dots\dots\dots\dots\dots\dots\dots\dots\dots\dots\dots\dots\dots\dots\dots\dots\dots 2.6$$

where

Φ = mass fraction of microcapsule

m_c= mass of one microcapsule

The quantity of healant delivered per unit crack area (m) can be determined by,

$$m = \frac{m_h}{A} \dots\dots\dots\dots\dots\dots\dots\dots\dots\dots\dots\dots\dots\dots\dots\dots 2.7$$

where,

m_h= amount of healant delivered expecting all microcapsules bisected by the crack plane are ruptured

Combining eq. 2.4-2.7 yields,

$m = \rho_s . \phi . D$ 2.8

where

ρ_s = sample density,

Φ = mass fraction of microcapsules

D = microcapsule diameter

The effect of increasing microcapsule loading on the amount of healant delivered per unit area of crack plane is shown in Figure 2.23 and Table 2.3. It is to be noted however, that for the sake of calculation, it is assumed that the shell wall around the healant is infinitely thin, i.e., the core content is close to 100%.
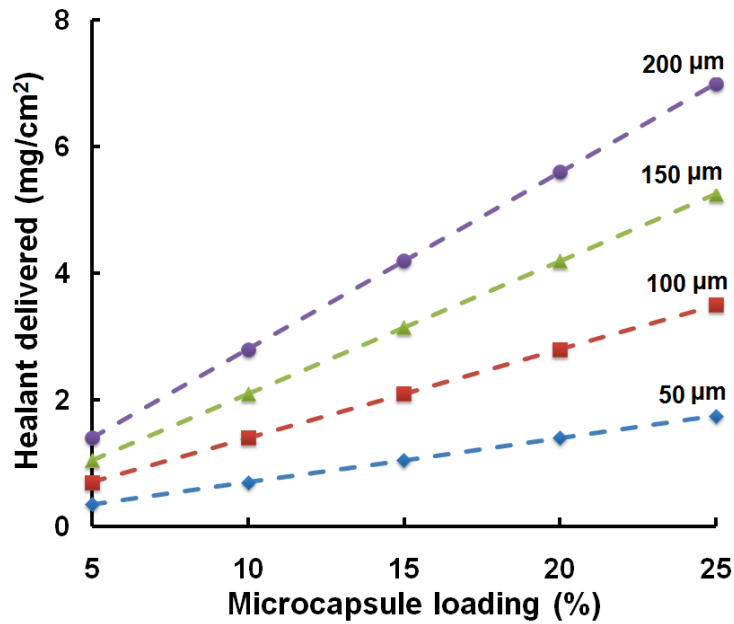
Figure 2.23: Effect of increasing microcapsule loading on healant delivery for reservoir type microcapsule (assuming extremely thin shell wall)

Table 2.3: Effect of mass fraction and microcapsule diameter on the amount of resin delivered per unit area of crack plane

Mass percent	Estimated healant delivered (mg/cm^2) with microcapsules of varying diameter *			
	50 µm	100 µm	150 µm	200 µm
5	0.35	0.7	1.05	1.4
10	0.7	1.4	2.1	2.8
15	1.05	2.1	3.15	4.2
20	1.4	2.8	4.2	5.6
25	1.75	3.5	5.25	7

*Assuming density of sample to be invariantly equal to 1.4 g/cm^3

2.4.8. Comparison of "reservoir" and "monolithic" microcapsules

A comparison in terms of the amount of healant delivered as a function of microcapsule loading for both "reservoir" and "monolith" type configuration for two representative microcapsule diameters (150 and 200 µm) is presented in Figure 2.24. At core contents 50% and higher, the predictions of monolithic and reservoir are essentially same.

However, it can be seen that the difference between reservoir and monolithic morphology is pronounced at relatively smaller dimensions and lower core contents (< 50%). Plots corresponding to different microdroplet diameter (D_d= 20-80µm) for a fixed core content (core$_{mic}$= 40%) are shown in the figure and the detailed calculations are presented in Table 2.1. It is apparent that as the microdroplet dimensions increase, the monolith type configuration essentially converges to that of a reservoir.
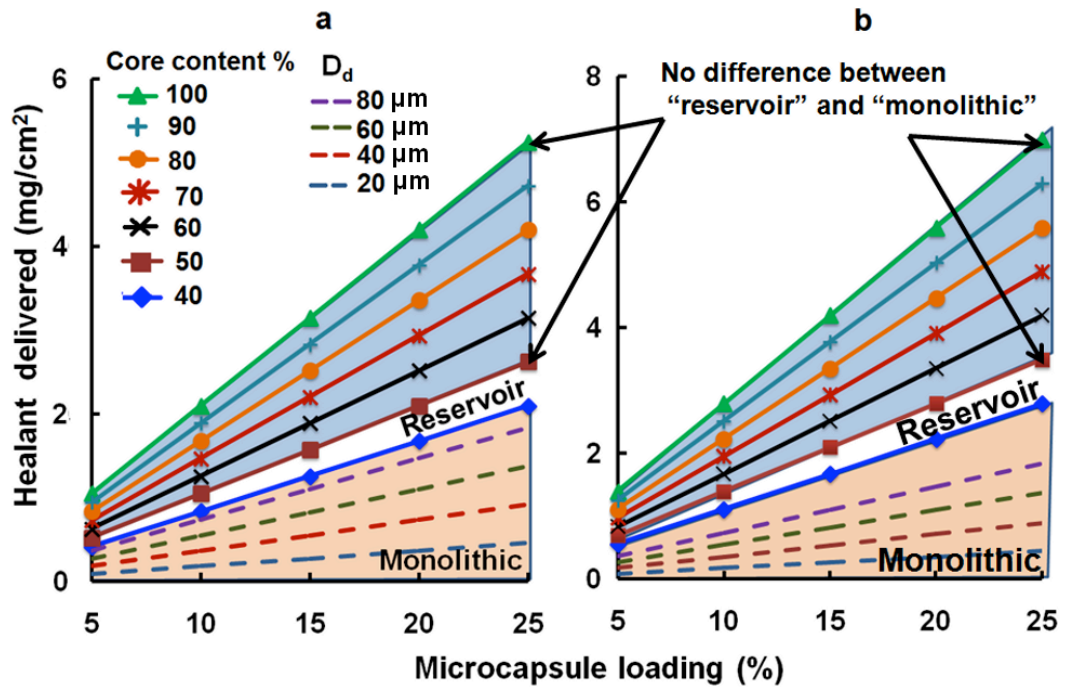
Figure 2.24: Healant delivered as a function of volume fraction and micro-droplet diameter due to rupture of microcapsules of D = a) 150μm and b) 200μm with different internal microstructure

It can hence be concluded that for endowing self healing functionality to epoxy resin, the introduction of microcapsules with "reservoir" type morphology is more beneficial, especially if the core content is less and the microdroplets within the capsule exhibit smaller dimensions.

CHAPTER III

ENCAPSULATION OF REACTIVE AMINES

3.1. Introduction

The first generation self-healing systems were based on monomeric healants capable of undergoing ring opening polymerization, e.g., endo-dicyclopentadiene, 5-ethylidiene-2-norbornene[112]. Lately, this elementary theme has been extended to encompass diverse healing chemistry, e.g., siloxane[33], epoxy-amine system[62,116] with the latter being most extensively studied in view of the associated economic factors. It is imperative to mention here that though there exist a number of successful methodologies for encapsulation of liquid epoxy, but encapsulation of the liquid hardener still remains a major challenge in view of its hydrophilic nature. To address this issue, several strategies have been adopted including encapsulation of amine in polyurea shells using reverse emulsion technique[117] and interfacial polymerisation[118]. Alternatively, hollow microballoons of urea-formaldehyde and silica have also been explored as amine containment structures[119,120]. However, these microcapsules usually exhibit low core contents, which has led researchers to explore other alternatives.

In this chapter, we have demonstrated the applicability of physical entrappment and interfacial polymerisation route towards encapsulation of water soluble amines, a process far more challenging than the one previously reported. We adopted a "physical" entrapment technique for immobilisation of triethylenetetramine hardener for potential application in self-healing applications. Surprisingly, porous siliceous substrates e.g., SBA-15, MCM-41, which are routinely employed towards enzyme immobilization[121-123] have not yet been explored for immobilizing amines. In view of their extremely high surface areas, and suitable pore sizes, these materials apparently possess excellent candidature as amine containments. The liquid amine can be immobilized within the

extended interconnected channels of SBA-15, and can be made available to the flowing epoxy in the event of crack propagation. The feasibility of such a system has also been experimentally demonstrated in this chapter.

Another technique, namely interfacial polymerisation has also been used for encapsulating triethylenetetramine (TETA) hardener in mechanically robust epoxy micro-containers. A polymeric surfactant was employed to stabilize the amine-oil suspension with an aim to modulate the particle size of microcapsules. Encapsulation of the amine was achieved by its reaction with epoxy at the interface to form a crosslinked shell, leaving behind excess amine unreacted within the core, which can subsequently serve as an epoxy curing agent for smart applications.

3.2. Experimental

3.2.1. Materials

TETA based hardener (HY 951; amine content 24 eq kg^{-1}) and aliphatic epoxy resin (Araldite CY 230; epoxy equivalent 200eq g^{-1}) were purchased from Ciba Geigy and used as received. Liquid Paraffin (Heavy) (CDH, kinematic viscosity 300 cSt) and polymeric surfactant, Hypermer A70 (Croda) was used without further purification. Conc. HCl, was obtained from CDH and poly(ethylene-alt-maleic anhydride) (EMA), tetraethyl orthosilicate (TEOS), poly(ethylene oxide)-poly(propylene oxide)-poly(ethylene oxide) ($EO_{20}PO_{70}EO_{20}$), were purchased from Sigma-Aldrich. Distilled water was used throughout the course of this work.

3.2.2. Encapsulation of amine hardener on mesoporous silica (SBA-15)

3.2.2.1. Preparation of SBA-15

SBA-15 was prepared by a polymer-templated route, a schematic of which is depicted in Figure 3.1[124]. In brief, 1.22 g of amphiphilic block-copolymer ($EO_{20}PO_{70}EO_{20}$) was dispersed in a mixture of 110 mL of 16 M HCl and 715 mL of water under stirring at 45 °C for 16 h to get a polymeric template. Subsequently, 50 mL of TEOS was added to this solution, and hydrolysis of TEOS was allowed to progress for 8 h under agitation. The precipitate was recovered by filtration and susequently washed with distilled water followed by drying at 110°C. The as synthesized product was then subjected to a controlled heating program at 1 °C min^{-1} up to 600°C.
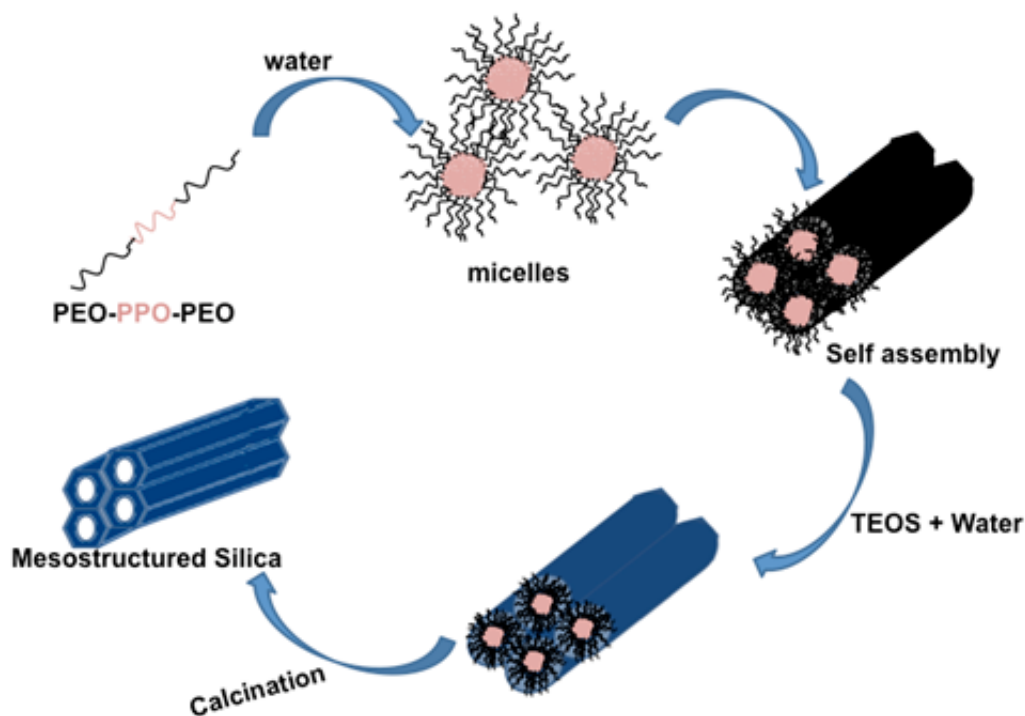
Figure 3.1: Schematic of SBA-15 preparation

3.2.2.2. Amine immobilization in mesoporous silica (SBA-15)

Liquid hardener was entrapped within the pores of SBA-15 by vacuum infiltration technique[119,120]. For the purpose of immobilization, an accurately weighed amount of SBA-15, thermally activated at 200°C for 12 h, was placed in excess triethylenetetramine under vacuum at 25 °C. The hardener infiltrated into the pores of SBA-15, which led to its settling to the bottom of the vessel. After 24 h, the sample was centrifuged at 600 rpm for 5 min, filtered and washed with ethanol to remove excess amine adhering to the surface. The ratio of entrapped amine to the initial mass of SBA-15 was estimated to quantify the extent of loading

$$Immobilized\ amine = \frac{Ef - E_0}{E_0}$$ 3.1

where E_f is the mass of amine immobilized SBA-15 and E_o is the mass of SBA-15 initially taken for immobilization.

3.2.3. Microencapsulation of amine by interfacial polymerisation

The immiscibility of triethylenetetramine in liquid paraffin was substantiated by capturing the optical images of the suspensions prepared by stirring vigorously for 5 min (1000 rpm) using a computer-interfaced microscope (Magnification 40 ×). Subsequently, crosslinked epoxy microcapsules filled with amine were prepared by interfacial polymerisation of TETA hardener with epoxy resin with the latter being added in less amounts, while keeping them suspended in liquid paraffin oil. The reaction was carried out under varying temperatures (50-75°C), stirring rates (400- 600 rpm) and altering

resin: hardener ratio (10:1.2-10:4.3). Based on stoichiometry, a epoxy: amine ratio of 10:1.2 is required, as established by calculations presented in Appendix B.

For the purpose of encapsulation, the amine hardener (5 g) was initially suspended in paraffin (100 ml) under ambient conditions while stirring at 600 rpm. The temperature of the medium was slowly increased to the desired temperature, followed by introduction of predetermined amount of epoxy resin through a syringe. The reaction was allowed to progress for extended time periods, followed by cooling to room temperature and the resultant microcapsules were filtered, washed repetitively and air dried. The ratio of mass of the microcapsules obtained to the total mass of reactants (epoxy resin and hardener) was calculated to quantify the microcapsule yield. The quantification of core content of the free flowing amine encapsulated microcapsules could be done by refluxing them in water for 12 h followed by estimation of the difference in the mass resulting due to extraction. A schematic of the entire procedure is presented in Figure 3.2.
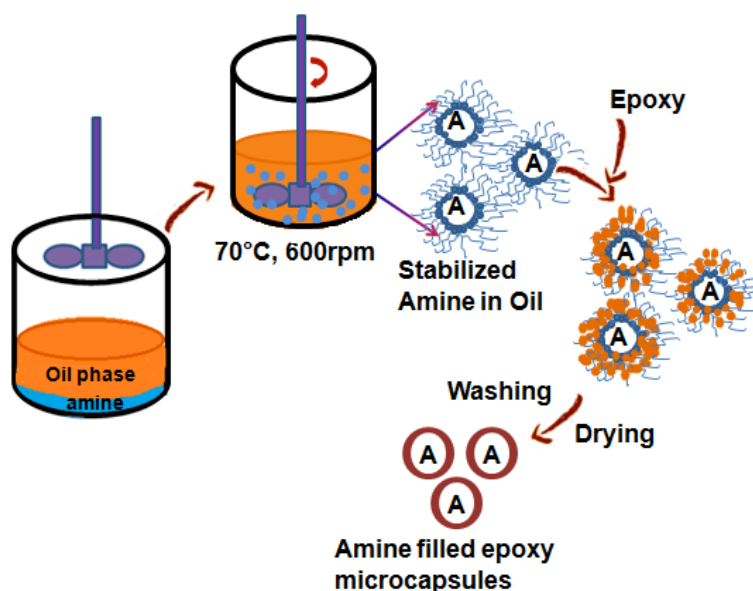
Figure 3.2: Schematic of the encapsulation process

3.3. Characterization

The surface analysis of amine encapsulated microcapsule was performed using a scanning electron microscope (Zeiss EVO MA15) under an acceleration voltage of 1 kV. Samples were prepared by placing it on aluminium stubs follwed by sputter-coating with gold (10 nm) using a sputter coater (QuorumSC7620) operating at 10-12 mA for 120 s. Average microcapsule size along with standard deviations were determined by using ImageJ software. Optical images of dispersed micro-droplets were imaged using optical microscope (MOTIC B3-223PL). A Thermoscientific FTIR (NICOLET 8700) analyser with an Attenuated Total Reflectance (ATR) crystal accessory was used for structural characterization of microcapsules by recording FTIR spectra in the wavelength range 4000 - 600 cm^{-1}. Perkin Elmer Diamond STG-DTA was used to investigate the thermal degradation behaviour of the amine filled microcapsules. For the study, requisite amount of sample mass (5.0 ± 0.5 mg) was subjected to heating in the temperature range 50-600 °C at a heating rate of 10 °C/min under N_2 atmosphere. Dynamic DSC scans were performed on a Differential Scanning Calorimeter (TA instruments Q 20) with a sample size of 10 ±2 mg. For each experiment, the samples were sealed in aluminum pans, and heated from 50 to 200°C at 10°C /min under flowing N_2 (50 mL/min). Before performing the experiments, the instrument was calibrated for temperature and enthalpy using standards (indium and zinc). The exothermic reaction was considered to be finished when the signal levelled off to the baseline. For estimation of heat of curing, the total area under the exothermic curve was determined.

3.4. Results and Discussion

3.4.1. Encapsulation of amine hardener on mesoporous silica (SBA-15)

3.4.1.1. Characterization of SBA-15

The SEM image of SBA-15 is illustrated in Figure 3.3 which clearly shows the rod like structure of the mesoporous silica.
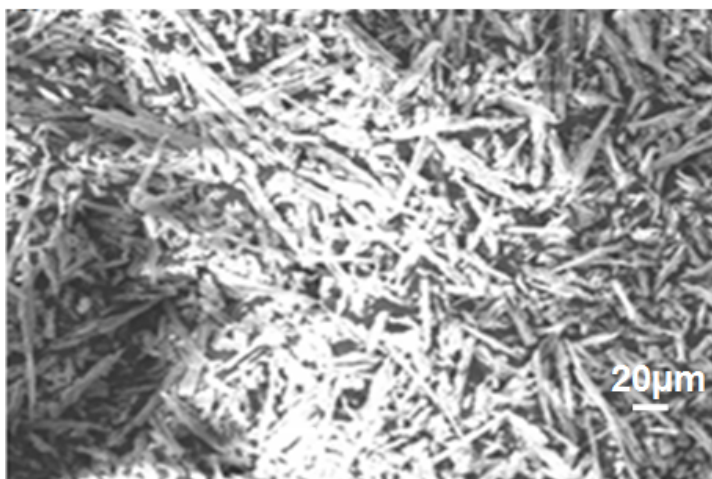
Figure 3.3: SEM image of SBA-15

To establish the mesoporous nature of SBA-15, N2 adsorption-desorption experiment was preformed and the resulting isotherm is presented in Figure 3.4. The isotherm shows a type II hysteresis loop in the N_2 adsorption-desorption isotherm (type IV) which is characteristic of mesoporous materials. From the isotherm, the surface area of SBA-15 was estimated to be 808 m^2/g. For determination of the pore size distribution Barrett–Joyner–Halenda (BJH) method was used. The desorption branch of the isotherm revealed that the SBA-15 have uniform pores with a average diameter of 5.4 nm, as presented in the inset of Figure 3.4.
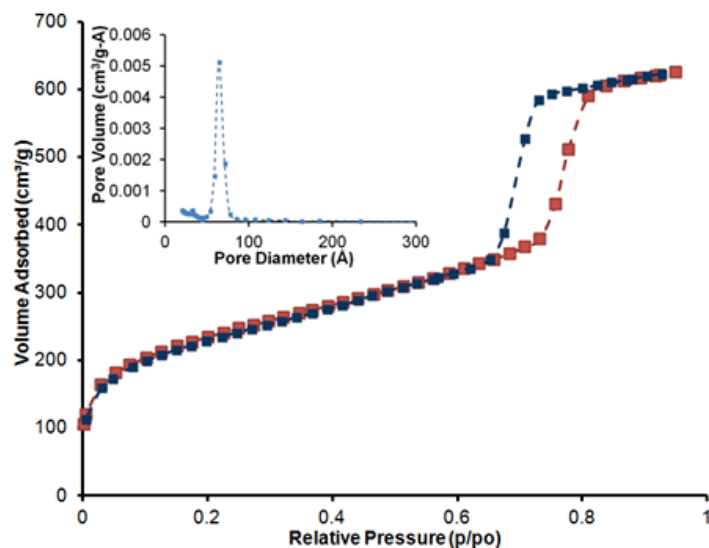
Figure 3.4: N₂ adsorption-desorption isotherm (pore size distribution in the

inset) of SBA-15

The powder X-ray diffraction (PXRD) pattern of the SBA-15 is depicted in Figure 3.5. The d (100) value (8.84 nm) established from the diffractogram matched excellently with those reported in the literature[125]. The wall thickness was calculated using d (100) value and pore diameter and it was found to be 4.8 nm.
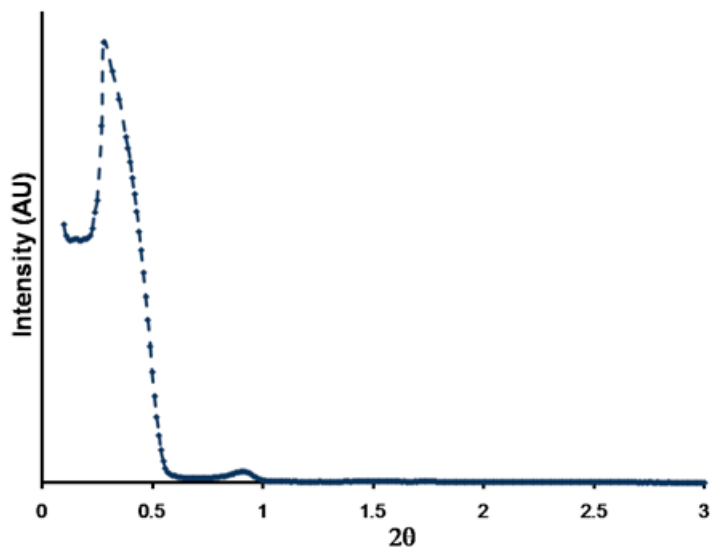
Figure 3.5: Powder X-Ray Diffraction (PXRD) pattern of SBA-15

3.4.1.2. Loading of SBA-15 with amine

Vacuum infiltration of TETA led to its entrapment within the porous structure of SBA-15 with the loading amount as high as 5 g/g. Such high loadings could be due to the presence of surface hydroxyl functionalities, which led to strong chemical interactions between the siliceous substrate and the amine, particularly hydrogen bonding and acid–base interactions. Another reason for the high loading of TETA is the dimension of both moieties. The dimensions of TETA (0.307 nm × 0.294 nm × 1.173 nm) are sufficiently in order so as to permit its diffusion within the pores of SBA-15 (pore size 5.4 nm, Figure 3.6).
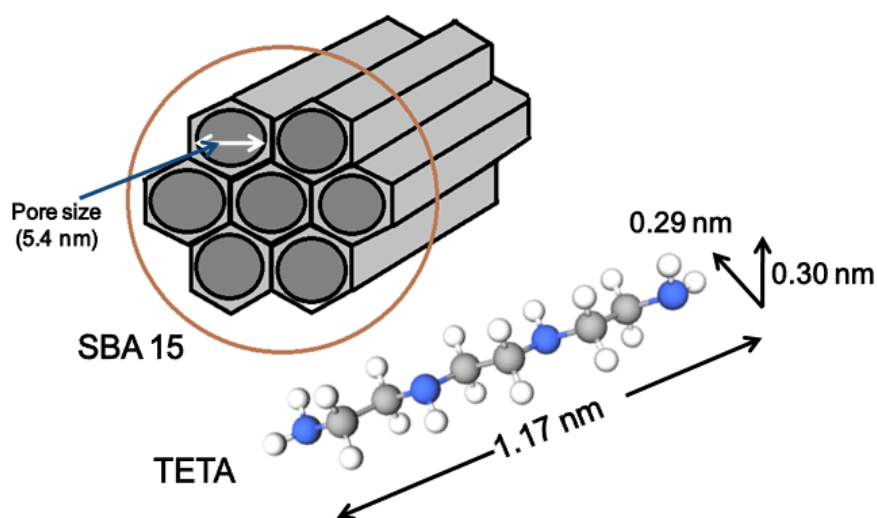
Figure 3.6: Three-dimensional representation of the substrate showing the dimensions of TETA and the pore size of SBA-15

TG traces of SBA-15, both before and after amine entrapment is shown in Figure 3.7, which confirms the high loadings revealed by gravimetric analysis. In the TG trace

72

of the neat SBA-15, ~3% w/w mass loss was observed initially (T < 150 °C), which could be due to the extraction of condensed water present within the pores of SBA-15.

The vaporization of the entrapped amine was assessed through isothermal thermogravimetric analysis. For this purpose, amine loaded silica was subjected to isothermal conditions (40, 70 and 100°C) for extended time periods and the mass loss profile with time is depicted in Figure 3.7. Interestingly, even at temperature as high as 100°C, complete loss of the amine could not be effected, with ~40% amine entrapped within the pores of the substrate.
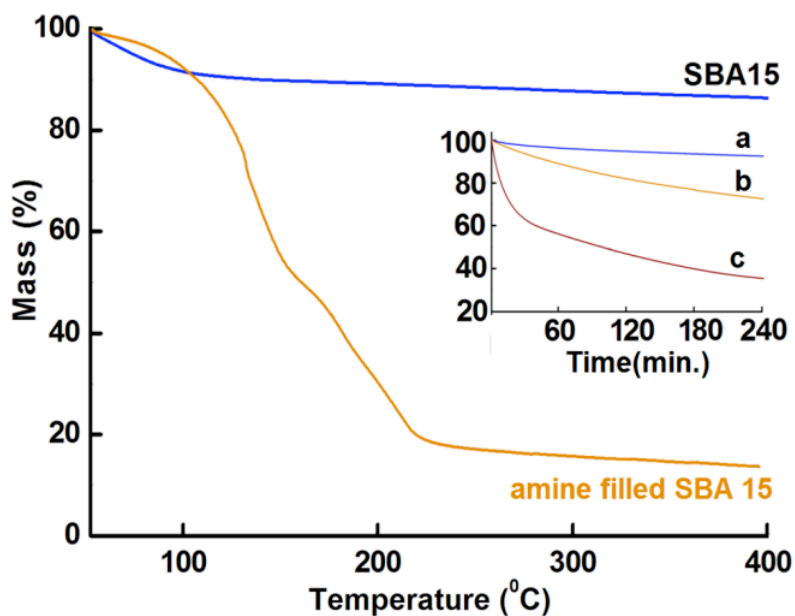
Figure 3.7: TG traces of SBA-15 and amine immobilized SBA-15. Isothermal TG traces at different temperatures a) 40°C, b) 70°C and c) 100°C

3.4.1.3. Curing studies

Silica nanoparticles have been reported to alter the curing kinetics of epoxy[124], and in view of the siliceous nature of SBA-15, its contribution towards altering the curing

behaviour of epoxy matrix was studied. For this purpose, the curing studies were performed with increasing temperature at different heating rates, and a plot of degree of conversion (α) with temperature at a representative heating rate (β = 5 °C/min) is shown in Figure 3.8. It can be clearly observed from the figure that the curing kinetics remained practically unaffected due to introduction of epoxy encapsulated urea-formaldehyde microcapsule and amine loaded SBA-15.
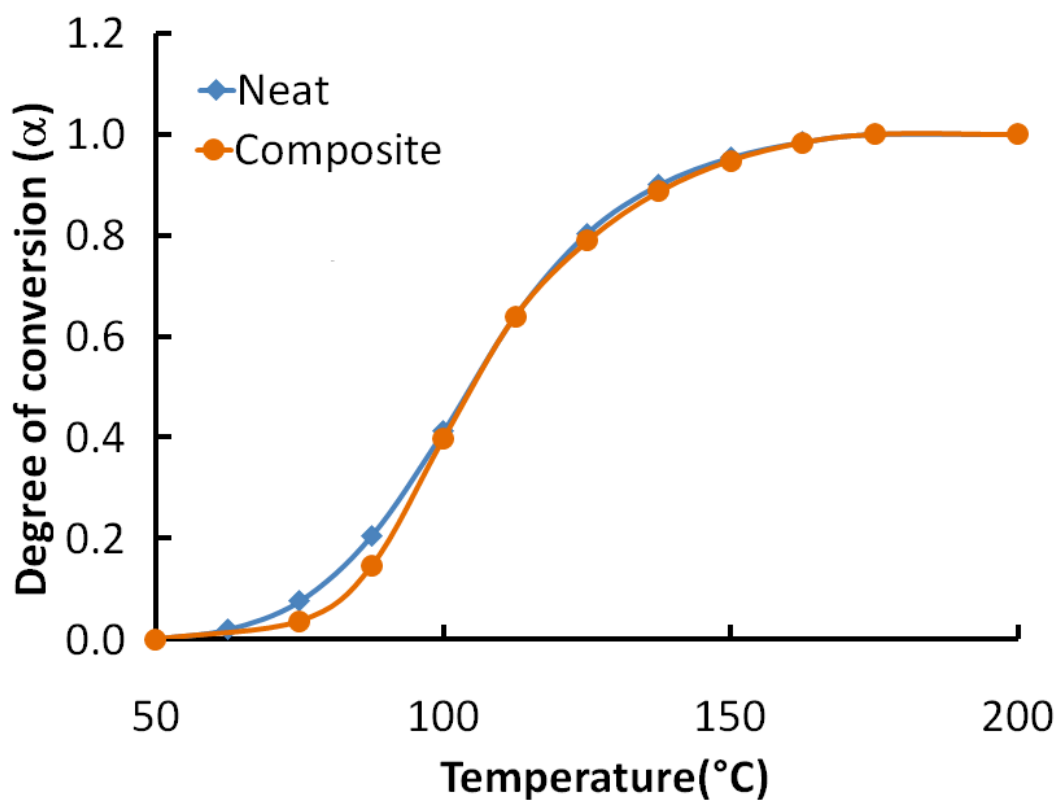
Figure 3.8: Effect of temperature on the degree of conversion of epoxy and self-healing composite (β = 5 °C/min)

3.4.1.4. Chemical reactivity of immobilized amine

Preliminary studies were carried out to investigate the chemical reactivity of amine loaded SBA-15. For this purpose, the epoxy resin and amine, in stoichiometric

ratio were transferred to a DSC pan and subjected to a controlled heating program at 10°C/min. A single exothermic peak was observed (Figure 3.9a), with an onset temperature of ~70°C. DSC studies were also performed, where the amine was derived from TETA entrapped in SBA-15 (Figure 3.9b). A third set of experiment was performed in the presence of crushed microcapsules, which served as the epoxy source and TETA loaded SBA-15 which served as the amine source (Figure 3.9c). In all the cases, similar profile was observed, with the only difference being the amount of heat liberated.
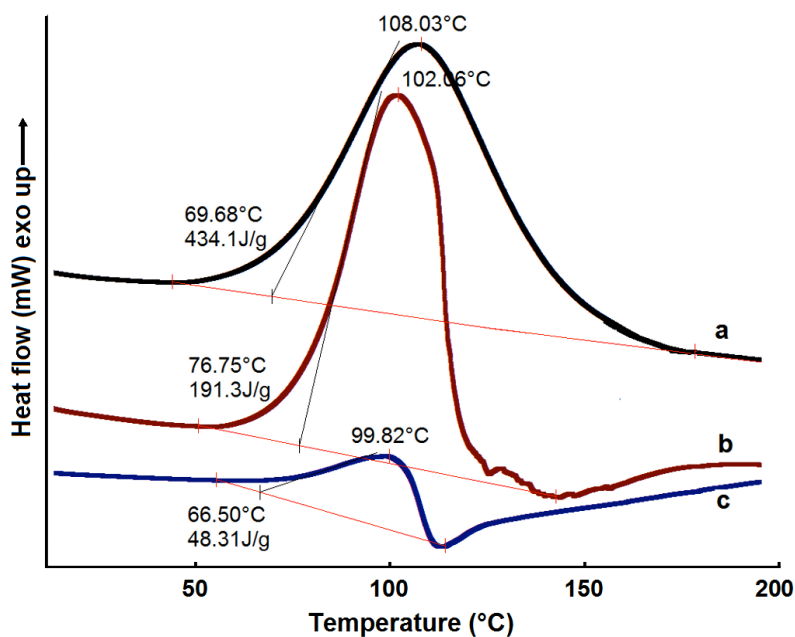
Figure 3.9: DSC trace associated with the curing behavior (a) epoxy-hardener (b)

encapsulated epoxy- hardener and (c) encapsulated epoxy- immobilized hardener

3.4.2. Microencapsulation of amine by interfacial polymerisation

The most common encapsulation technique relies on the formation of a polymeric shell around the liquid healant suspended in a dispersion medium. Unfortunately, this

encapsulation methodology cannot be applied for amine encapsulation, in view of the solubility of the amine in aqueous medium, which does not permit the formation of a stable separate phase. For encapsulation of these water soluble substances, inverse emulsion polymerisation (water in oil) is the norm[126], and this inspired us to investigate the possibility of interfacial polymerisation approach. In the present study, the water soluble amine was dispersed in paraffin medium followed by the controlled introduction of reactive epoxy in non-stoichiometric amounts, lesser than the amount required for complete curing. Amine filled microcapsules were formed by the reaction of the epoxy with TETA hardener at the paraffin-amine interface.

The use of paraffin as the dispersion medium has been well reported[126], although not for amine based systems. Theoretical predictions were made to assess the possibility of amine-paraffin phase separation. The solubility parameters of liquid paraffin, epoxy and TETA were estimated based on the group contribution models of Hoy[3]. The structures of the molecules along with detailed calculations are shown in the Appendix B. The difference in the solubility parameter of TETA and paraffin, i.e., 10.8 $cal^{1/2}$ $cm^{3/2}$ mL^{-1} and 8.25 $cal^{1/2}$ $cm^{3/2}$ mL^{-1} respectively, permits the existence of TETA as phase separated microdroplets under stirring in paraffin medium. To confirm the same, optical images of TETA-paraffin suspension were captured (Figure3.10), which clearly indicate the immiscibility of TETA in paraffin.
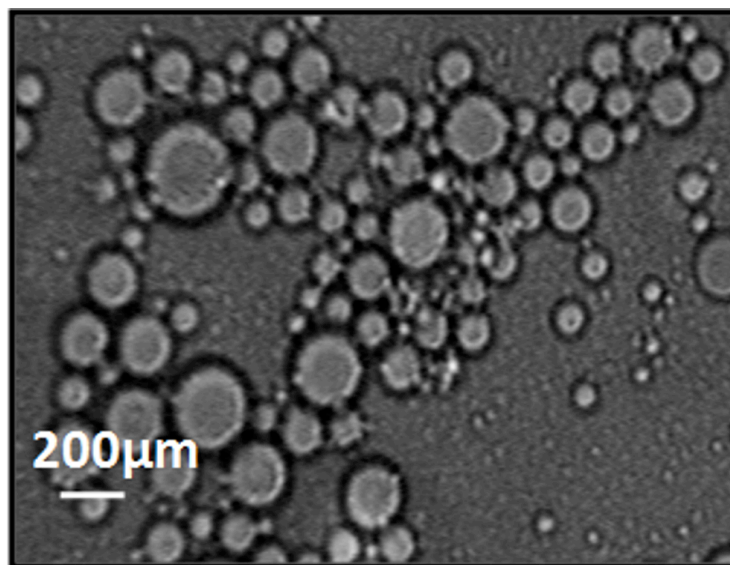
Figure 3.10: Optical image of TETA-paraffin suspension in the absence of surfactant

It is to be noted that stabilization of a water in oil (w/o) emulsion pose a challenge in encapsulation process[2,117]. In view of the same, we were not surprised to observe the instability of the amine-paraffin dispersion where the coalescence of the amine droplets was evidenced (Figure 3.10). Different surfactants were explored towards their ability of stabilising the obtained dispersion, namely Sodium dodecyl sulphate (SDS), Pluronic 61 (PEO-PPO-PEO), Polyvinyl alchol (PVA) and Hypermer A 70, the latter three being polymeric surfactants. The optical image of the dispersions obtained using surfactant are presented in Figure 3.11. It can be seen that the Hypermer A70, was most effective in stabilizing the amine droplets. The optical images showing uniformity in the size distribution is shown in Figure 3.11d
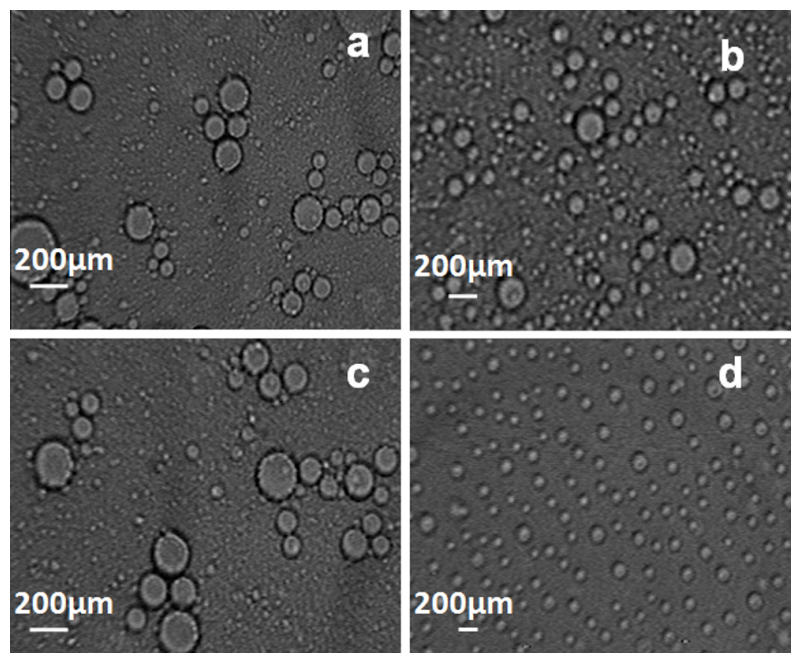
Figure 3.11: Optical image of the dispersions obtained using different surfactants a) Sodium dodecyl sulphate (SDS), b) Pluronic 61 (PEO-PPO-PEO), c) Polyvinyl alchol (PVA) and d) Hypermer A 70

Upon introduction of epoxy resin to the amine-paraffin suspension, ring opening of the oxirane functionality initiates at the oil-amine interface resulting in the formation of prepolymer around the amine droplets. The reaction then proceeds with the diffusion of both the monomers (epoxy and hardener) towards the interface, till complete exhaustion of the limiting reagent, if any. However, it is to be noted that there exists a distinct possibility of formation of microcapsules with monolithic morphology in this case as the epoxy and amine both are miscible with each other.

It is to be noted that the microcapsule dimensions are strongly dependant on the experimental parameters. Extensive studies were carried out to attain the optimal conditions, especially in terms of reaction temperature, time and stirring speed. Prior to

encapsulation experiments, the curing studies of the epoxy resin with TETA was performed using non-isothermal calorimetric studies. The influence of increasing heating rate viz. 2.5, 5, 10 and 15 °C min^{-1} on the curing behaviour of neat epoxy is presented in Figure 3.12.
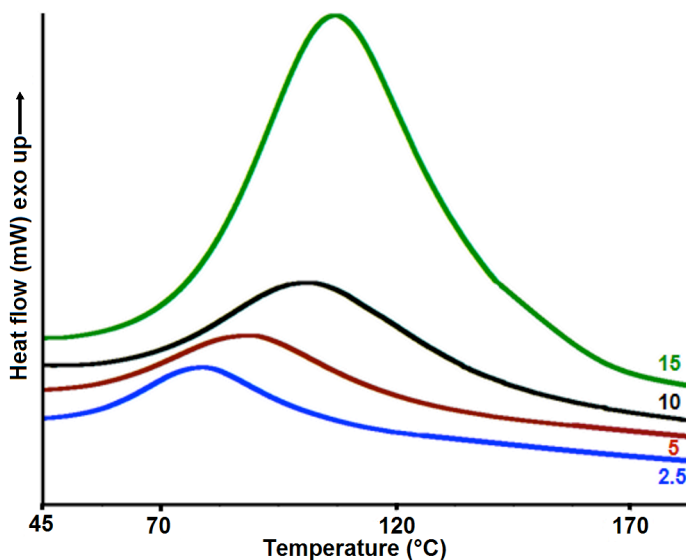
Figure 3.12: Effect of heating rate on the curing profile of epoxy

Representative thermal parameters i.e. ΔH_{cure}, T_{onset} and T_{peak} are summarised in Table 3.1.

Table 3.1: Characteristic curing parameters of epoxy

Sample	β (°C/min)	T_{onset}(°C)	T_{peak}(°C)	ΔH_{cure}(J/g)
Epoxy	2.5	54.1	79.2	320.3
	5	56.2	89.5	323.5
	10	65.3	102.3	342.8
	15	75.3	107.0	321.7
	15	74.3	101.8	307.6

79

As anticipated, increasing the heating rate (β) results into a coherent shift in the curing behaviour towards higher temperatures. Kissinger–Akahira–Sunose method[127] was applied for determination of activation energies (E_α) from the plot of $ln\left(\dfrac{\beta_i}{T^2_{\alpha,i}}\right)$ against $1/T_\alpha$.

$$ln\left(\frac{\beta_i}{T^2_{\alpha,i}}\right) = \text{Constant} - \frac{E_\alpha}{RT_{\alpha,i}} \quad\dots\dots\dots\dots\dots\dots\dots\dots\dots\dots\dots\dots\dots\dots\dots\dots\dots\dots\dots 3.2$$

Where,

β = heating rate,

T_α = temperature associated with a particular conversion (α) at the corresponding heating rate,

E_α = activation energy at a particular degree of conversion (α)

R = gas constant.

The linear plots at few representative conversions are also shown in Figure 3.13[128]. Our studies clearly reveal that the exothermic curing process can initiate under ambient conditions, however the same would require impractical durations, in view of which encapsulation studies were carried out in the temperature range 50 to 75 °C.
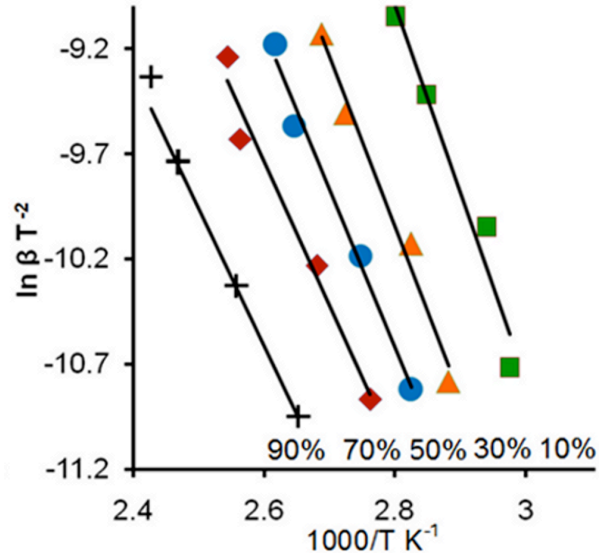
Figure 3.13: Isoconversional plots at different conversions using Kissinger-Akahira-Sunose method

The SEM images of the microspheres, prepared using stoichiometric amounts of epoxy and amine (epoxy: amine:: 10:1.2), obtained at different temperatures are depicted in Figure 3.14.
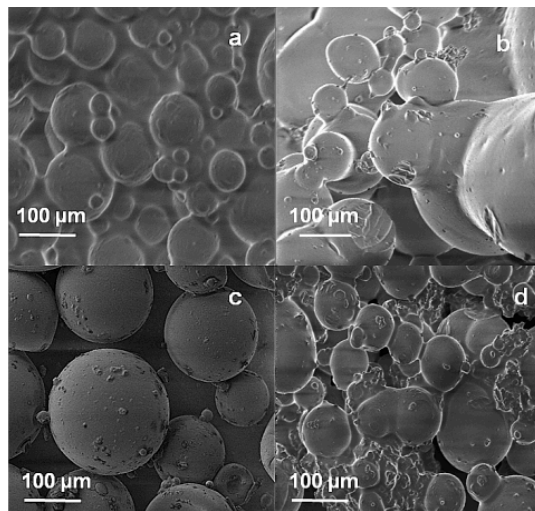
Figure 3.14: SEM images of microcapsules obtained at different temperatures a) 50 °C, b) 60°C, c) 70 °C and d) 75°C (stirring speed = 600 rpm)

81

It seems that at lower temperatures (T< 65°C) only partial curing takes place, even after extended periods (~36 h) which was evidenced by the formation of agglomerated microcapsules. As the temperature of the reaction media is raised to 70°C, the extent of curing increases, leading to the formation of free flowing microcapsules within 20 h. Increasing the temperature further led to significant vaporization of the amine, which in turn led to further imbalance in stoichiometry over extended time periods. To support this, a set of isothermal thermogravimetric experiments were performed on TETA, where the mass loss was studied with respect to time at various temperatures ranging from 50-90°C. Few representative isothermal TG traces are illustrated in Figure 3.15. As expected, mass loss increased with increase in temperature. Over extended durations, especially at higher temperatures, the vaporisation of amine is expected to lead to a imbalance of stoichiometry which in turn result in partial curing and agglomeration of the microcapsules. Therefore, exhaustive studies on the influence of other operating parameters, i.e. stirring speed and epoxy: hardener ratio were carried out while keeping the reaction medium at 70°C.
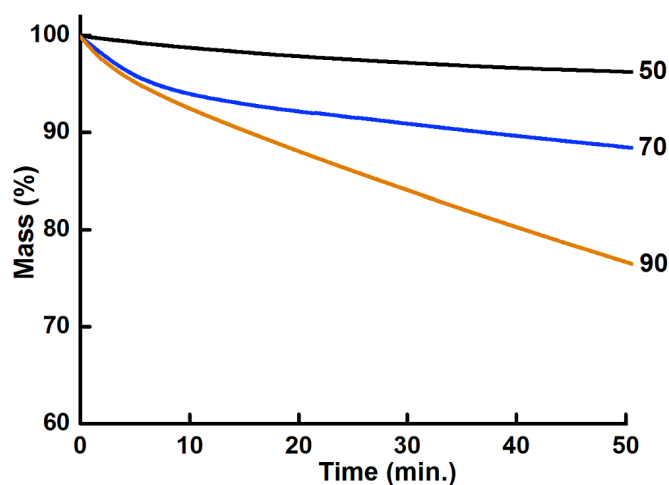
Figure 3.15: Representative isothermal TG traces of amine hardener at different temperatures

3.4.2.1. Effect of epoxy: amine on yield and core content

The effect of varying the ratio of epoxy: amine on the microcapsule yield and the amine core content is illustrated in Figure 3.16. Core content is indicative of the amount of liquid amine actually available in the microcapsules for healing purposes, which was quantified as the ratio of mass loss during water reflux to original mass of sample taken.
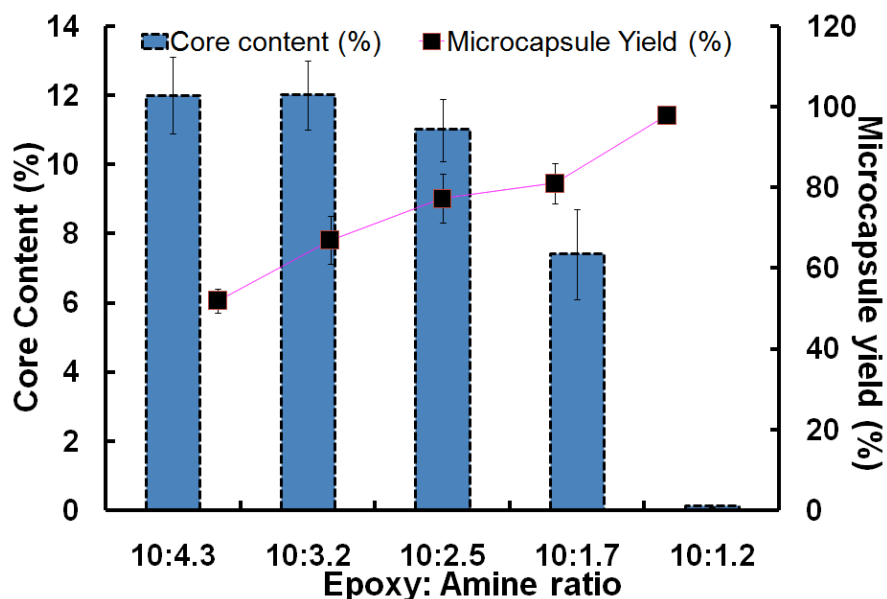
Figure 3.16: Effect of the ratio of resin: hardener on the core content and yield of amine filled microcapsules

As expected, yield of amine filled microcapsules increases with increasing epoxy concentration till the stoichiometric ratio of 10:1.2 is reached. However this increase in yield was associated with a related decrease in the core content. It is to be noted that microcapsules could not be obtained as the concentration of the epoxy: amine was reduced to less than 10:4.3. Although, obtaining larger core content is a key target of any encapsulation process, further increase in core content was not possible probably due to

the tacky nature of the microcapsules and resulted into the agglomeration of microcapsules on increasing the amine content in the feed[129].

It is to be noted that in view of the miscibility of epoxy and amine (closeness of solubility parameter), the formation of "monolithic" epoxy microcapsules is expected[130]. SEM image of a broken microcapsule is shown in Figure 3.17, which distinctly reveals the presence of microdroplets of amine dispersed within the epoxy shell.
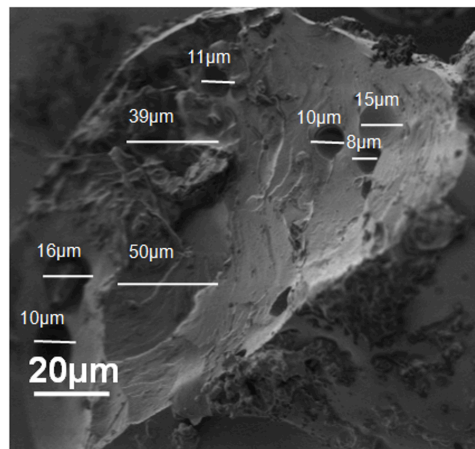
Figure 3.17: SEM image of broken microcapsule prepared using epoxy: amine ratio 10:3.2

3.4.2.2. Effect of stirring speed on morphology and particle size distribution of microcapsules

Among the experimental parameters: agitation rate particularly, determines the equilibrium between interfacial tension and shear forces of the distinct phase separated droplets[108]. The SEM micrographs of microcapsules prepared at different stirring speed are shown in Figure 3.18 and the related particle size distribution is presented in Figure 3.19. As predicted, with increase in stirring speed, the average particle size shifted

towards lower dimensions, which could be due to the extensive shearing of the large droplets into smaller microdroplets. It was noticed that free flowing microcapsules could not be produced upon reducing the stirring speeds to below 400 rpm. Increasing the stirring speed beyond 600 rpm was anticipated to result into the formation of relatively lower diameter microcapsules and thus finding less practical applicability. Under most effective reactions conditions, i.e., stirring speed of 400 rpm, reaction temperature of 70°C and resin: hardener ratio 10:3.2, spherical microcapsules could be obtained.
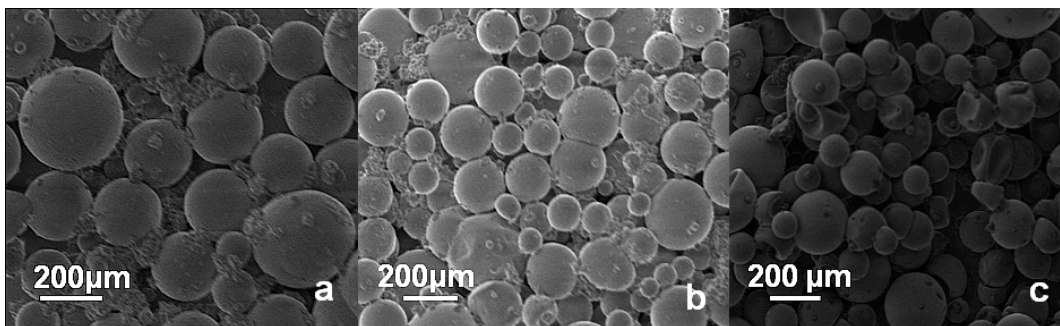
Figure 3.18: Effect of stirring speed on the size of amine filled microcapsules a) 400 b) 500 and c) 600 rpm
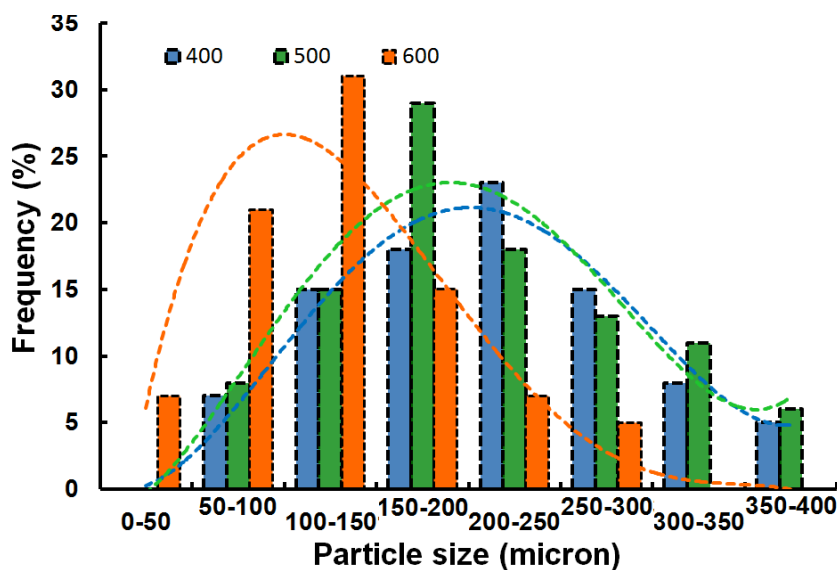
Figure 3.19: Effect of stirring speed on the particle size distribution of amine filled microcapsules

The TG traces of the liquid amine hardener and amine filled microcapsules is depicted in Figure 3.20. Derivative of TG (DTG) is also presented in the same figure. As evident, liquid amine undergoes oxidative degradation at T ~210 °C. As expected, the encapsulation of the amine led the degradation temperature to shift towards higher temperature (T_{onset} = 400°C).
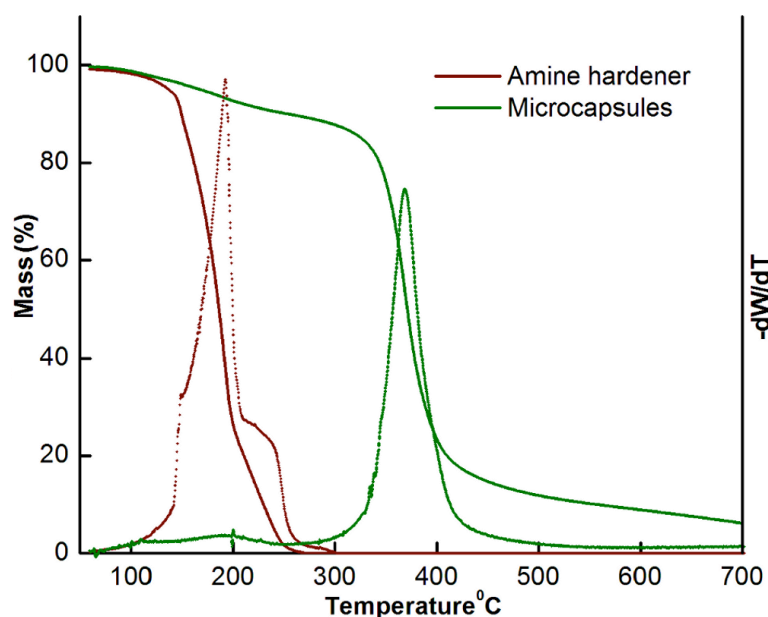
Figure 3.20: TG-DTG traces of a) TETA hardener b) TETA encapsulated microcapsules. DTG traces are also presented as dotted lines

The FTIR spectra of microcapsules and liquid epoxy resin are shown in Figure 3.21. As evident from the figure, the reaction of epoxy with amine resulted in the reduction of the intensity of the absorption band due to –C-O-C (oxirane ring : 915 cm^{-1})[131]. It was not possible to determine epoxy content in microcapsules prepared using 10:3.2 epoxy: hardener concentration.
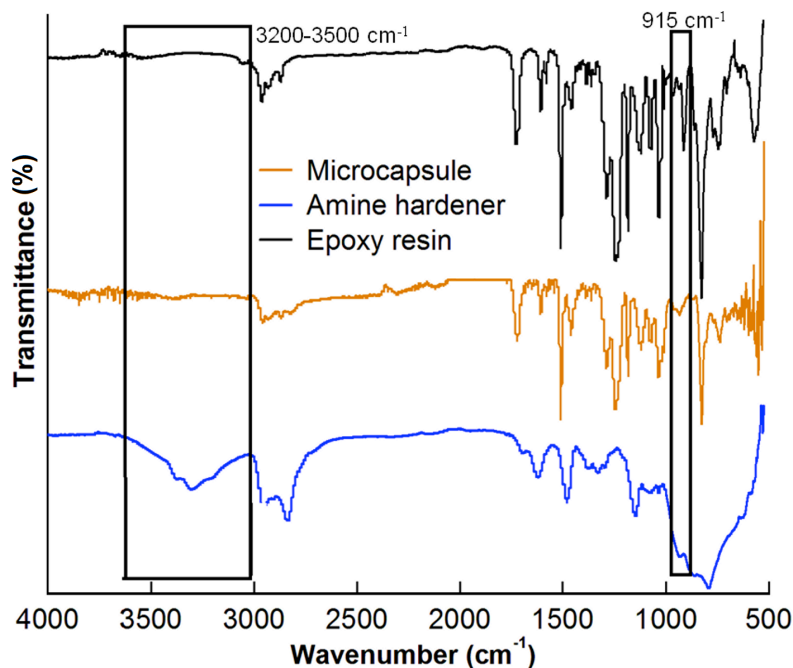
Figure 3.21: FTIR spectra of amine hardener, epoxy resin and amine filled microcapsules prepared using epoxy: hardener ::10:3.2

3.4.2.3. Stability of the microcapsules

The stability of the microcapsules was established by placing them under isothermal conditions (30 °C) over extended time periods (3 months) and estimating the mass loss as a function of time. Negligible mass loss was observed over the entire period which clearly highlights the potential of these microcapsules for practical applications.

3.4.2.4. Reactivity of the encapsulated amine

Curing behaviour of epoxy resin with encapsulated amine was performed using non-isothermal calorimetry. The slurry formed after rupture of the microcapsules with epoxy was placed in a DSC pan and subjected to a controlled temperature program and the resulting curing profile is shown in Figure 3.22. The profile of neat epoxy-amine is

also presented for reference. It is apparent from the figure that the ring opening reaction shifts towards higher temperature in the case of microcapsule-epoxy slurry. In addition, the degree of heat evolved was ~12-13 % of the heat associated with the curing of neat epoxy: an observation in accordance with the core content determined gravimetrically.
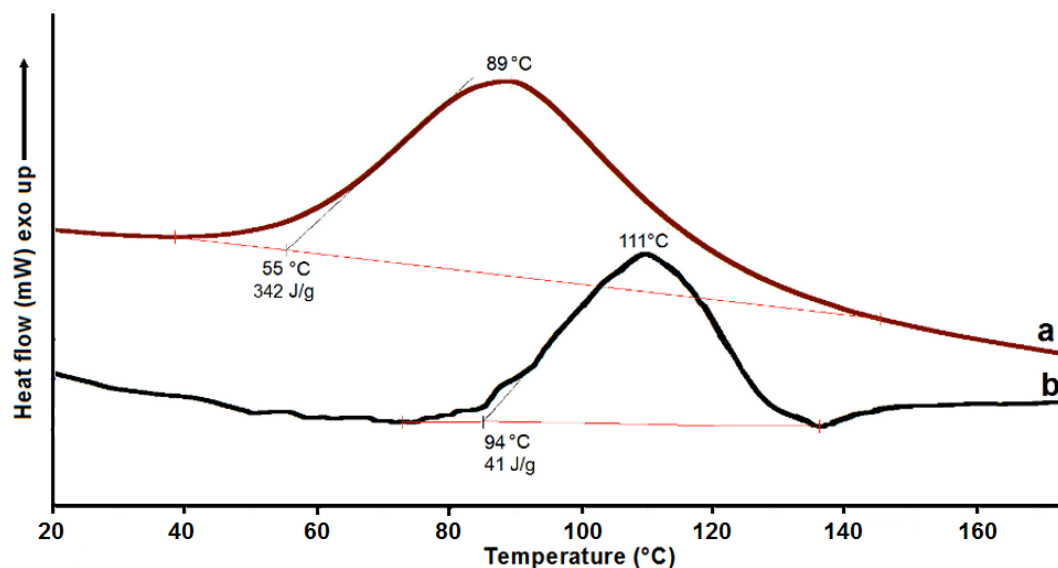
Figure 3.22: Curing profile of epoxy with a) amine, b) crushed amine

encapsulated microcapsules

To summarise, in this chapter we have discussed the encapsulation of amine through interfacial polymerisation as well as through physical entrapment method. The core content of the microcapsule prepared using interfacial method was significantly low. Physical entrapment of amine in SBA-15 led to high loadings. The detailed self healing studies using the will be discussed in subsequent chapter.

CHAPTER IV

CURING KINETICS OF SELF HEALING EPOXY THERMOSETS

4.1. Introduction

In view of the enormous potential of self healingmaterials in the future, it is very significant to be aware of the effect of these self-healing additives on the curing kinetics, as this process governs the polymer morphology[132-134]. Majority of studies in this area deal with improving the efficiency of self healing process, but surprisingly very few studies deal with the kinetics of the curing process of such compositions[135,136]. Of particular importance is to establish the role of common encapsulating materials, e.g. urea-formaldehyde which possess 2° amino functionalities capable of reacting with epoxy resins. In fact, urea-formaldehyde resin has also been used as an effective hardener for epoxy resins, nonetheless the curing can be effected only at higher loadings (100 phr)[137]. Moreover, the silica nanoparticles have also been reported to alter the curing kinetics of epoxy[138], and in view of the siliceous nature of SBA-15, its contribution towards altering the curing behaviour of epoxy needs to be studied.

This chapter discusses the influence of self-healing fillers on the curing kinetics of a cycloaliphatic epoxy resin with triethylenetetramine hardener. For this, non-isothermal DSC experiments have been performed and empirical methodologies are used to predict the kinetics of the curing.

4.2. Experimental

Differential Scanning Calorimeter (TA instruments Q 20) was used for calorimetric studies. The resin and TETA were mixed at a stoichiometric epoxide/amine ratio (100:12) at low temperatures (0-5°C). For non-isothermal DSC scans, the requisite amount of samples (10 ±2 mg) were sealed in aluminum pans, and subjected to

programmed heating from 0 to 250°C at four different heating rates 2.5, 5, 10 and 15 °C/min. During the curing process, nitrogen gas was purged at the flow rate of 50 ml/min to minimize oxidation of the sample. Isothermal runs were performed on selected samples at 60°C for 1h. Before performing the experiments, the temperature and enthalpy calibration of the instrument was carried out using standard indium and zinc. The area under the exothermic curve was estimated for quantification of the heat of curing. The amount of microcapsule loading in epoxy was selected based on reported previous studies[60], and the amount of loaded SBA-15 was decided on the basis of stoichiometric requirements. The samples have been labelled to as EP followed by the concentration of UF microcapsules (% w/w) and concentration of mesoporous silica, e.g., epoxy containing 10% UF microcapsules and 2 % mesoporous silica isreferred to as EP10UF2MS and neat epoxy is referred to as EP throughout the text.

4.3. Results and Discussion

Epoxy encapsulated UF microcapsules were prepared by dispersion polymerisation technique, as discussed in Chapter II and TETA hardener (HY 951) was immobilized within the pores of mesoporous silica (SBA-15) as discussed in Chapter III. Self healing epoxy composites were prepared by dispersing known amount of the microcapsules and immobilized amine hardener in epoxy resin and the curing behaviour of the compositions was studied by non-isothermal calorimetry to understand the effect of self healing fillers on the curing kinetics of epoxy resin.

90

4.3.1. Curing behaviour

The DSC traces of neat epoxy and microcapsule filled compositions under a representative heating rate (5 °C/min) are presented in Figure 4.1. It is apparent from the figure that all the compositions exhibit a single exothermic peak, which is characteristic of the epoxy curing process. The presence of UF microcapsules or amine immobilised SBA-15 did not seem to affect the curing process appreciably and all the compositions exhibit similar T_{onset} (onset cure temperature) and T_{peak} (peak cure temperature) values.
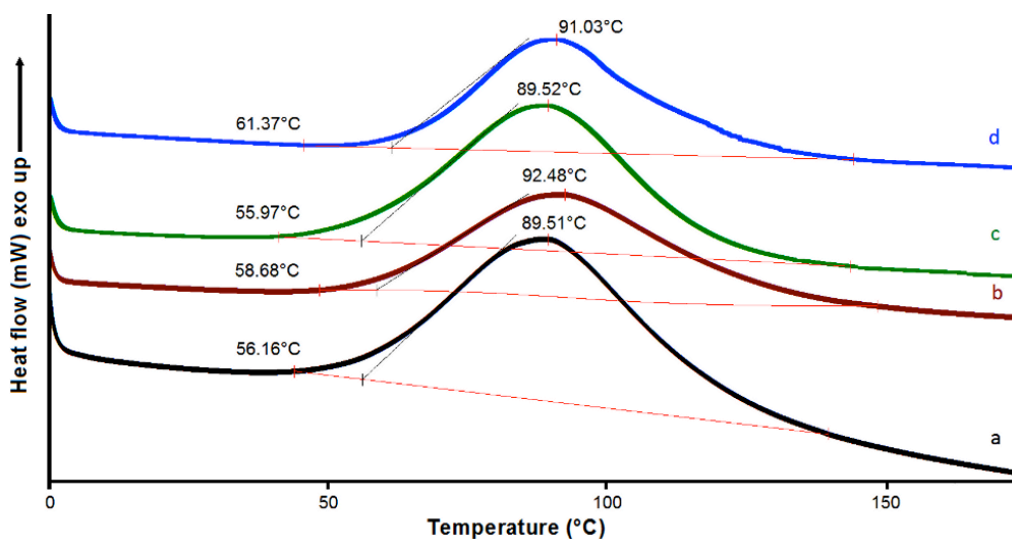
Figure 4.1: Curing profile of epoxy based compositions a) Neat epoxy, b) EP5UF, c) EP10UF, d) EP10UF2MS

DSC thermograms of a representative epoxy composite at various heating rates viz. 2.5, 5, 10 and 15 °C/min are depicted in Figure 4.2. As anticipated, an ordered shift in the traces towards higher temperatures was observed while increasing the heating rate (β). The curing reaction, being primarily a kinetic event, is a function of both time and temperature. When subjected to a higher rate of heating, the reactants receive lesser time

to respond at any specific temperature and thus lead to the noticed phenomenon. The characteristic thermal parameters, i.e., ΔH_{cure}, T_{onset} and T_{peak} are summarized in Table 4.1.
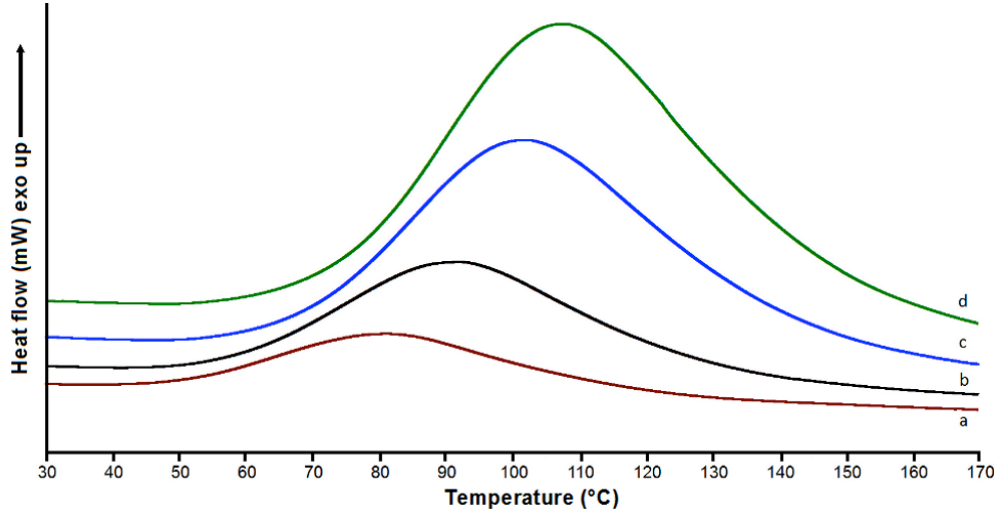
Figure 4.2: Effect of rate of heating on the DSC traces of microcapsule filled epoxy (EP5UF) a) 2.5, b) 5, c) 10 and d) 15 °C/min

Table 4.1: Curing parameters of epoxy and its composites

Sample	β (°C/min)	T_{onset} (°C)	T_{peak} (°C)	ΔH_{cure} (J/g)
Epoxy	2.5	54.1	79.2	320.3
	5	56.2	89.5	323.5
	10	65.3	102.3	342.8
	15	75.3	107.0	321.7
EP5UF	2.5	49.9	81.6	305.6
	5	58.7	92.5	311.3
	10	67.2	102.4	309.4
	15	72.5	108.1	294.3
EP10UF	2.5	48.6	80.3	319.5
	5	55.9	89.5	328.2
	10	66.3	104.9	327.8
	15	82.7	112.1	321.6
EP10UF2MS	2.5	56.4	81.4	300.5
	5	61.4	91.0	310.2
	10	69.2	101.3	312.8
	15	74.3	101.8	307.6

It is apparent from the data that there is no significant effect on the heat of curing (ΔH_{cure}) due to increasing rates of heating. The degree of conversion (α), at any particular temperature (T_a) was estimated as the ratio of the areas under the exothermic DSC peak:

$$\alpha = \frac{\Delta H_{T_\alpha}}{\Delta H_{cure}} \dots\dots\dots\dots\dots\dots\dots\dots\dots\dots\dots\dots\dots\dots\dots\dots\dots\dots\dots\dots\dots 4.1$$

where

ΔH_{T_α} = heat of reaction of moderately cured samples (till temperature T_a)

ΔH_{cure} = total heat of curing reaction

The increase in the extent of conversion (α) with temperature for EP, and EP5UF, EP10UF and EP10UF2MS at a particular rate of heating (5 °C/min) is shown in Figure 4.3. It can be seen that increase in microcapsule loading does not affect the curing behavior significantally as far as the degree of conversion is concerned.
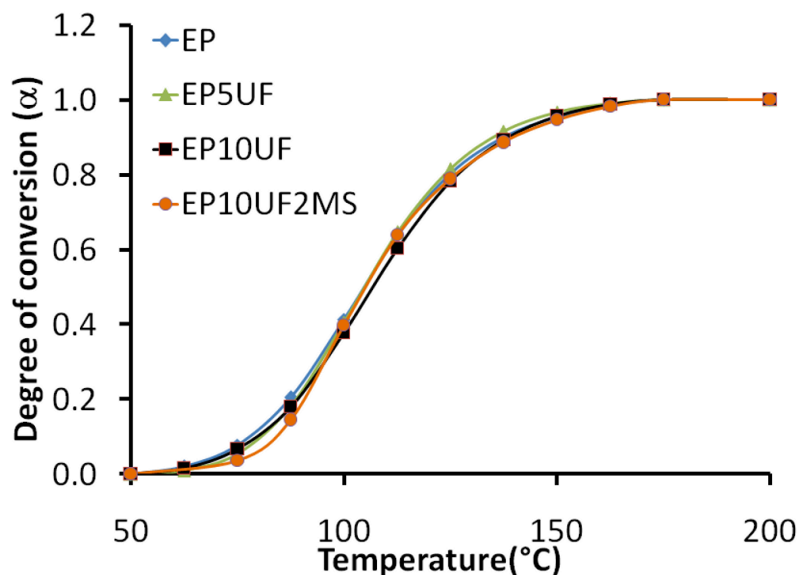
Figure 4.3: Effect of temperature on the degree of conversion of epoxy as well as self-healing composition (β = 5°C/min)

As expected[139], with increase in heating rates, the traces shift towards higher temperatures, as is apparent from the data presented in Figure 4.4.
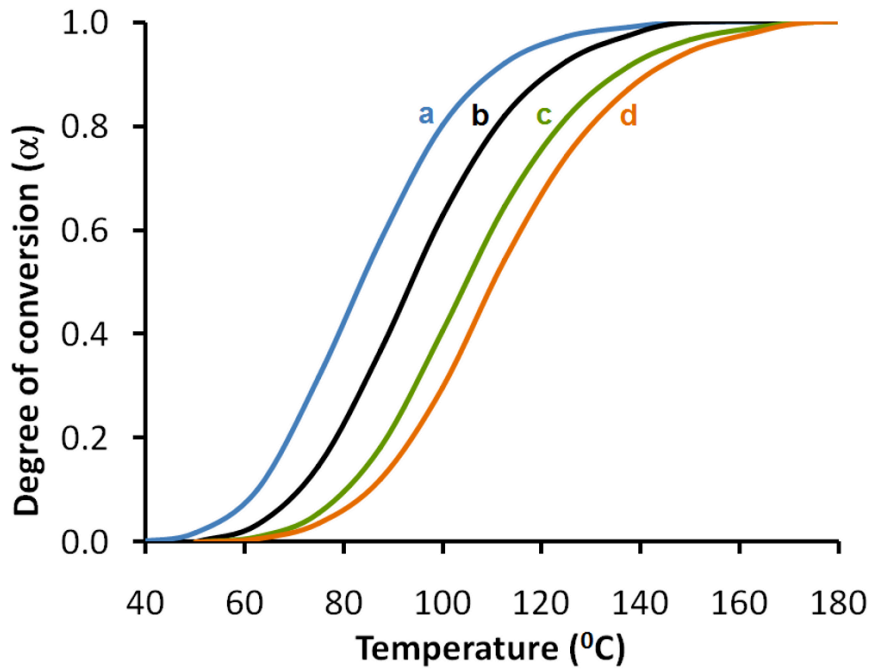
Figure 4.4: Effect of temperature and heating rate on the extent of epoxy curing a) 2.5, b) 5, c) 10 and d) 15 °C/min

4.3.2. Isoconversion methods

The rate of a reaction is primarily dependent on three major variables: temperature (T); extent of conversion (α) and pressure (P) as follows:

$$\frac{d\alpha}{dt} = k(T)f(\alpha)h(P) \dots\dots\dots 4.2$$

The pressure term, ($h(P)$) is generally ignored for a majority of kinetics methods, and the reaction rate can be rewritten as.

$$\frac{d\alpha}{dt} = k(T)f(\alpha) \dots\dots\dots 4.3$$

Generally, the temperature dependent term ($k(T)$) is assumed to exhibit Arrhenius type dependency

$$k(T) = A\exp\left(-\frac{E}{RT}\right) \dots\dots\dots\dots\dots\dots\dots\dots\dots\dots\dots\dots\dots\dots\dots\dots 4.4$$

Combining Eq. 4.3 and Eq. 4.4:

$$\frac{d\alpha}{dt} = A\exp\left(-\frac{E_\alpha}{RT}\right)f(\alpha) \dots\dots\dots\dots\dots\dots\dots\dots\dots\dots\dots\dots\dots 4.5$$

Where,

$f(\alpha)$ = model of reaction,

T (K) = absolute temperature,

A (s^{-1}) = pre-exponential factor,

E_a(kJ mol^{-1}) = activation energy

R = universal gas constant

For different heating rates (β_i), Friedman method gives Eq. 4.6 at specified α:

$$\ln\left(\frac{d\alpha}{dt}\right)_\alpha = \ln\left(A_\alpha f(\alpha)\right) - \frac{E_\alpha}{RT_\alpha} \dots\dots\dots\dots\dots\dots\dots\dots\dots\dots\dots 4.6$$

By substituting a new parameter $C_f(\alpha) = ln(A_\alpha f(\alpha))$, Eq. 4.6 may be written as

$$\ln\left(\frac{d\alpha}{dt}\right)_{\alpha i} = C_f(\alpha) - \frac{E_\alpha}{RT_{\alpha i}} \dots\dots\dots\dots\dots\dots\dots\dots\dots\dots\dots\dots 4.7$$

At a particular conversion (α); parameters$\left(\dfrac{d\alpha}{dt}\right)_{\alpha i}$ and $T_{\alpha,i}$ values can be determined experimentally at different heating rates. This can be used to arrive at E_α and $C_f(\alpha)$ from the plot of $\ln\left(\dfrac{d\alpha}{dt}\right)_{\alpha i}$ vs $\dfrac{1}{T_{\alpha,i}}$ for at least three heating rates.

Alternatively, Kissinger–Akahira–Sunose method can be used for determination of activation energy $(E_a)^{[127]}$. For this method, $\left(\dfrac{d\alpha}{dt}\right)$ can be equated to $\dfrac{d(\alpha)}{dT}\beta$, and Eq. 4.5 can be further rearranged.

$$\frac{d\alpha}{f(\alpha)} = \frac{A}{\beta}\exp\left(-\frac{E_\alpha}{RT}\right)dT \dotfill 4.8$$

Integrating Eq. 4.8 and introducing Doyle's approximation[140], leads to

$$g(\alpha) = \int_0^\alpha \frac{d(\alpha)}{f(\alpha)} = \frac{A}{\beta}\int_{T_0}^T \exp\frac{E}{RT}dT \cong \frac{ART^2}{\beta E}\exp\left(-\frac{E}{RT}\right) \dotfill 4.9$$

By taking logarithm of Eq. 4.9 the following equation can be derived for various heating rates under a constant degree of conversion α,

$$\ln\left(\frac{\beta}{T_\alpha^2}\right) = \ln\left(\frac{RA_\alpha}{E_\alpha g(\alpha)}\right) - \frac{E_\alpha}{RT_\alpha} \dotfill 4.10$$

which can further be written as

$$\ln\left(\frac{\beta}{T_\alpha^2}\right) = C_k - \frac{E_\alpha}{RT_\alpha} \dotfill 4.11$$

where $C_k(\alpha) = \ln\left(\dfrac{RA_\alpha}{E_\alpha g(\alpha)}\right)$

Hence, E_a can be obtained using the KAS method from the slope of $ln\left(\dfrac{\beta_i}{T_{\alpha,i}^2}\right)$

against $\dfrac{1}{T_\alpha}$.

The linear plots (at selected conversions) used to arrive at the activation energy using KAS and Friedman method for EP5UF is depicted in Figure 4.5.
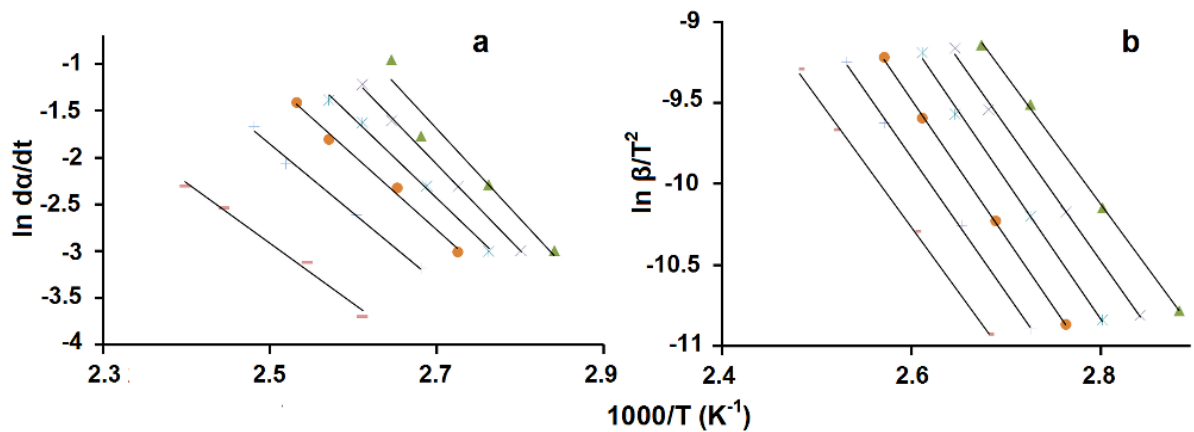
Figure 4.5: Isoconversional plot for a representative composition (EP5UF) at different degree of conversions (a) Friedman method (b) Kissinger-Akahira-Sunose method

The difference in activation energy with variation of degree of conversion *(α)* for neat epoxy and the self healing compositions, as determined by both the methods is presented in Figure 4.6.
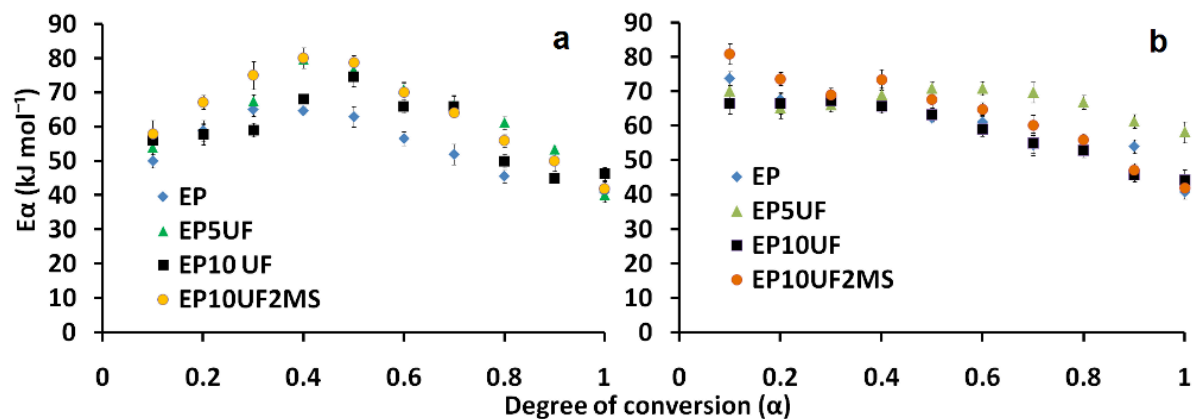
Figure 4.6: Variation of activation energy (E_a) with degree of conversion (a) Friedman method (b) Kissinger-Akahira-Sunose method

It can be seen that the range of activation energies for all the composition is between 40 and 90 kJ/mol, irrespective of the model employed. In general, a progressive decrease in the activation energies was observed. It was interesting to note that the introduction of UF fillers or amine loaded SBA-15 does not affect the activation energy–conversion profile. The reaction of the epoxy groups with amine leads to formation of a solid polymer[141], which is expected to switch the kinetically controlled process to one that of diffusion controlled, thereby expected to lead to an increase in the E_a. However, the exothermic curing process, results in an increase in the energy of the reactants, indirectly lowering the energy required to cross the energy barrier. In view of the higher reactivity of the 1° amine groups with epoxy, this reaction predominates in the early stages of curing ($\alpha < 0.6$). This is followed by the reaction with 2° amines, which continues until $\alpha = 0.8$[142]. Other reactions like homopolymerisation of epoxide groups and etherification have also been reported toward the end of the curing process, i.e., at higher temperatures. It is the combined result of all of the above processes that manifests

in the observed E_a - α profile. Interestingly, the curing of epoxy has been effected by UF at higher loadings (50:50)[137], however our results suggests, that although 2° amino groups are available on the surface of UF resin, these do not directly participate in the curing reaction, as the primary amino groups in the liquid TETA are more easily accessible.

4.3.3. Prediction of dynamic cure of self-healing epoxy resin

In view of its simplicity, KAS method was applied to predict the curing behavior of self-healing epoxy composites, when cured under different heating rates. For this purpose, $C_k(\alpha)$ and E_a derived from the data obtained at $\beta = 2.5, 5, 10$ and 15 °C/min were replaced into Eq. 4.11 to quantify the temperature related with different values of α under a particular heating rate (β). The model was further validated by performing dynamic DSC run at 30 °C/min, and the experimental data are shown in the Figure 4.7.
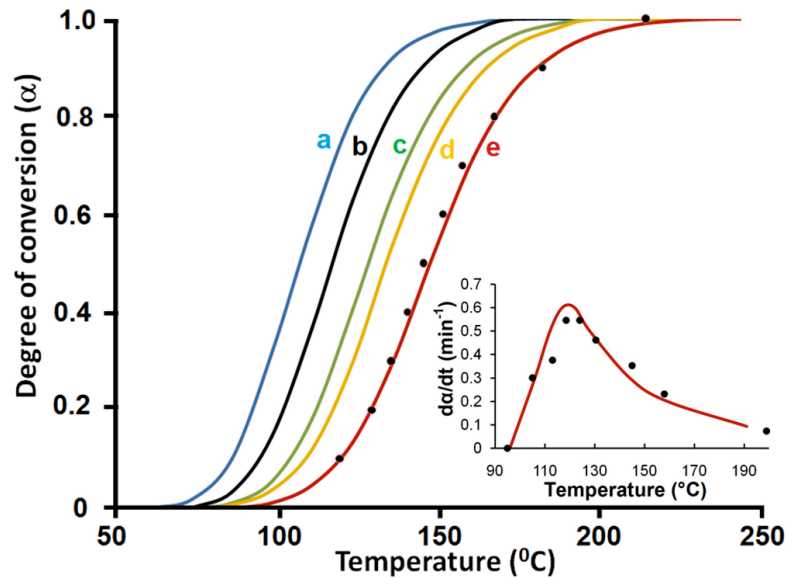
Figure 4.7: Experimentally determined curing degree at different heating rates (a) 2.5, (b) 5, (c) 10, (d) 15 and (e) 30°C/min. Inset shows the experimental and KAS predicted reaction rate at 30 °C/min

The variation of rate of reaction $\left(\dfrac{d\alpha}{dt}\right)$ with temperature for the specified rate of heating (30°C/min) is shown in the inset of Figure 4.7. It can be observed that the predicted values are in close agreement with the data obtained experimentally.

To establish the potential of the proposed self-healing system comprising of epoxy encapsulated UF microcapsules and amine immobilised on SBA-15, curing was also effected on a mixture containing stoichiometric amounts of crushed microcapsules and SBA-15. The resulting calorimetric trace is presented in Figure 4.8.
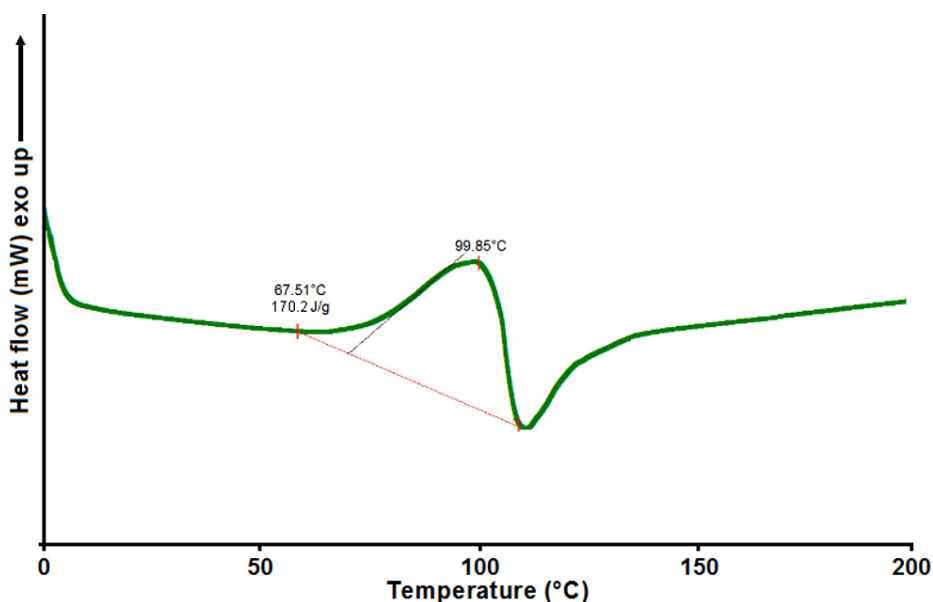
Figure 4.8: Curing profile of epoxy encapsulated UF microcapsules with SBA-15

immobilized amine hardener

The profile exhibits a single exothermic peak, characteristic of curing process connected with the epoxy released from the microcapsules with the hardener. However, the heat of curing (ΔH_{cure}) was found to be 170.2 J/g as compared to 342.8 J/g for neat epoxy under similar experimental conditions (10°C/min), which relates well with the core content of the microcapsules.

100

To summarise, in this chapter, we discuss the effect of self-healing fillers on the curing behavior of epoxy resins. Non-isothermal DSC studies reveal that although secondary amine groups are accessible on the surface of urea-formaldehyde, the same did not interfere with the curing behavior of the base resin.

EFFECT OF MICROCAPSULE ADDITION ON MECHANICAL PROPERTIES AND HEALING EFFICIENCY

5.1. Introduction

Due to the fragile nature of microcapsules, their inclusion into the polymeric resin is anticipated to result in substantial deterioration in the mechanical properties[143]. However, to the best of our knowledge, no systematic investigations have been performed to quantify the effect of shell wall material of microcapsule on the mechanical behaviour of self healing compositions. Majority of literature in this area deal primarily with improving the repairing efficiency,[93] but studies on the influence of microcapsule introduction on other mechanical properties under dynamic mode and quasi-static mode are rather scarce. Here, in this chapter we have quantified the influence of microcapsules on the quasi-static and dynamic properties of a representative cycloaliphatic epoxy resin. Healant encapsulated microcapsules with different shell walls (UF and polystyrene) were prepared by dispersion polymerization and solvent evaporation techniques, and dispersed within the epoxy matrix to prepare self healing formulations. The effect of inclusion of these microcapsules on the mechanical properties of cured composite was studied under both dynamic as well as quasi-static modes. Our studies revealed that the mechanical properties of the resulting composite decreased due to microcapsule introduction, the extent of which was found to increase proportionally with increasing loading. Certain level of improvement in the fracture toughness of the base matrix was observed, which was attributed to underlying mechanisms like crack bowing, crack pinning, microcracking and crack path deflection as evidenced by fractographic investigations.

In this chapter, we also discuss experimental studies to validate the model for predicting the amount of healant, which is released in the crack plane in the event of microcapsule rupture. The model has been discussed in detail in Chapter II. For the experiments, healant encapsulated microcapsules, with varied microstructure along with

suitable catalysts were included in the formulation to obtain mendable compositions. The healing efficiency has been estimated in terms of the ratio of impact strength both before and after healing.

5.2. Experimental

5.2.1. Materials

Epoxy monomer, (Araldite CY 230; epoxy equivalent 200 eq/g) as well as triethylenetetramine(TETA) based curing agent (HY 951; amine content 32 eq/kg) was received from Ciba Geigy, and used without any further purification. Methyl Imidazole (2-MeImidH) (97%, Sigma Aldrich), $CuCl_2.\ 2H_2O$ and $NiCl_2.\ 6H_2O$ (A.R., CDH) were used without further purification. The materials along with the methodology adopted for the preparation of healant encapsulated microcapsules and immobilised amine has been discussed in previous chapters (Epoxy encapsulated in UF and polystyrene microcapsules: Chapter II, immobilised amine on SBA-15: Chapter III). Distilled water was used throughout the course of this work.

5.2.2. Preparation of metal imidazole complexes

Metal imidazole complexes (latent hardener for epoxy) were synthesised as per the method reported in the literature[144]. For the preparation of copper complex, $CuCl_2.2H_2O$ (5.6 g) and 2-MeImidH (10.7 g) were separately dissolved in 25 ml and 12.5 ml of methanol to maintain a molar ratio of salt: 2-MeIm of 1.5 to 2.0. The solutions were mixed and stirred for 3-4 h, following which, acetone (75 ml) was added, which led to the precipitation of the coloured complex. Thus formed precipitate was filtered, washed with acetone and dried under vacumm at 70 °C for 12h. For the preparation of

nickel complex, [Ni(2-Me-ImidH)$_4$Cl]Cl, the same methodology was adopted with NiCl$_2$.6H$_2$O as the metal ion source.

5.2.3. Preparation of epoxy-microcapsule composites

Epoxy-microcapsule composites containing different amounts of either urea-formaldehyde or polystyrene microcapsules (5-30 % w/w) were prepared by curing of epoxy with amine hardener at room temperature. The general methodology adopted for the epoxy-microcapsule composites preparation is presented in Figure 5.1.
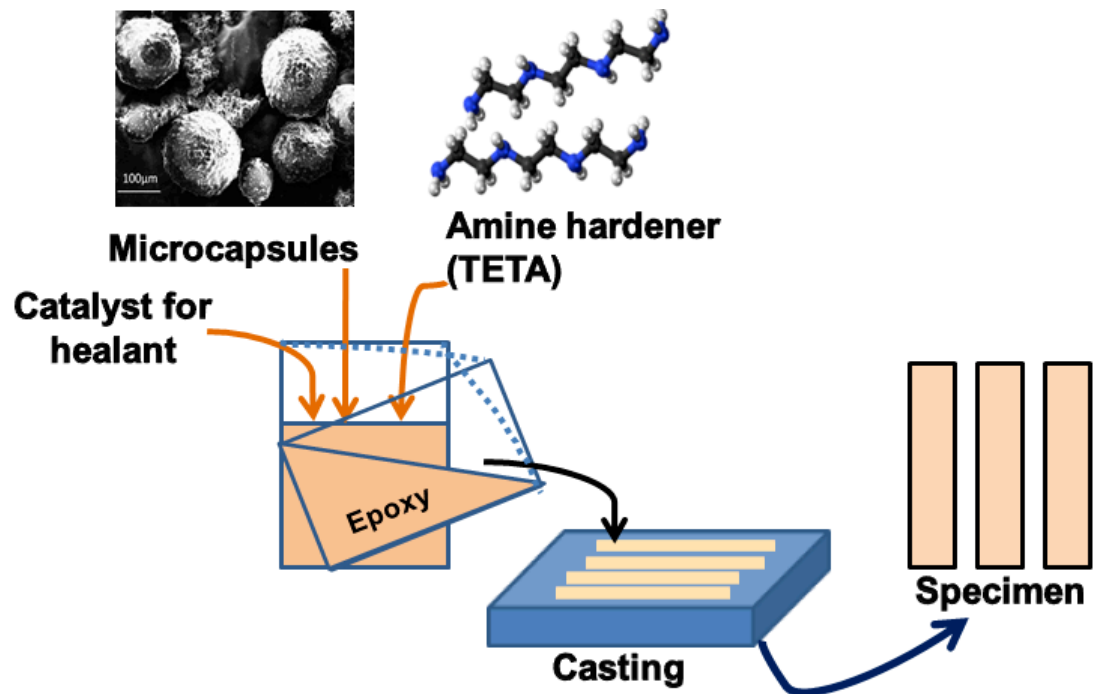
Figure 5.1: Pictorial representation of composite specimen preparation

The healant encapsulated microcapsules were first strained through a 40-100 mesh (BSS), to get microcapsules of desired particle dimensions (150-425 μm), which were subsequently homogenized in the epoxy resin with the aid of ultrasonicator. Requisite amount of TETA hardener was added, and then the dispersion was degassed

under vacuum and poured into greased silicone moulds. The curing reaction was allowed to progress at 30 °C for 24 h. Neat epoxy samples were also prepared using similar methodology, which will be designated as EP in the subsequent text. The compositional details of all the composites prepared along with their sample designations are depicted in Table 5.1. All the cured epoxy formulations containing microcapsules will be designated as EpxZ where x relates to the amount of loading (% w/w) and Z refers to type of microcapsules (UF or PS) used for the preparation of composite. For example, a cured epoxy composition containing 5% (w/w) UF microcapsules can be designated as EP5UF.

Table 5.1: Details of sample designation and composition

Sample Designation	Amount (g)		
	Epoxy resin	Hardener	Microcapsule
EP	100	13	-
EP3Z	100	13	3.4
EP5Z	100	13	5.6
EP10Z	100	13	11.3
EP15Z	100	13	16.9

Z refers to the type of microcapsule (UF: Urea-formaldehyde, PS: Polystyrene)

5.2.4. Determination of healing efficiency

Healing efficiency (η) was determined as the ratio of impact strength of healed and virgin sample as per the reported literature[79]. For this, first the specimens of requisite dimensions (63.5 mm × 12.5 mm ×3.0 mm) for the Izod impact testing were prepared as per ASTM D 256. The impact strength was estimated using an impact strength testing

machine (International Equipments, India). Post-fracture, both the faces were aligned and gently pressed by hand for a few seconds and clamped to ensure close contact for a period of 6 h under specified conditions. A representative photograph of clamped sample is presented in Figure 5.2. The healed specimens were re-subjected to impact tests after 24 h and the self healing efficiency was quantified as per eq 5.1:

$$\eta = \frac{\sigma_{Healed}}{\sigma_{virgin}} \dots\dots\dots\dots\dots\dots\dots\dots\dots\dots\dots\dots\dots\dots\dots\dots\dots\dots\dots\dots\dots\dots\dots\dots\dots 5.1$$

where

σ_{Healed} = Impact strength of healed sample

σ_{virgin} = Impact strength of virgin sample

A control set of experiments was performed with an aim to quantify the intrinsic healing ability of neat epoxy in the absence of microcapsules. For this purpose, fractured epoxy samples were exposed to conditions mentioned previously and the impact strength both before and after fracture was compared. Five identical specimens were tested for each composition and the average of all the results along with the standard deviation have been reported.
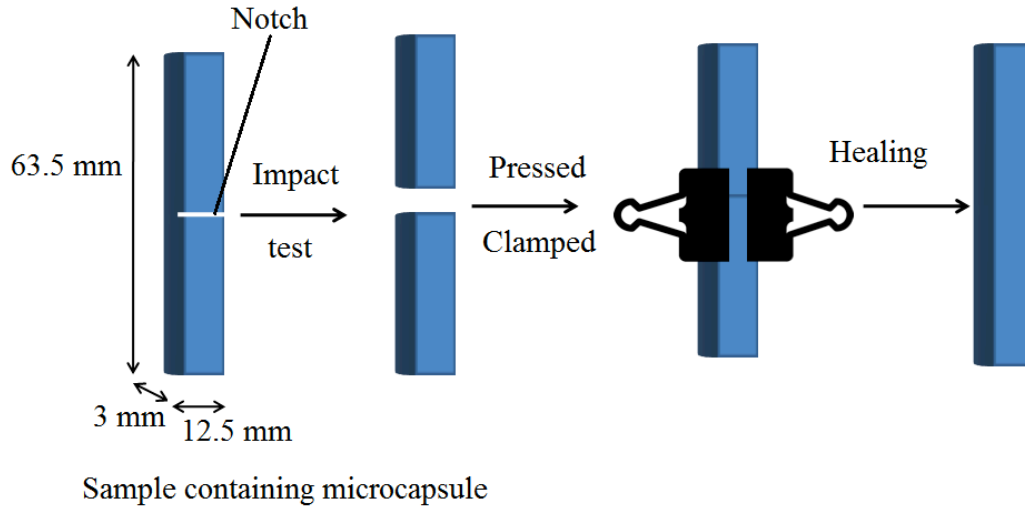
Figure 5.2: Schematic procedure adopted for evaluating healing efficiency

5.3. Characterisation

The mechanical properties of the specimen were determined under quasi-static loading as per ASTM method D638 using a Universal Testing System (International equipments) at ambient temperature. For tensile testing, the dog-bone shaped specimens 165 mm long, 3 mm thick, and 13 mm wide along the centre of the casting, were used. The specimens were subjected to a cross head speed of 50 mm/min. The flexural testing was performed under three point single edge notch bending mode using the same instrument. For this testing, specimens with required dimensions (127 mm length x 12.5 mm width x 3.5 mm thickness and 3 mm notch) were prepared and then subjected to a deformation rate of 2 mm/min under a span length of 60 mm. The mode I critical stress intensity factor (K_{IC}) of the samples was determined as per equation 5.2[145]:

$$K_{Ic} = \frac{3 \times P \times L \times a^{1/2}}{2 \times B \times w^2} Y(\frac{a}{w}) \dots\dots\dots\dots\dots\dots\dots\dots\dots\dots\dots\dots\dots\dots\dots\dots 5.2$$

where,

P = load at break

L = span length

B = thickness of sample

The geometry factor, $Y(\frac{a}{w})$ is calculated using the formula 5.3,

$$Y(\frac{a}{w}) = 1.93 - 3.07 \times (\frac{a}{w}) + 14.53 \times (\frac{a}{w})^2 - 25.11 \times (\frac{a}{w})^3 + 25.8 \times (\frac{a}{w})^4 \ldots\ldots\ldots\ldots\ldots\ldots 5.3$$

where

a = notch length

w = width of the sample

The fracture energy (G_{IC}) was estimated using the following equation

$$G_{IC} = \frac{K_{IC}^2 (1 - v^2)}{E} \ldots\ldots\ldots\ldots\ldots\ldots\ldots\ldots\ldots\ldots\ldots\ldots\ldots\ldots\ldots\ldots\ldots\ldots\ldots\ldots\ldots\ldots 5.4$$

where

K_{IC} = mode I critical stress intensity factor

E = flexural modulus of the polymer

v = Poisson's ratio of epoxy $(0.35)^{146}$

Five identical specimens were tested for each composition and the average of all the results along with the standard deviation have been reported. The fractured surface of the composite was studied with thw aid of a Scanning Electron Microscope (Zeiss EVO MA15) under a 20 kV acceleration voltage. For this, fractured specimens were placed on

aluminium stubs and coated with gold (10 nm) using a sputter coater (Quorum-SC7620) operating at 10-12 mA for 120 s.

5.4. Results and Discussion

5.4.1. Epoxy-microcapsule composites

Epoxy-microcapsule composites were obtained by dispersing varying quantities of either polystyrene or urea-formaldehyde microcapsules in epoxy resin using aid of ultrasonicator, subsequently curing under ambient conditions. The DSC traces of neat epoxy and microcapsule filled compositions under a programmed heating rate (5 °C/min) are illustrated in Figure 5.3. It is evident from the figure that all the compositions exhibit a single peak, which is characteristic of the exothermic nature of the curing process. Interestingly, the presence of UF or PS microcapsules did not affect the curing process appreciably and all the compositions exhibit similar onset cure temperature (T_{onset}) and peak cure temperature (T_{peak}) values.
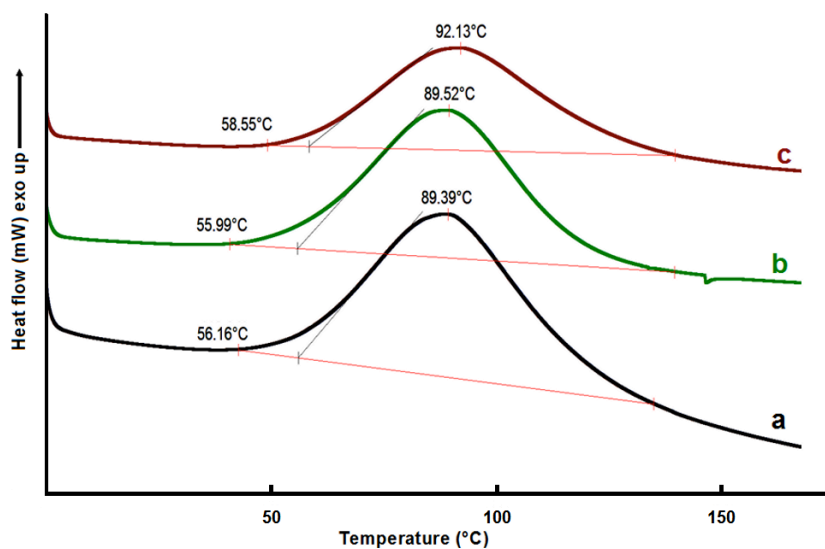
Figure 5.3: Curing profile of epoxy based compositions a) Neat epoxy, b) EP10UF, c) EP10PS

109

The TG trace of neat epoxy and epoxy-microcapsule composites with different microcapsules is illustrated in Figure 5.4. It can be observed that the incorporation of epoxy encapsulated microcapsules reults into a slight reduction in the thermal stability of the base polymer. Temperature corresponding to 5% mass loss ($T_{5\%}$) of epoxy (220 °C) reduced to 175 °C and 147 °C due to introduction of PS and UF microcapsules (15% w/w) respectively. Also, in comparison to neat epoxy, the char content of the microcapsule loaded samples is slightly lower, which can be attributed to the presence of uncured resin within the microcapsules.
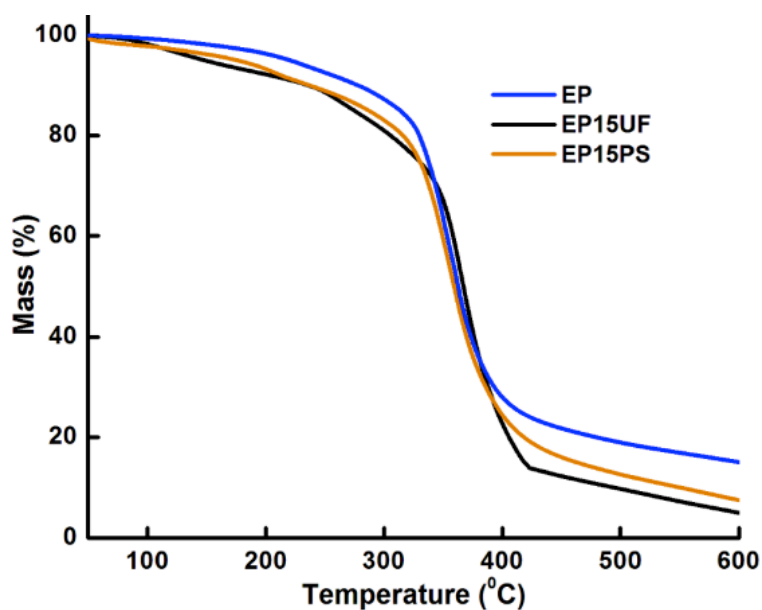
Figure 5.4: TG traces of composites formed with microcapsules

The FTIR spectrum of cured epoxy and composites prepared in the presence of microcapsules is presented in Figure 5.5. As expected an increased absorption in the region above 3300-3000 cm^{-1} is observed in the composites, which could be attributed to

the absorption due to hydroxyl, imino, amino and C-H (ar.) groups present in the shell wall of the microcapsules.
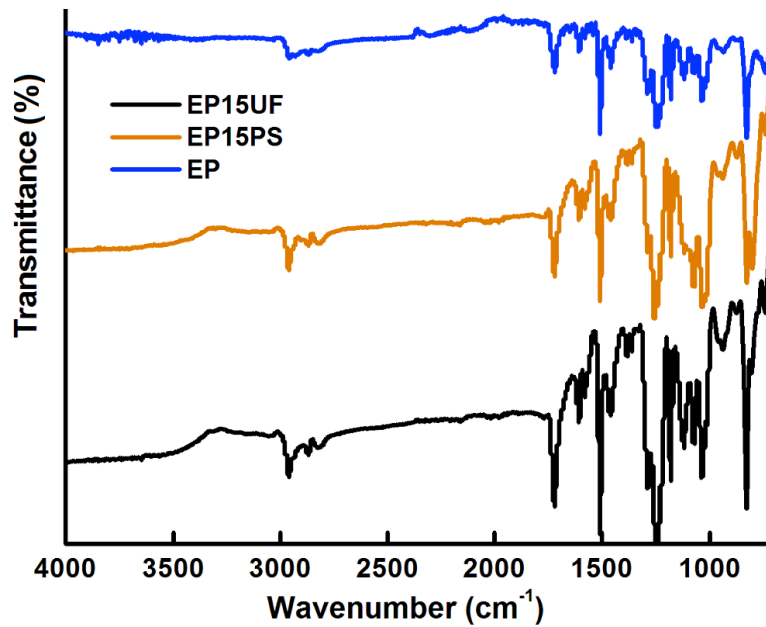
Figure 5.5: FTIR spectra of epoxy and its composites

Figure 5.6 and 5.7 presents the difference in mechanical properties of the epoxy-microcapsule composite as a function of loading (%, w/w) of UF and PS microcapsules. It is evident from the figure that the introduction of microcapsules resulted in a reduction in both the tensile strength as well as tensile modulus and the decrease is proportional to the amount of microcapsule loading. Due to the fragile nature of microcapsules, their contribution to the load bearing capability of epoxy seems to be practically negligible, which can be used to explain the observed reduction in the mechanical properties of the resultant epoxy-microcapsule composites. Our results clearly show that the shell of the microcapsule does not play any key role in defining the mechanical properties, which were found to depend only on the extent of loading.
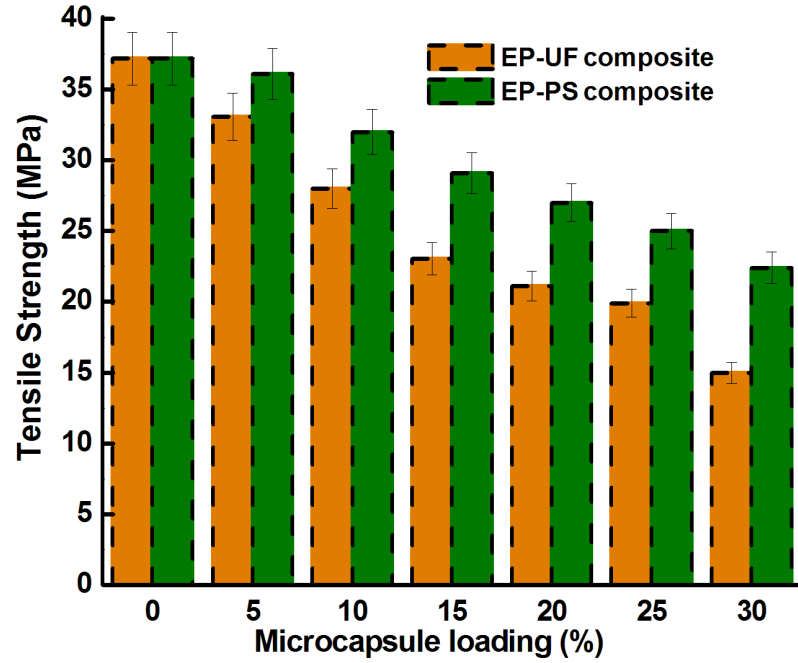
Figure 5.6: Effect of introduction of UF and PS microcapssules on the tensile strength of epoxy
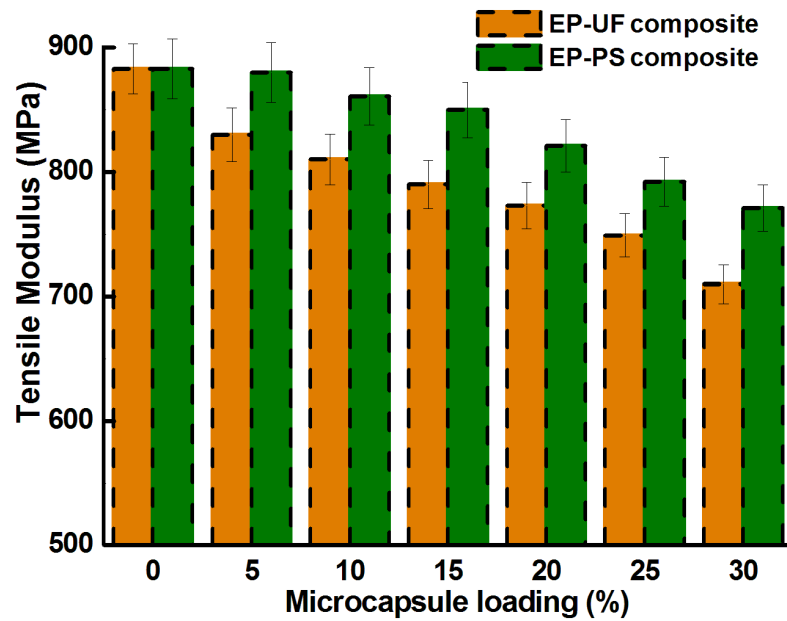
Figure 5.7: Effect of incorporation of UF and PS microcapsules on the tensile modulus of epoxy

The introduction of microcapsules also resulted into a proportional decrease in the impact strength of epoxy, as is apparent from data shown in Figure 5.8. The impact strength decreased from 24±1.5 (for neat resin) to 12 ±1 J/m after inclusion of 15% (w/w) UF microcapsules. Similar extent of impact strength lowering has been reported previously on epoxy samples containing healant encapsulated UF microcapsules[147]. The extent of decrease was relatively less pronounced in the case of PS microcapsules, where for a similar loading the impact strength was ~18 J/m.
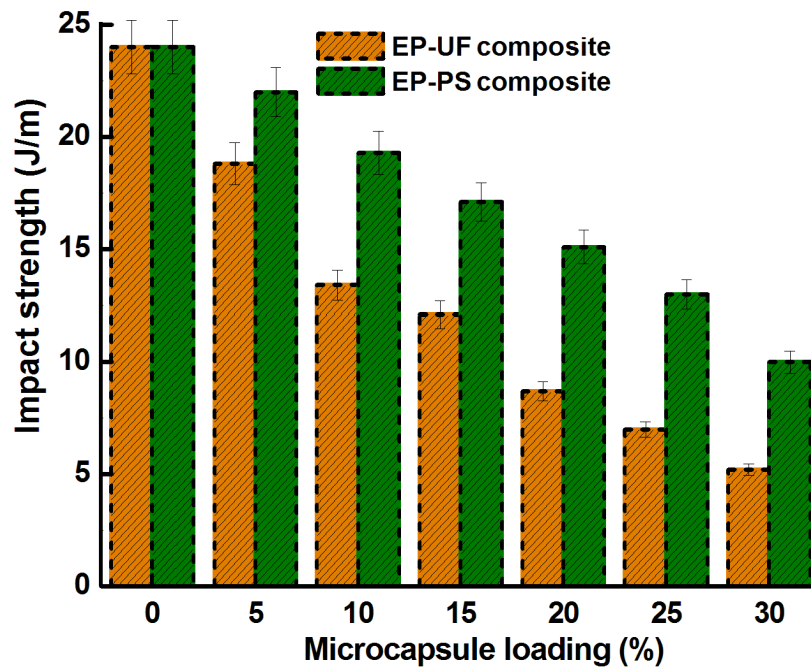
Figure 5.8: Decrease in impact strength of epoxy due to inclusion of UF and

PS microcapsules

The stress-strain response of the epoxy-microcapsule compositions in flexural mode is depicted in Figure 5.9. Interestingly, the composites exhibited slightly higher strength and modulus, when compared with that of the unmodified epoxy. The mechanical

response of notched specimens is also presented in Figure 5.9 (Inset), which evidently shows the detrimental effect of notch on the flexural strength, which can be due to concentration of stress from the smaller cross-sectional area of notch.

Single edge notch bend (SENB) geometry is the most common mode for quantification of fracture toughness of polymeric samples[145], however for self healing compositions, the use of TDCB geometry has been preferred[77]. In the present study, we have determined the toughness, using the SENB geometry in order to allow comparison with our previous studies[148,149].
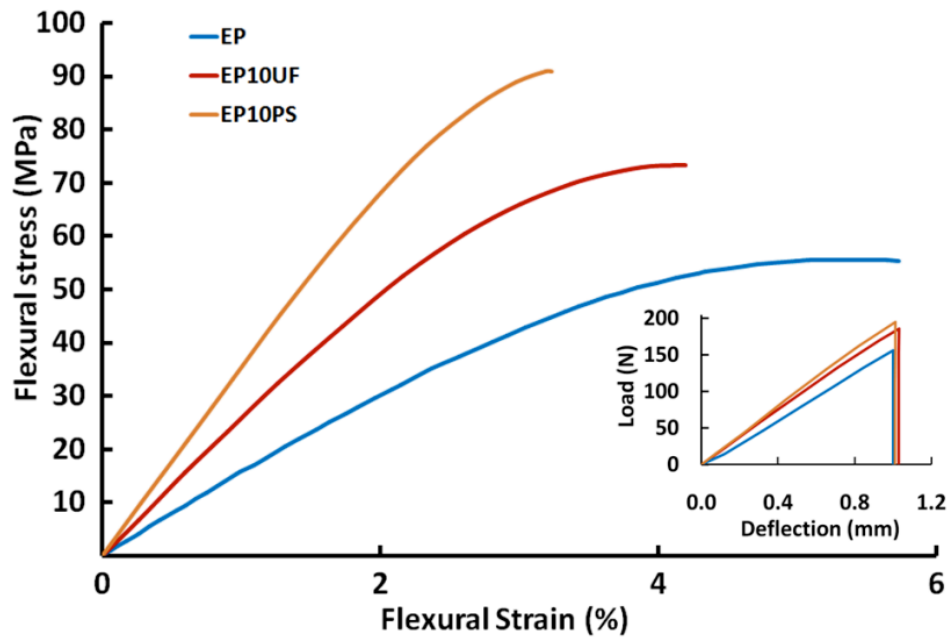
Figure 5.9: Stress-strain curves (flexural mode) of epoxy and its composites with UF and PS microcapsules. (Inset presents the influence of notch on the flexural response of specimens)

Normalized critical stress intensity factor (K_{IC}) and fracture energy (G_{IC}) of compositions were compared as a function of microcapsule loading and the results are

illustrated in Figure 5.10. For the purpose of calculation, the Poisson's ratio of epoxy was assumed to be 0.35[146]. The figure shows that the stress intensity factor K_{IC} of epoxy increased by $\sim 38.2 \pm 6$ % on the introduction of UF microcapsules (10% w/w). This is however much lesser than the value of 127% reported previously, an incongruity which may be attributed to the TCDB geometry used for toughness determination[60] as compared to SENB geometry used in the present work. The stress intensity factor (K_{IC}) was further used to estimate the fracture energy, which was found to increase substantially, from a mean value of 5.05 kJ/m^2 (unmodified epoxy) to 9.5 $\pm$0.4 kJ/m^2 after loading of microcapsules (10 % w/w) irrespective of shell wall material.
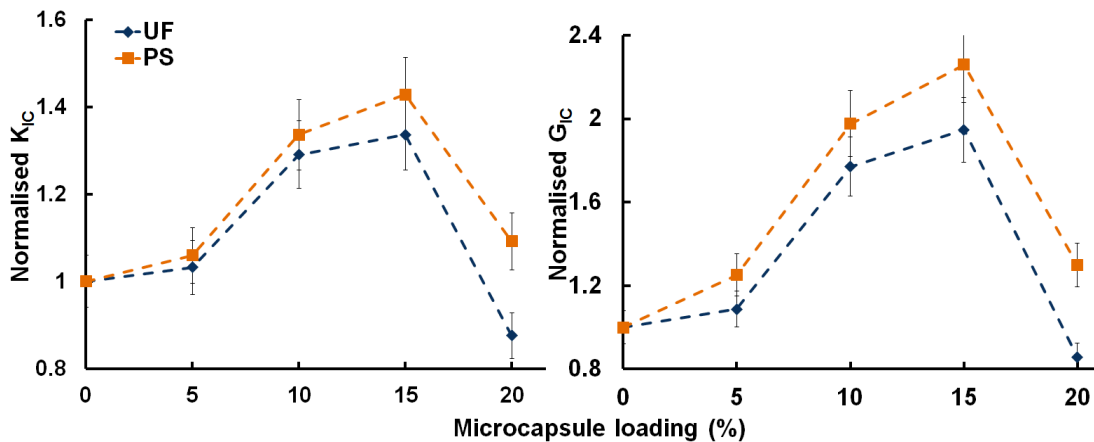
Figure 5.10: Increase in the normalized critical stress intensity factor (K_{IC}) and

normalized fracture energy (G_{IC}) due to inclusion of microcapsules

It was interesting to note the difference in the fracture toughness values estimated from impact and single edge notched bending tests. Comparison of Figure 5.8 and 5.10 reveals that the izod impact toughness decreases, while the SENB fracture toughness increase with microcapsule addition. This may be attributed to the difference in the strain

rate employed, with the latter being performed at much lower strain rates $(8.1 \times 10^{-2}s^{-1})$ giving the polymer enough time to respond to the applied stress.

5.4.2. Toughening mechanism

Fractography was performed on the cracked surfaces and the results are shown in Figure 5.11 and 5.12. The featureless and smooth surface of neat epoxy is characteristic of fracture in a brittle thermosetting polymer, which shows no signs of plastic deformation (Figure 5.11)[150,151]. The presence of feather-like hackle markings resulting from small-scale secondary crack formation could be observed just after the plastic zone which extends to the stress zone. The hackle markings transition into striations in the direction of crack propagation and finally there is a complete transition to a mirror fracture surface, as reported previously[60].
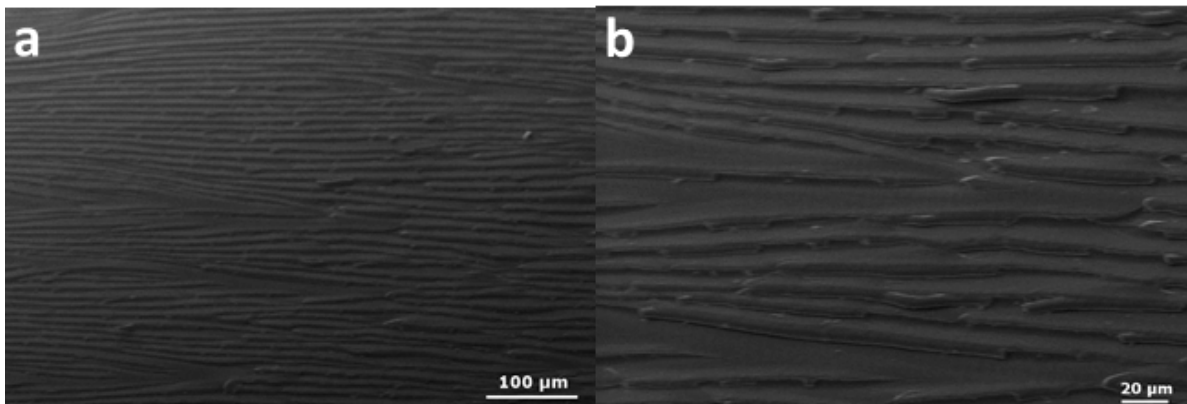
Figure 5.11: SEM image of fractured epoxy at different magnifications

As compared to neat epoxy, the fractured surface of the epoxy containing microcapsules is relatively rough throughout the crack plane. "Crack pinning" is

most commonly cited to explain the toughening in epoxy-microcapsule composite. According to this, the role of second phase is to cause the crack to bow out, propagation of which requires much larger quantity of energy. Indirect proof of the existance of this mechanism is the presence of 'tails' connected with the embedded microcapsules (Figure 5.12 a). In some cases, the tip of crack is compelled to alter its path as it reaches the microcapsules, an event frequently known as crack bowing, (Figure 5.12 b), which results in increased surface area. In addition, the mode I character of the crack opening is also reduced, which mandate larger energy for its progression.
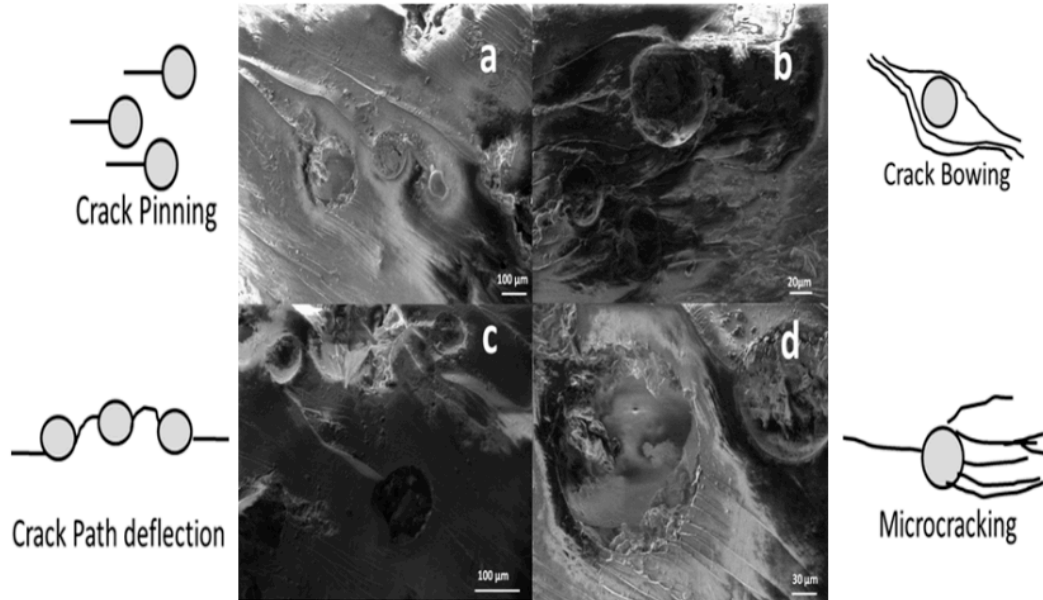
Figure 5.12: Underlying toughening micromechanism and SEM images of fracture surface revealing a) crack pinning, b) crack bowing, c) crack path deflection, d) microcracking

As expected, a number of "broken" microcapsules were noticed on the surface of the composite. It appears that the "breaking" of the microcapsule leads to the flow of the

117

encapsulated healant into the crack plane. In rigid particle-epoxy composites[152], crack pinning by the filler material is expected to contribute significantly towards increasing the toughness of the composite. However, in the present scenario, due to the fragile nature of the microcapsules, the contribution of this route is practically negligible. However, clear evidence of "Crack path deflection" (Figure 5.12c) and "Microcracking" (Figure 5.12d) was found during fractography[153], which could be used to understand the toughened nature of the microcapsule containing composite samples.

5.4.2. Healing epoxy composites containing microencapsulated epoxy

To experimentally validate the predictions for the amount of healant released into the crack plane in the event of microcapsule rupture, the healing efficiency of epoxy composites containing epoxy loaded microcapsules with different internal microstructures were dispersed within a representative epoxy matrix. The detailed characterization of microcapsules prepared is presented in the Chapters II. Introduction of either type of microcapsule is expected to endow the polymer with self-healing functionality, however as per the predictions, self healing efficiency should be lesser in samples containing monolithic microcapsules irrespective of resin core

For the purpose of demonstrating healing in composites containing epoxy loaded microcapsules, a set of latent epoxy hardeners (copper and nickel imidazolates) was prepared by the reaction of metal salts with methyl imidazoles.

5.4.2.1. Latent hardener for epoxy curing

The reaction of 2-MeImidH with copper and nickel ions reportedly leads to the formation of stable metal complexes with square pyramidal geometry, namely chlorotetrakis 2-methylimidazolemetal(II) chloride [M(2-Me-ImidH)$_4$Cl]Cl, where M = Cu and Ni[144]. Elevation of temperature leads to dissociation of this complex, leading to the release of imidazole moiety. This in turn, is capable of attacking the oxirane rings available with the epoxy resin (Scheme 5.1) resulting in the formation of a cured crosslinked network.
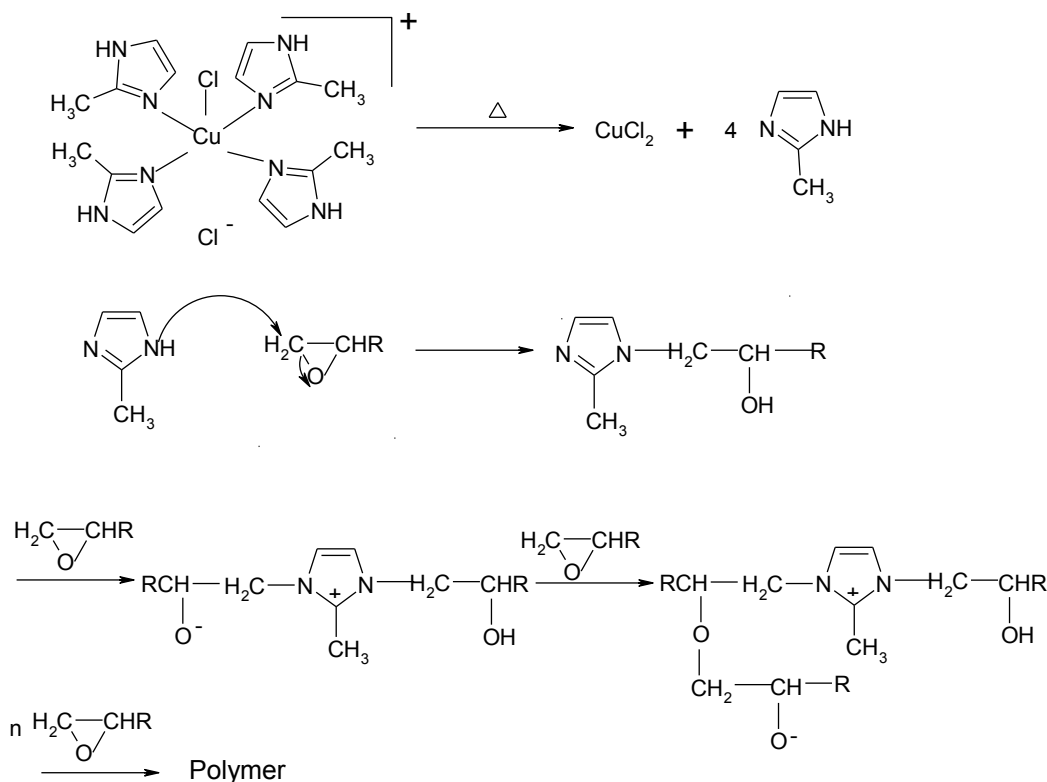
Scheme 5.1: Schematic representation of the functioning of copper-imidazole based latent hardener

The FTIR spectra of 2-MeImidH and both the metal complexes [M(2-Me-ImidH)$_4$Cl]Cl, M = Cu, Ni) are depicted in Figure 5.13. The broad absorption band in the resonance stabilised imidazole N−H···N hydrogen bond stretching (2200–3400 cm^{-1}) is absent in the spectrum of the metal complexes, which is clearly indicative of the coordination of 2-MeIm with the metal ion through the secondary amine functionality[116]. As expected, the characteristic absorption peaks at 756 cm^{-1} (N-H wagging), 1110 cm^{-1} (C-N stretching), 1600 cm^{-1} (C=N stretching) and 1440 cm^{-1} (C-H rocking) are visible in all the spectra, which are indicative of the availability of the imidazole moiety in the complex; an essential criteria for the functioning of a successful latent hardener.
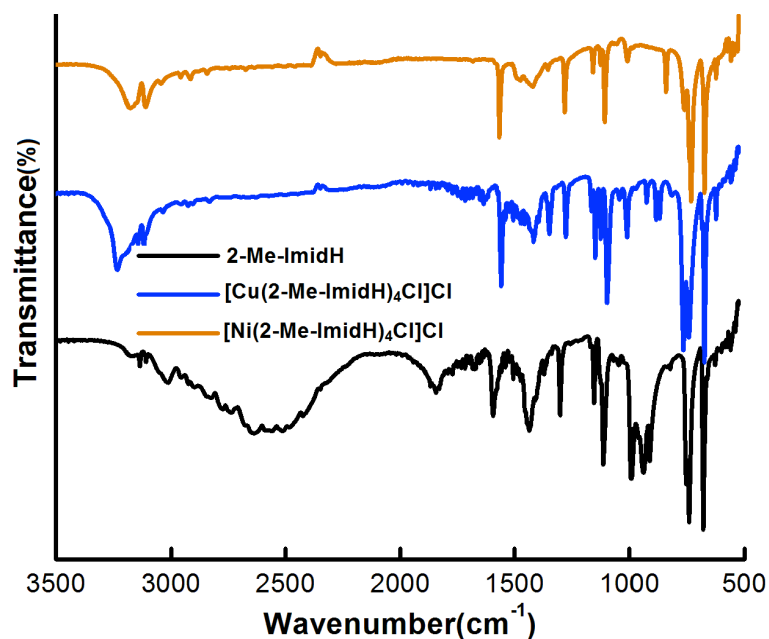
Figure 5.13: FTIR spectra of 2- MeImidH and [M(2-Me-ImidH)$_4$Cl]Cl, M = Cu, Ni

Thermal decomposition behavior of 2-methyl imidazole and the metal complexes is presented in Figure 5.14. It is evident from the TG traces that both the complexes are

120

thermally more stable than 2-methyl imidazole, which undergoes single step degradation at T_{onset}= 205°C. The presence of metal in the coordination complex leads to higher ash content, which is in accordance with the theoretical values (i.e. 28.3 % and 29.0 % for the Ni and Cu complex respectively).
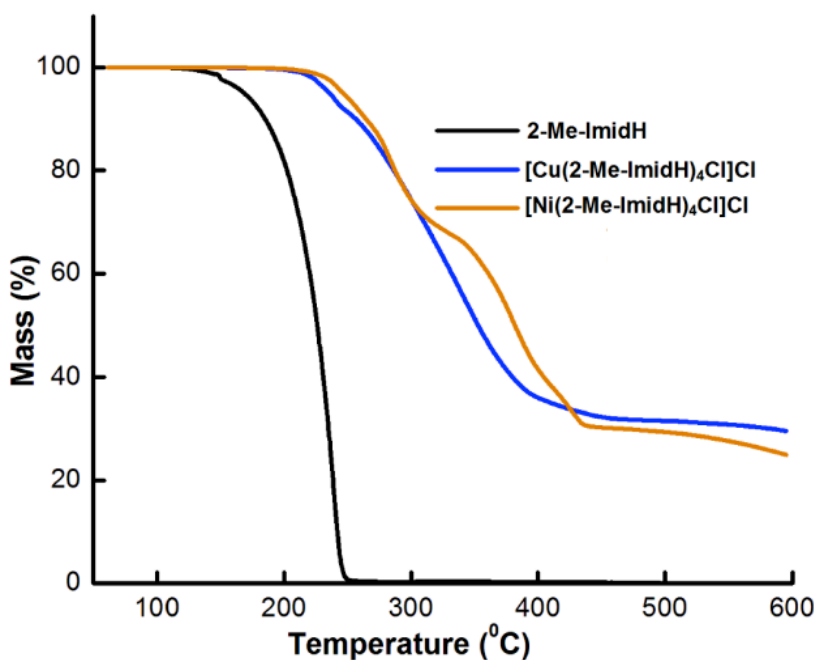
Figure 5.14: TG traces of 2-methyl imidazole and metal-(2-methyl imidazole)

complexes

5.4.2.2. Healing studies on microcapsules with "reservoir" type internal morphology

Composite specimens were prepared in the presence of epoxy loaded microcapsules and latent hardener, which were subjected to impact test and the impact strength both before and after healing was estimated to quantify the efficiency of healing.

The morphology of the cracked surface of neat epoxy and microcapsule containing composite samples after being subjected to impact tests was studied by scanning electron microscopy, the resulting SEM micrographs are shown in Figure 5.15 (a,b). The smooth and featureless surface of epoxy is characteristic of brittle fracture in thermosets, which elucidate absence of plastic deformation. In comparison, the fractured crack plane of the microcapsule loaded samples was relatively rough throughout. As expected, a number of "broken" microcapsules could be seen on the surface of crack plane (Figure 5.15 b).
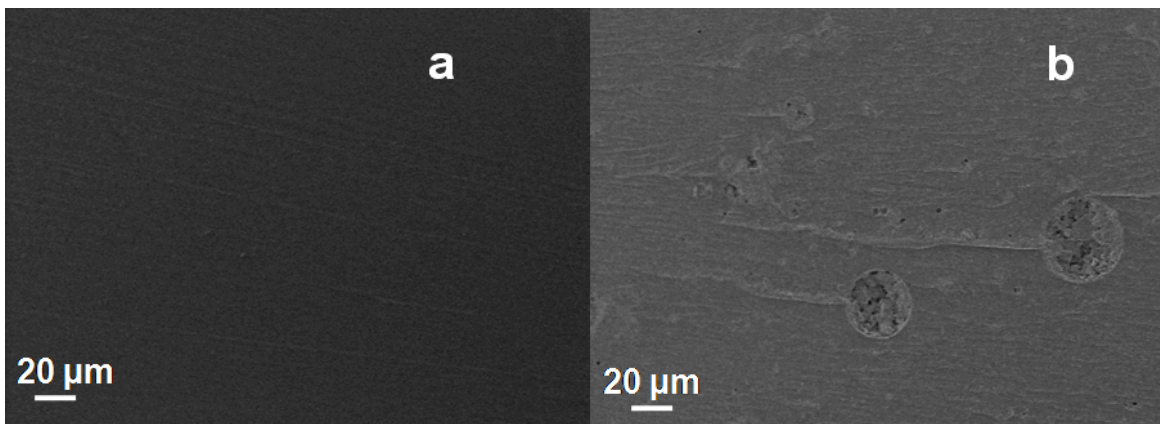
Figure 5.15: SEM micrographs of fractured surface of a) neat epoxy and b) epoxy-microcapsule composite

The healing efficiency was found to increase with increasing microcapsule loading, reached a maximum (100%) and levelled off subsequently (30 % microcapsule loading and 1% latent curing agent, 150 °C), as illustrated in Figure 5.16.
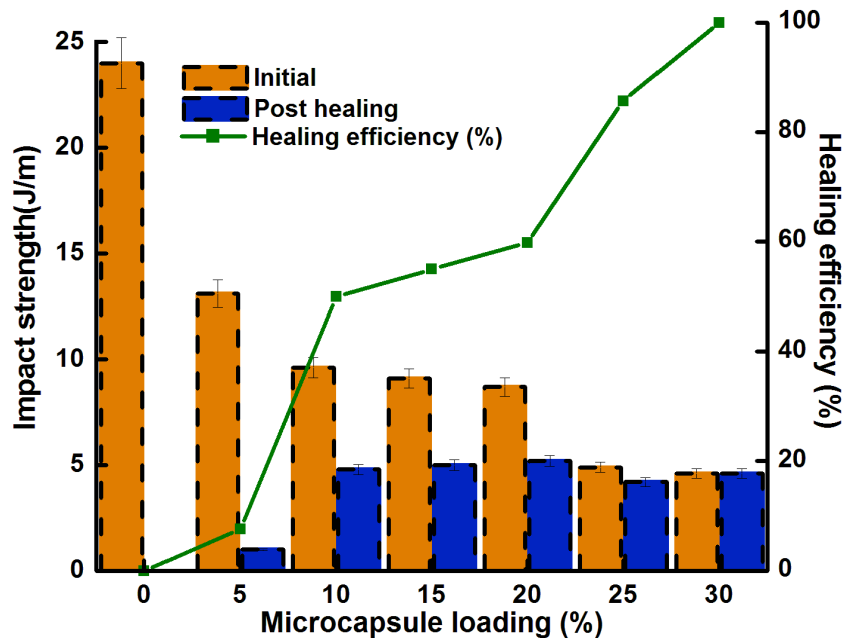
Figure 5.16: Effect of increasing epoxy encapsulated microcapsule loading "reservoir" type morphology on the impact strength (primary axis) and healing efficiency with latent hardener (secondary axis) (secondary axis) of epoxy composite

Healing in composites having epoxy loaded microcapsules is also demonstrated with immobilized amine on SBA-15 at 70 °C. The detailed procedure of SBA-15 preparation and immobilization of amine on to it has been presented in Chapter III. The healing efficiency was found to reach a maximum of 100% at 20% microcapsule loading, as presented in Figure 5.17.
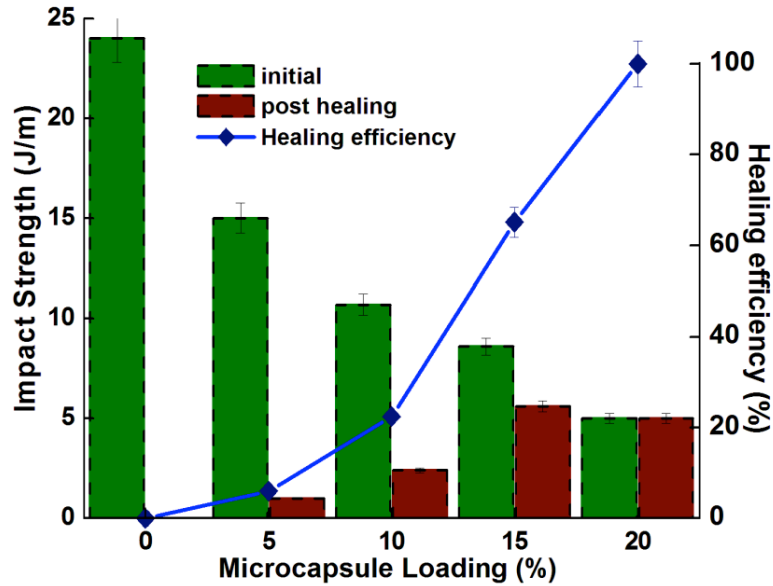
Figure 5.17: Effect of increasing microcapsule loading with "reservoir" type morphology on the impact strength (primary axis) and healing efficiency (secondary axis) with amine immobilised SBA-15

5.4.2.3. Healing studies on microcapsules with "monolithic" type internal morphology

The effect of introducing microcapsules with monolithic morphology on the impact strength of epoxy is shownin Figure 5.18. It can be seen that in comparison to reservoir type microcapsules, introduction of microcapsules with monolithic morphology led to slightly lesser reduction in the properties of epoxy. However, the healing efficiency was substantially lower in the case of monolithic microcapsules. This was attributed to the relatively lower core content of the microcapsule. Moreover, as has been discussed in Chapter II, the entire contents of the healantare not released in the event of rupture of monolithic microcapsules, thereby leading to the lower self healing efficiency.
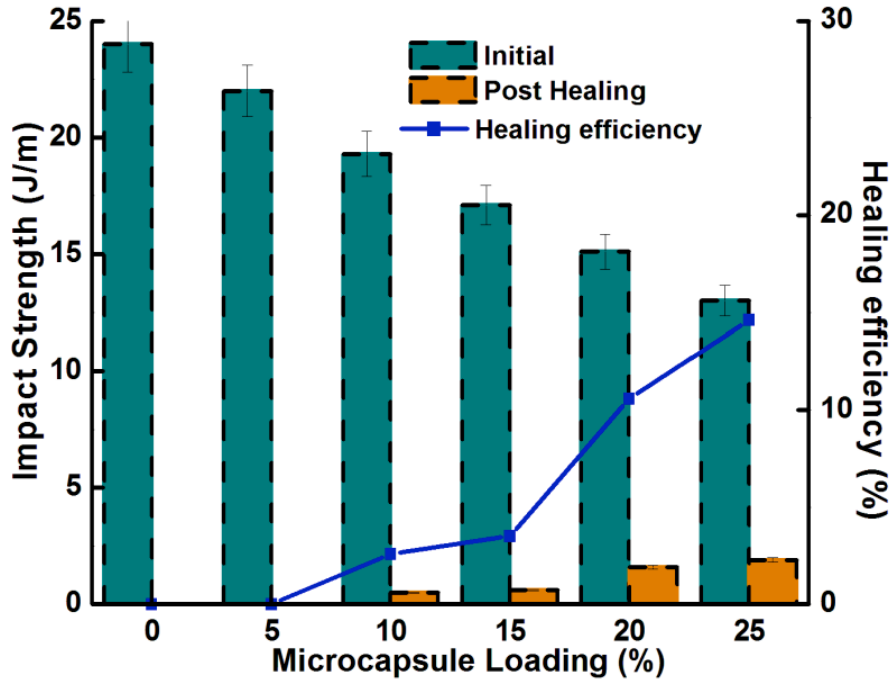
Figure 5.18: Effect of increasing epoxy encapsulated PS microcapsule loading with "monolithic" type morphology on the impact strength (primary axis) and healing efficiency (secondary axis) of epoxy composite

SEM image of fractured plane of a representative sample, containing monolithic microcapsule (20% w/w loading) is shown in Figure 5.19. The figure is annotated with the dimensions of few microdroplets. For the ease of calculation, the average diameter of the microdroplet was calculated, which was of the order of ~15 micron. With the diameter of a monolithic microcapsule being 130 micron, the healant released is expected to be only 16.4 % of the amount released in the event of rupture of an analogous "reservoir" microcapsule. Experimentally, the healing efficiency was found to be 17.7%, which is well within the range.
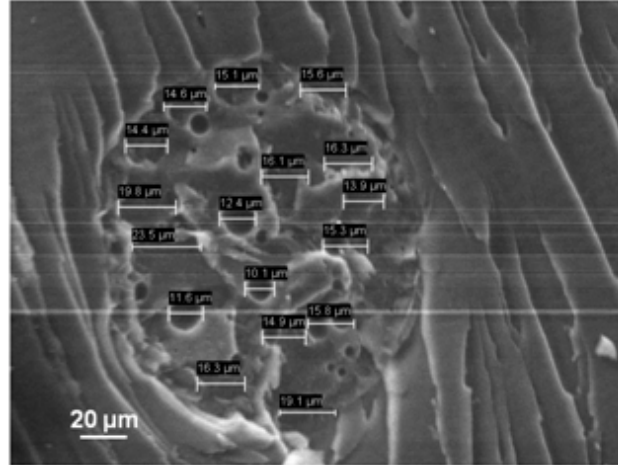
***Figure 5.19: Fractured surface of sample containing monolithic microcapsule
(microcapsule loading 20% w/w)***

The detailed calculation is presented in Table 5.2.

Table 5.2: Comparison of experimental and model predictions for a representative

microcapsule loading (20%)

Microcapsule Loading (%)	Self healing efficiency (%)		Fraction (%) monolithic/ reservoir	
	Reservoir	**Monolithic**	**Experimentally observed**	**Model predictions**
20	59.77	10.59	17.71	16.44

As discussed earlier part of this chapter, introduction of microcapsules led to

deterioration in the mechanical properties, the extent being much larger in microcapsules

with reservoir type structure[90]. In line with our expectations, the self healing efficiency

was lower in the case of samples containing monolithic microcapsules. Complete healing

was observed at higher loadings (>20% v/v) for reservoir type microcapsule, while under

similar loadings, the healing efficiency was much lower for monolithic microcapsules. It

is however, to be noted that the core-content of the monolithic microcapsules was $\sim$ 38$\pm$ 2%, while that of the microcapsules with reservoir microstructure was 65$\pm$ 4%. Our experiments validate the developed model, discussed in detail in Chapter II.

CHAPTER VI

SUMMARY AND

CONCLUSIONS

Self-healing composites are advanced materials, which present an interesting autonomic route for repairing damage, thereby extending the lifetime of the composite. Usually, this property is bestowed by introducing compartmentalized healing agent in the matrix either in the form of capsules or hollow fibers/tubes or microvascular networks. Upon damage, the healant flows into the crack by capillary action, undergo polymerization thereby healing the matrix. Several different types of containment structures have been reported for encapsulating healing agents, starting from microcapsule to microvascular network with the former being the simplest to produce. Microencapsulation of healing agent can be achieved by various techniques like in-situ dispersion polymerisation, interfacial polymerization and solvent evaporation, to name a few. The internal microstructure is dependent on the method of preparation, the dispersion polymerization leading to reservoir type of internal morphology while solvent evaporation leading to microcapsules with "monolithic" microstructure.

In this work, the effect of introduction of self-healing additives on the curing behavior, mechanical and healing properties of epoxy thermoset have been explored. Liquid epoxy resin and its amine hardener both were encapsulated separately by various techniques and incorporated in epoxy matrix to get epoxy based self-healing composites. These were subsequently evaluated for their mechanical properties and healing efficiency.

6.1. Encapsulation of cycloaliphatic epoxy as healing agent

- Liquid epoxy was encapsulated in urea-formaldehyde and polystyrene microcapsules using dispersion polymerisation and solvent evaporation techniques in two different

128

shell wall materials i.e. urea-formaldehyde and polystyrene. Dispersion polymerization led to the formation of microcapsules with "reservoir" type internal morphology while solvent evaporation resulted in "monolithic" microcapsules.

- The yield of the microcapsules obtained by adopting either type of methodology, as determined by gravimetric analysis, was found to be $72 \pm 5\%$.

- The effect of operating parameters particularly stirring speed, on the microcapsule dimensions was determined. It was found that the microcapsule diameter decreased with increasing stirring speed.

- The core content of the microcapsules was determined and was found to be $65 \pm 4 \%$ for microcapsules formed by dispersion polymerization and $38 \pm 2 \%$ for microcapsules formed by solvent evaporation method.

- An analytical model was developed to predict the amount of healant released into the crack plane in the event of microcapsule rupture. Of particular interest was to establish the effect of internal microstructure. Theoretical predictions revealed that with increasing core content, the monolithic morphology essentially converged to that of reservoir (core content >50%). The developed model clearly highlighted the advantages associated with the "reservoir" microstructure in the context of self-healing applications. The differences between reservoir and monolith microcapsules were particularly pronounced when the microdroplet dimensions and core content were low.

- Healing studies were experimentally performed for validation of the developed

model. For this purpose,healant encapsulated microcapsules, with varied microstructure along with suitable catalysts were included in the formulation to obtain healable compositions. The healing efficiency has been quantified in terms of the ratio of impact strength both before and after healing. The experimental results were found to be in line with the theoretical predictions.

6.2. Encapsulation of reactive amine as curing agent for epoxy

- Triethylenetetramine (TETA) hardener was encapsulated by interfacial polymerisation and physical entrapment method in crosslinked epoxy shell and mesoporous substrate (SBA-15) respectively.

- For encapsulation of amine by interfacial polymerisation process, reaction parameters especially epoxy: hardener ratio, stirring rate and medium temperature was found to have a pronounced effect on the microcapsule morphology, particle size distribution and the core content.

- Under optimal conditions, i.e. stirring rate of 600 rpm, reaction temperature of 70°C and epoxy: hardener ratio 10:3.2, spherical microcapsules were obtained in excellent yields (100%) with a core content of 12 %.

- Triethylenetetramine hardener was filled within the pores of SBA 15 by vacuum infiltration technique. The extent of amine immobilisation was determined gravimetrically to be 5 g/g.

6.3. Effect of inclusion of microcapsules on curing behavior

- The curing behavior of a TETA cured epoxy and representative self-healing compositions prepared by dispersing UF microcapsules and SBA-15 immobilised amine was systematically studied using the non-isothermal differential scanning calorimetric technique.

- Curing studies were performed at different heating rates (2.5-15°C/min) and the data was used to estimate the activation energy at different stages of curing, using both Friedman and Kissinger–Akahira–Sunose method.

- The activation energy was found to vary from 40-90 kJ/mol, irrespective of the method used for its estimation. The studies revealed a progressive decrease in the activation energy for all compositions, irrespective of the presence of microcapsules or SBA-15 in the composition in the concentration range studied.

- KAS method was further used to predict the curing behaviour at elevated heating rate 30°C/min, which was subsequently validated with dynamic DSC experiments.

6.4. The effect of inclusion of microcapsules on the mechanical and healing properties

- The effect of inclusion of both reservoir (UF) and monolithic (PS) microcapsules on the thermal, structural and mechanical properties of a representative cycloaliphatic thermosetting epoxy resin was studied under quasi-static and dynamic loadings.

- Mechanical properties like tensile strength, modulus and impact strength were found

to decrease proportionally with microcapsule loading. However significant improvement in the toughness of the base resin was evidenced (38.2 ± 6 %), which was quantified in terms of critical stress intensity factor (K_{IC}) and fracture energies (G_{IC}).

- Fractography of the cracked surface was performed to gain insight into the underlying mechanisms behind the improved toughening. Clear evidence of crack pinning, crack bowing, micro-cracking and crack path deflection was observed during morphological investigations, which could be used to explain the toughened nature of the composites.

- The presence of UF or PS microcapsules did not affect the curing behaviour of epoxy and all the compositions were found to exhibit similar onset (T_{onset}) and peak cure temperatures (T_{peak}).

- Latent curing agents were prepared by complexation reaction of metal chlorides of copper and nickel with 2-methyl imidazole. Calorimetric studies were carried out to establish the curing profile of epoxy in the presence of latent hardener.

- To validate the developed model, epoxy resin encapsulated microcapsules with different internal microstructures (loadings 5-30% w/w) and fixed loading of curing agents (latent curing agent as well as amine immobilized SBA-15) (1% w/w), were dispersed in an epoxy matrix to yield self-healing compositions.

- In line with the theoretical predictions, the healing efficiency was significantly higher in composites containing microcapsules with "reservoir" type morphology. Complete

healing (~10%) was observed at higher loadings (>20% w/w) for reservoir type microcapsule, while under similar loadings, the healing efficiency was significantly lower (~10%) for monolithic microcapsules.

- Introduction of reservoir type microcapsules led to complete healing (healing efficiency =100 ± 2 %) at 30 % loading for UF microcapsule-latent hardener system, and at 20% loading for UF microcapsule- amine immobilized SBA-15 system.

6.5. Encapsulation of unsaturated polyester (USP)

- Liquid unsaturated polyester-filled microcapsules in urea-formaldehyde (UF) and polystyrene (PS) shell were successfully synthesized by dispersion polymerization route and solvent evaporation technique respectively.

- By adopting dispersion polymerization route, free flowing microcapsules (~130 ± 49 μm) with a core content of 58 ± 4% could be obtained in high yields upon filtration and drying.

- Upon adoption of solvent evaporation route, under optimal conditions, microcapsules of diameter 135 ± 15 μm, with a core content of 40 ± 4% were formed.

- Introduction of unsaturated polyester loaded microcapsules led to a decrease in the characteristic mechanical properties of the base matrix; however healing functionality was successfully introduced, as quantified in terms of the ratio of impact strength of healed to virgin samples.

- Calorimetric   studies were   used   to   arrive at   the optimal temperature

conditions desired for curing in the presence of AIBN as the free radical initiator.

- For reservoir type microcapsules, healing efficiencies of the order of 100% could be reached at 20% (w/w) loading of microcapsules. The healing efficiency was substantially lower in the case of monolithic microcapsules. This was attributed to the relatively lower core content (40 ± 4%) and the monolithic internal morphology of the microcapsules as compared to the reservoir type microcapsules with core content (58 ± 4%).

EFFECT OF INTRODUCTION OF UNSATURATED POLYESTER ENCAPSULATED MICROCAPSULES ON PROPERTIES OF EPOXY

A.1. Introduction

Among many, the most desirable feature for potential application in the field of self healingsystem is that the healing chemistry should not be strongly dependant on stoichiometry and be economically feasible. Commonly used healing agents in literature are DCPD[9,60], Epoxy[38,90,154,155] and PDMS[156]. There are advantages and disadvantages of all these healing systems, which have been discussed in detail in previous chapters. For the present work, unsaturated polyester (USP) was selected as a healant and an attempt was made towards eliminating previously mentioned limitations, especially the stoichiometry dependence associated with epoxy-amine chemistry.

A.1.1. Unsaturated polyesters

Unsaturated polyester (USP) is one of the most extensively used matrix material in fiber-reinforced composite, its popularity arising from its excellent mechanical properties, chemical resistance, low cost, and ease of processing and excellent fiber wettability. The resin is synthesized by the reaction of a glycol with a diacid in the presence of an anhydride, which is usually unsaturated e.g. maleic anhydride (Scheme A.1).
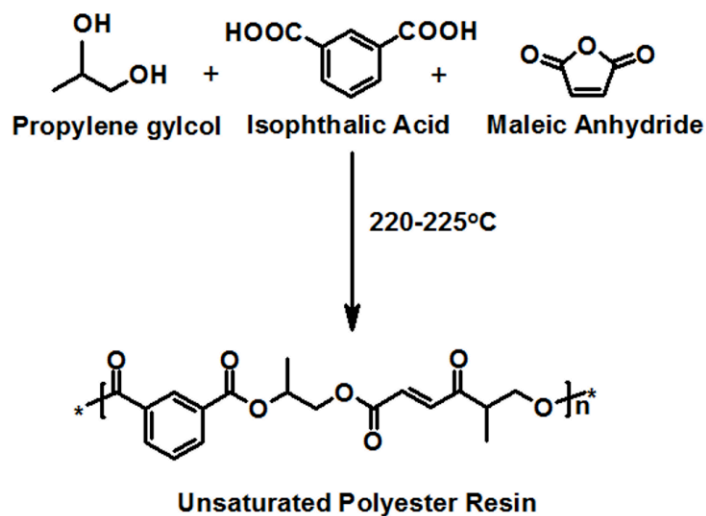
Scheme A.1: A representative synthetic process for preparation of polyester

resin

Conventional unsaturated polyesters are generally solution of unsaturated polyester with a diluent, commonly styrene. The curing process results in the cross-linking of polyesters chains through poly(styrene) linkages at the unsaturated sites, thereby forming an amorphous cross-linked structure. In order to obtain a rigid structural material, the pre-polymer solution in styrene is cross-linked into a rigid thermoset through a free radical copolymerization between the styrene moieties and the double bonds present in the polyester macromolecule Scheme A.2. However, this crosslinked network is inherently brittle, which restricts its usage in highly demanding applications.
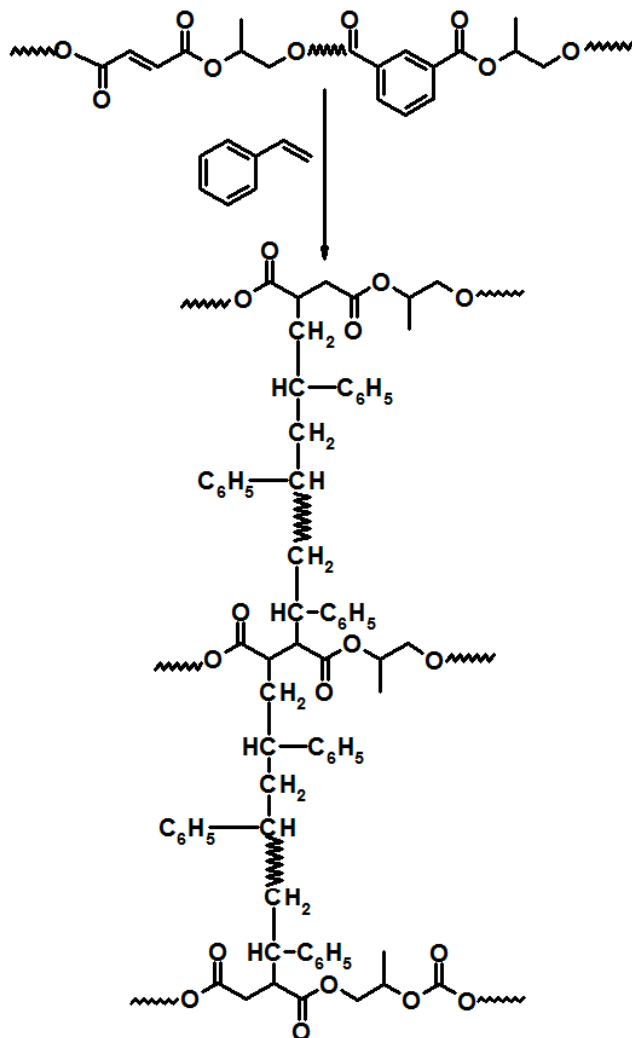
Scheme A.2: Crosslinking of unsaturated polyester resin

A.1.2. Curing agents for unsaturated polyester (USP)

Due to the presence of styrene in the formulation, it is possible to cure the resin using free radical initiators such as 2, 2'-Azobisisobutyronitrile (AIBN), benzoyl peroxide etc. AIBN is one of the most important initiators under the broad category of azocompounds that undergoes decomposition at 50–70ºC. AIBN is safer to use than benzoyl peroxide in view of the reduced risk of explosion. It is always desirable to perform curing reactions under ambient conditions; therefore the use of redox

initiators is rather common. The most common initiator system used is a combination of methyl ethyl ketone peroxide (MEKP) and cobalt naphthenate.

The curing reaction is highly exothermic, and the temperature can increase up to 100-200°C, depending on the compositon of the resin, thickness of laminate, and the initiator system. Unsaturated polyester (USP) resin is highly viscous in nature. For healing applications, the flowability of the resin is an essential criteria, which has been achieved by dilution of the resin with ethyl acetate, which is a common solvent favored in view of its low cost, low toxicity, and agreeable odor.

A.2. Experimental

A.2.1. Materials

Isophthalic acid based unsaturated polyester resin (USP RPL211, Revex) with a styrene content of 32% was used for the study.

A.2.2. Microencapsulation of epoxy in polystyrene shell

The procedure adopted for encapsulation of USP in polystyrene was similar to that adopted for epoxy encapsulation, which has been discussed in detail in Chapter II. In brief, a predetermined amount of unsaturated polyester and polystyrene was dissolved in dichloromethane which was then added to aqueous PVA solution (2.5%, w/w) under stirring at room temperature to produce oil in water emulsion. Thus resulting emulsion was transferred into 150 ml of aqueous PVA solution with continuous stirring at varying speed (350-550 rpm). After evaporation of solvent, the reaction mixture was cooled, and

the unsaturated polyester encapsulated polystyrene microcapsules were filtered, washed repeatedly with water and finally dried under vacuum.

A.2.3. Microencapsulation of USP in UF shells

Dispersion polymerisation route was adopted for the preparation of USP encapsulated urea-formaldehyde shells, and the procedure was similar to that of epoxy encapsulation as discussed in Chapter II. In brief, 100 mL distilled water was mixed with 25 ml EMA solution (2.5%, w/v) by stirring at room temperature (~ 450 rpm). To this solution, 2.5 g urea, 0.25 g ammonium chloride and 0.25 g resorcinol was added. After complete dissolution, the pH of the solution was adjusted to 3.2 ± 0.2. Subsequently, ~ 60 ml of the healing agent solution (USP: ethyl acetate:: 1:1 w/w) was slowly added over a period of 20 minutes. Thereafter, requisite amount (6.33 g) of formalin was introduced and the temperature of the reaction mixture was increased to 50-55°C, while maintaining a constant stirring rate between 250-450 rpm. The reaction was allowed to proceed for 4 h, followed by filtration of the microcapsules and air drying for 24 h, which resulted in free-flowing powder. The general schematic is presented as Scheme A.3
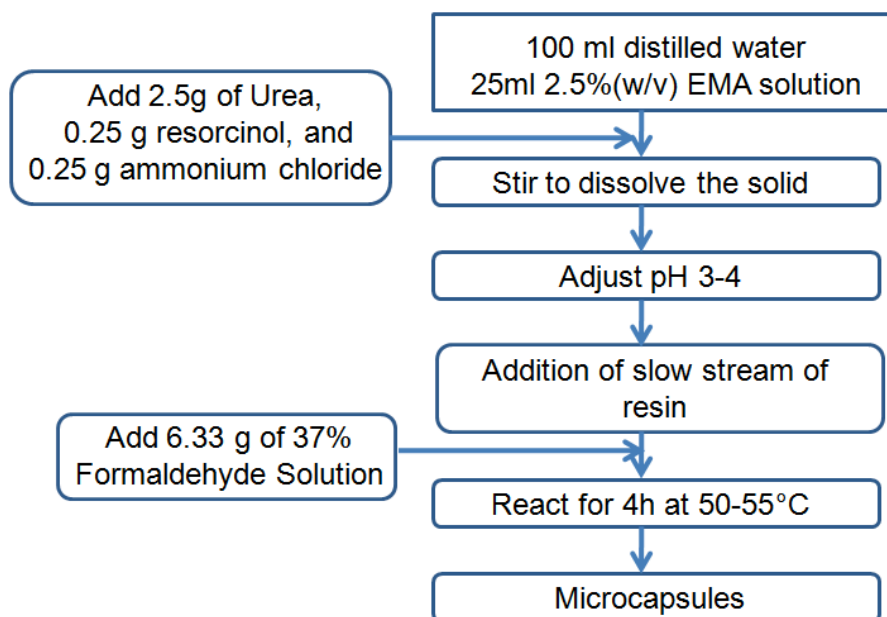
Scheme A.3: Schematic for preparation of USP encapsulated urea-formaldehyde microcapsules

The extent of encapsulation in the microcapsules was estimated by acetone extraction process as per the procedure discussed in Chapter II.

A.3. Characterization

The USP encapsulated microspheres were characterised using the methods detailed in Chapter II.

A.4. Results and Discussion

A.4.1. Encapsulation of USP in polystyrene shells

A.4.1.1. Effect of stirring speed on encapsulation of USP in polystyrene shells

The influence of stirring rate on the morphology of microcapsulesis presented in Figure A.1. It can be seen that the prepared microcapsules were poly-dispersed and

spherical in shape withsmooth texture and sub-micron debris on their shell. The yield of the microcapsules, as determined by gravimetric analysis, was found to be 72 ± 5%.
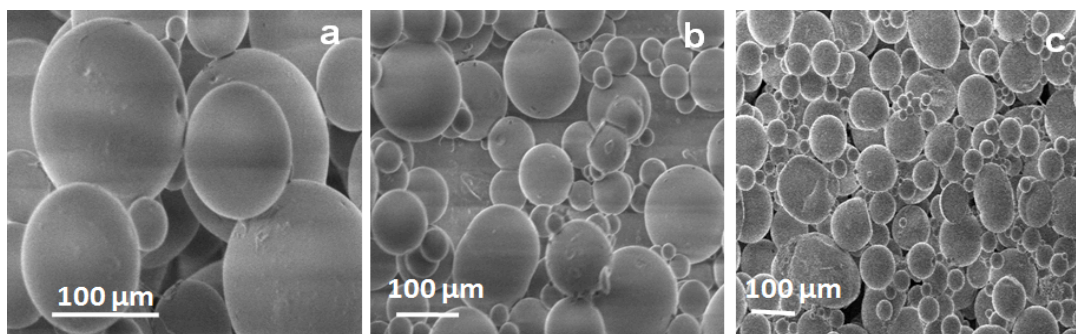
Figure A.1: Effect of increasing stirring speeds on the size of USP encapsulated polystyrene microcapsules a) 350, b) 450 and c) 550 rpm

As expected, with increase in stirring rate, the average particle size distribution of the microcapsules shifted to lower dimensions, as can be seen in Figure A.2.For studying the self healing efficiency of samples, microcapsules of diameter 135±15μm were used with a core content of 40 ± 4%.
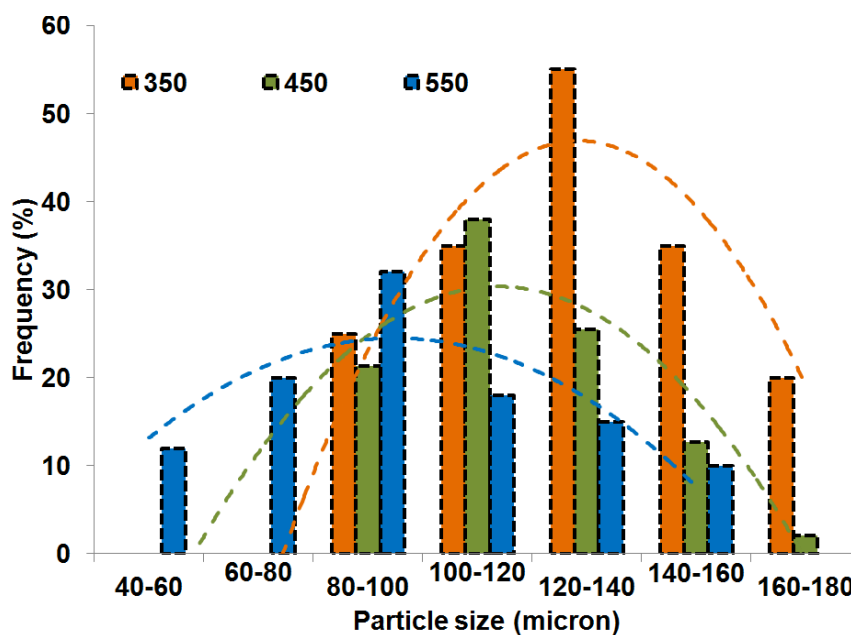
Figure A.2: Particle size distribution of microcapsules prepared by solvent evaporation

A.4.1.2. Thermal properties

Figure A.3 shows the TG traces of USP encapsulated polystyrene microcapsules, liquid USP and polystyrene. The TG traces of liquid USP reveals a three step degradation behavior. The first mass loss at T< 200°C can be due to the loss of volatile styrene present in the polyester composition. Increase in temperature leads to the polymerisation of the polyester and styrene chainsand the second mass loss at 300-400°C can be attributed to the degradation of the polystyrene chain. The final mass loss 400-550°C is due to decomposition of cross-linked structure of USP. The TG traces of microcapsules exhibit a two-step degradation. The first mass loss (300-400°C) is due to degradation of shell, i.e., polystyrene and subsequent mass loss subsequent mass loss (400-550°C) occurs due to the decomposition of core, i.e., USP.

On the other hand, polystyrene exhibits a single step degradation at 300-400°C. The major degradation product of polystyrene consists of a mixture of unsaturated and saturated compounds. It has been reported that the degradation products of polystyrene include 40% monomer, with decreasing amounts of dimer, trimer, tetramer and pentamer. The polystyrene degradation is reportedly initiated at weak links inherent to the polymer, particularly peroxy and hydroperoxy structures.
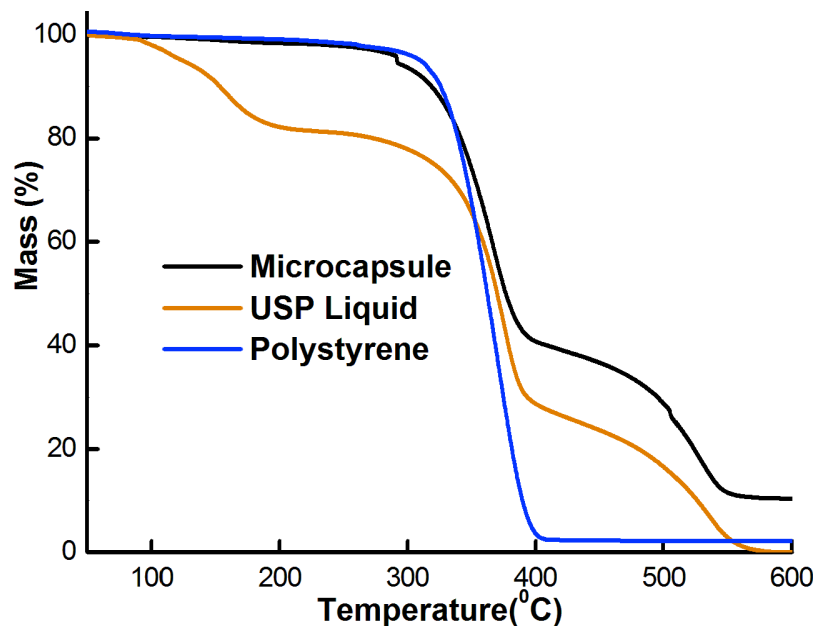
Figure A.3: TG trace of microcapsules, unsaturated polyester (USP) liquid and polystyrene shell

A.4.1.3. Structural properties

The FTIR spectra of the USP resin both before and after curing, and microcapsules are shown in Figure A.4. Liquid polyester resin exhibit strong absorption at 777 cm^{-1} and a weak band at 1073 cm^{-1} due to -C-H bending arising from 1 and 3 positions in benzene ring. The broad absorption band at 1153 cm^{-1} can be attributed to the C-O-C- vibration of the ester linkage. The absorption at 1289 cm^{-1} is associated with the unsaturated sites (–C=C–) available with the polyester and the medium absorption band at 1456 cm^{-1} can be attributed to –C-H bending. The presence of –C=O and symmetric –C-H stretching was confirmed by the presence of strong band at 1717 cm^{-1} and 2983 cm^{-1} respectively[157]. The absence of these characteristic bands in the spectra of microcapsules is clearly indicative of the complete encapsulation of the

143

liquid resin in poly(styrene) shell. The microcapsules exhibit absorption bands at 3026 and 2922 cm^{-1}, which could be due to the -CH(ar) and -CH(al) stretchings respectively.
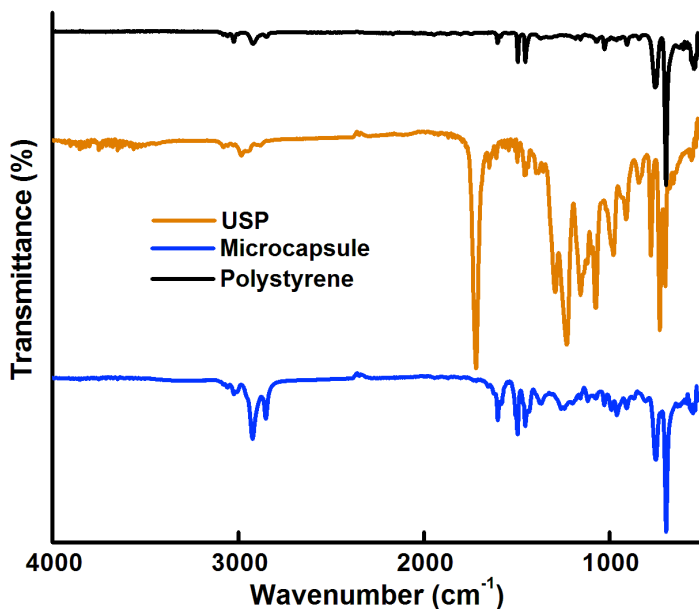
Figure A.4: FTIR spectra of unsaturated polyester resin before and after

encapsulation

A.4.2. Encapsulation of USP in urea-formaldehyde shells

SEM image of USP encapsulated urea-formaldehyde microcapsules is illustrated in Figure A.5 and a representative broken microcapsule is shown in the inset. It is to be noted that dispersion polymerisation route adopted for the preparation of microcapsules lead to the formation of microcapsules with 'reservoir' type internal structure as discussed in Chapter I.
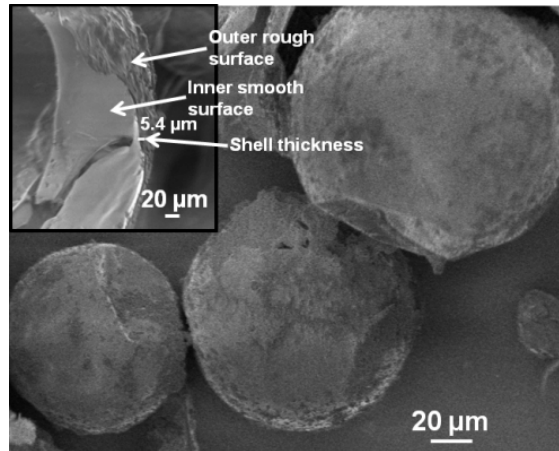
Figure A.5: SEM image of microcapsules containing unsaturated polyester resin. Inset shows the broken microcapsule

It can be seen that, the shell of the microcapsule has a rough porous outer surface while smooth inner surface. The roughness of outer surface can be ascribed to a number of factors, especially resulting from the interplay of the shell-determined elastic forces and fluid-induced shear forces[113].

A.4.2.1. Effect of stirring speed on encapsulation of USP in UF shells

Representative SEM images along with the average size of the microcapsules obtained by varying the stirring speed, keeping all other conditions constant is presented in Figure A.6.The associated particle size distribution is shown in Figure A.7. Our studies revealed that microcapsules of dimensions ~130 ± 49 μm and core content of 58 ± 4 % could be obtained, while maintaining stirring speed at 350 rpm. The shell thickness of the microcapsules was found to be 5.4 ± 1.3 μm.
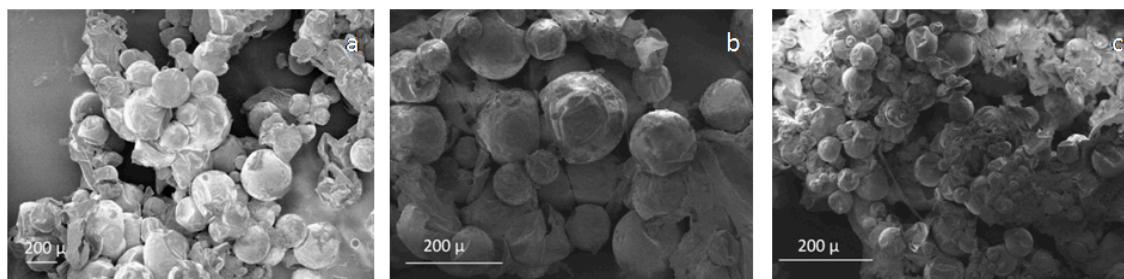
Figure A.6: Effect of increasing stirring speed on microcapsule size a) 250 rpm b)

350 rpm and c) 450 rpm
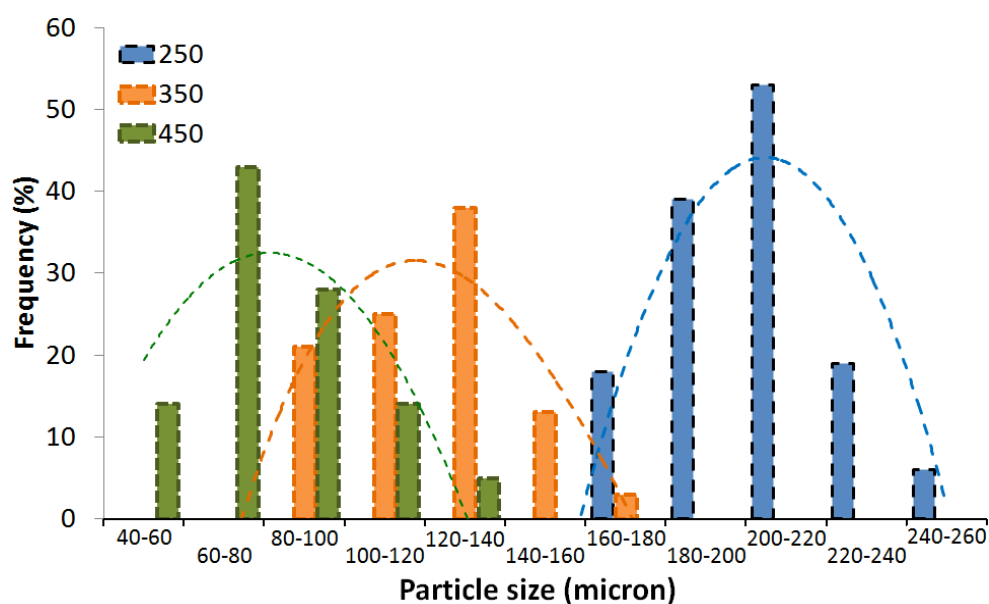
Figure A.7: Particle size distribution of USP encapsulated microcapsules prepared

using dispersion polymerisation route

A.4.2.2. Thermal properties

TG traces of unsaturated polyester encapsulated UF microcapsules are presented in Figure A.8. For comparison purposes, the TG traces of neat and cured USP along with urea-formaldehyde are also included. It can be seen urea-formaldehyde exhibit ~ 5% mass loss at T ≤ 150°C, presumably due to the loss of adsorbed water followed by a

precipitous decomposition at about 242°C (T_{max} ~ 270°C). Neat USP resin exhibits a mass loss of ~20 % at T < 150 °C due to vaporisation of the diluent, i.e. styrene. Programmed heating of the liquid resin leads to the formation of a cross-linked polymer, which subsequently undergoes thermal degradation at ~350°C and 450°C. It is interesting to note a two step degradation profile of USP encapsulated microcapsules. It is apparent that release of the core polyester occurs at slightly elevated temperature in comparison to the unencapsulated liquid. It appears thatthe encapsulating shell wall of urea-formaldehyde ruptures at 240°C, leading to the release of the core components, which further undergo similar degradation profile as exhibited by cured polyester.
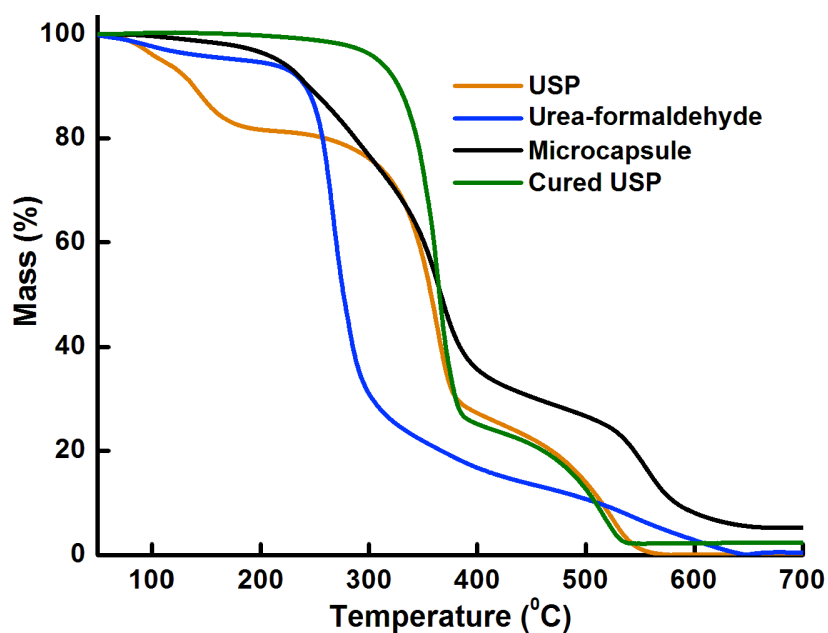
Figure A.8: TG traces of liquid USP resin, cured USP, microcapsules and urea-formaldehyde

A.4.2.3. Structural properties

The FTIR spectra of liquid USP, microcapsules and neat urea-formaldehydeis illustrated in Figure A.9. The spectrum of liquid USP has been discussed in earlier section (Figure A.4). Characteristic absorption bands at 3350 cm^{-1} (overlapping absorptions of hydroxyl, imino and amino functionalities), 2962 cm^{-1} (alkyl C–H stretching), 1255 and 1181 cm^{-1} (aliphatic C–N), 1649 cm^{-1} (NH-CO-NH stretching) and 1034 cm^{-1}(C–O–C stretching) were observed in the spectra of urea-formaldehyde[114]. It can be seen that the spectra of microcapsule is similar to that of urea-formaldehyde where the peaks associated with liquid unsaturated polyester are absent.
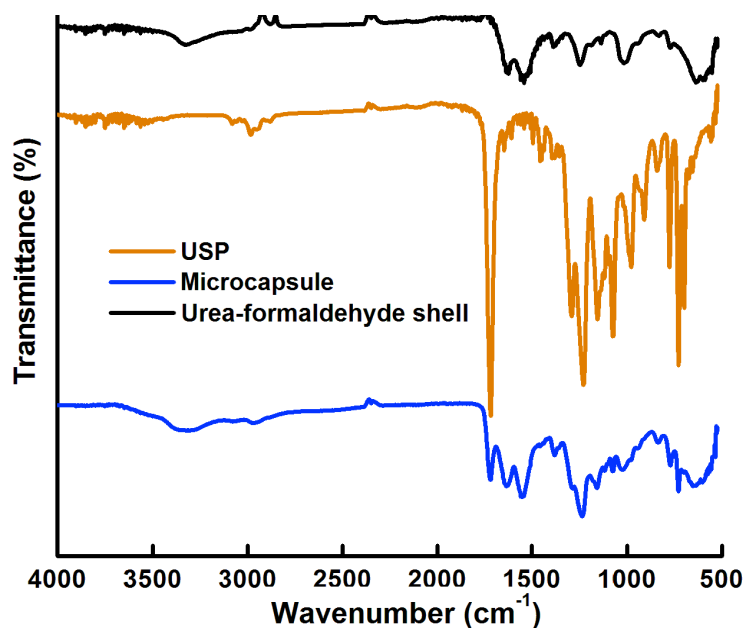
Figure A.9: FTIR spectra of unsaturated polyester resin (USP), microcapsules and urea-formaldehyde

A.4.3. Chemical reactivity of encapsulated USP

The chemical reactivity of the USP was assessed through calorimetric studies. The microcapsules were crushed and subjected to a controlled heating program to 200 °C. Studies were also performed on crushed microcapsules with a free radical initiator, AIBN (1% w/w of microcapsule) and the obtained traces are also included in Figure A.10.
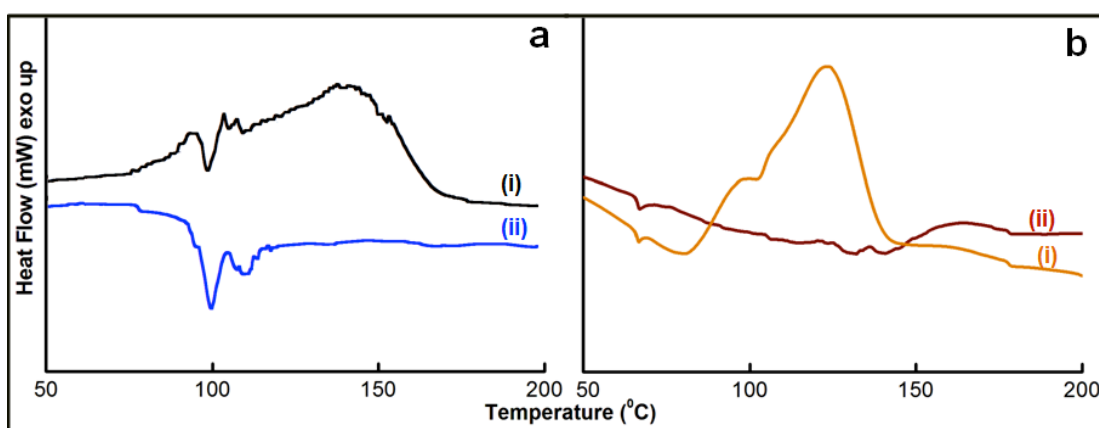
Figure A.10: DSC trace associated with the curing of USP in the presence of AIBN a) microcapsules of USP encapsulated in PS and b) USP "reservoir" encapsulated in urea-formaldehyde as (ii). The trace obtained in the absence of AIBN is also included as (i)

AIBN was selected as the initiator in view of its high decomposition rate (k_d) (Table A.1) and economic viability[158]. The released USP was found to undergo crosslinking as indicated the curing exotherm, confirming its chemical activity after being released from the shell, irrespective of the wall used for encapsulation. AIBN was

capable of initiating the curing reaction at temperatures as low as 80ºC, with T_{peak} at 106

ºC. However, in the absence of the initiator, curing could not commence, under the

temperature range (< 200°C) studied as indicated by the absence of the exotherm. It is to

be noted that these micrcocapsules do not alter the curing kinetics of epoxy resins as has

been established by non-isothermal DSC studies previously[128].

Table A.1:Decompositon rates and 10-hour half-life temperatures of common thermal

initiators[159]

S. No	Initiator	Solvent	Temperature (ºC)	$K_d(s^{-1})$	10 h Half-life Temperature (ºC) (solvent)
1.	4,4-azobis (4-cyanovalaric acid)	Acetone	70	4.6 x 10^{-5}	69 (water)
		Water	69	1.9 x 10^{-5}	
		Water	80	9.0 x 10^{-5}	
2.	1,1'-Azobis (cyclohexanecarbonitrile)	Toluene	80	6.5 x 10^{-6}	88 (toluene)
			95	5.4 x 10^{-5}	
			102	1.3 x 10^{-4}	
3.	2,2'-Azobis(isobutyronitrile) (AIBN)	Benzene	50	2.2 x 10^{-6}	65 (toluene)
			70	3.2 x 10^{-5}	
			100	1.5 x 10^{-3}	
4.	Benzoyl peroxide	Benzene	60	2.0 x 10^{-6}	70 (benzene)
			78	2.3 x 10^{-5}	
			100	5.0 x 10^{-4}	

A.4.4. Healing epoxy composites

Modelling studies on healant release, as detailed in Chapter II, reveal that

reservoir type microcapsules release comparitively larger amount of healant as compared

to monolithic microcapsules. The same has been experimentally validated using epoxy

encapsulated microcapsules as described in Chapter V. A similar attempt was made on USP encapsulated microcapsules. For this purpose, the healing efficiency of epoxy composites containing USP loaded microcapsules with different internal microstructures were dispersed within a representative epoxy matrix. Introduction of either type of microcapsule would endow the polymer with self-healing functionality, however as per the predictions, self healing efficiency should be lesser in samples containing monolithic microcapsules.

A.4.4.1. Healing studies on microcapsules with "reservoir" type internal morphology

Healing functionality was introduced in epoxy by introducing USP loaded microcapsules and AIBN (1% w/w microcapsule), both of which were dispersed homogenously within the matrix prior to curing. Specimens were subjected to impact test and the impact strength both before and after healing was determined to quantify the efficiency of healing.

Rupture of microcapsules led to the flow of the encapsulated USP into the crack plane, which subsequently undergo crosslinking in the presence of curing agent, leading to healing of the crack. The SEM micrographs of the fractured surface of specimen prepared in the presence of microcapsules after the post-healing impact testing is presented in Figure A.11. The image represents a scenario, where the encapsulated resin is released from a single ruptured microcapsule.
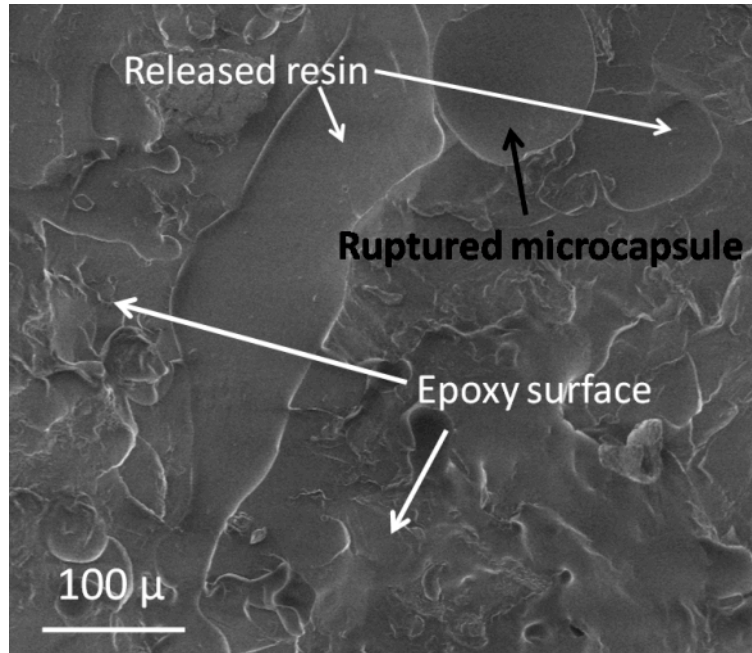
Figure A.11: Fracture surface of representative healed sample

The effect of increasing microcapsule loading on the impact strength of epoxy, both before and after healing is shown in Figure A.12. It was observed that inclusion of reservoir type microcapsules led to a pronounced decrease in the impact strength. The healing efficiency (quantified in terms of the ratio of impact strength of the samples, both before and after healing) is also included in the figure (secondary axis). It was observed that the healing efficiency increased with increasing microcapsule loading, reached a maximum (100%) at 20 % microcapsule loading.
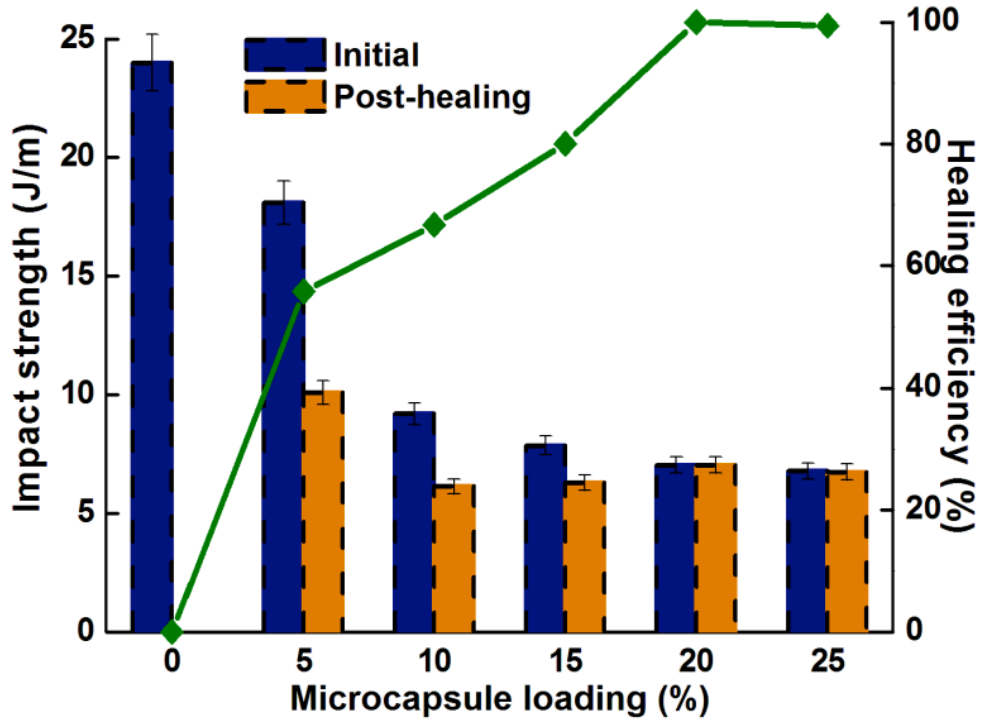
Figure A.12: Effect of increasing microcapsule loading "reservoir"type morphologyon the impact strength (primary axis) and healing efficiency (secondary axis) of epoxy-microcapsule composite

A.4.4.2. Healing studies on USP encapsulated microcapsules with monolithic morphology

The effect of introducing USP encapsulated microcapsules with monolithic morphology on the impact strength of epoxy matrix is illustrated in Figure A.13. It can be seen that in comparison to reservoir type microcapsules, introduction of microcapsules with monolithic morphology led to slightly lesser reduction in the properties of epoxy. However, the healing efficiency was substantially lower in the case of monolithic microcapsules. This was attributed to the relatively lower core content ($40 \pm 4\%$) and the

153

monolithic internal morphology of the microcapsules as compared to the reservoir type

microcapsules with core content (58 ± 4%).
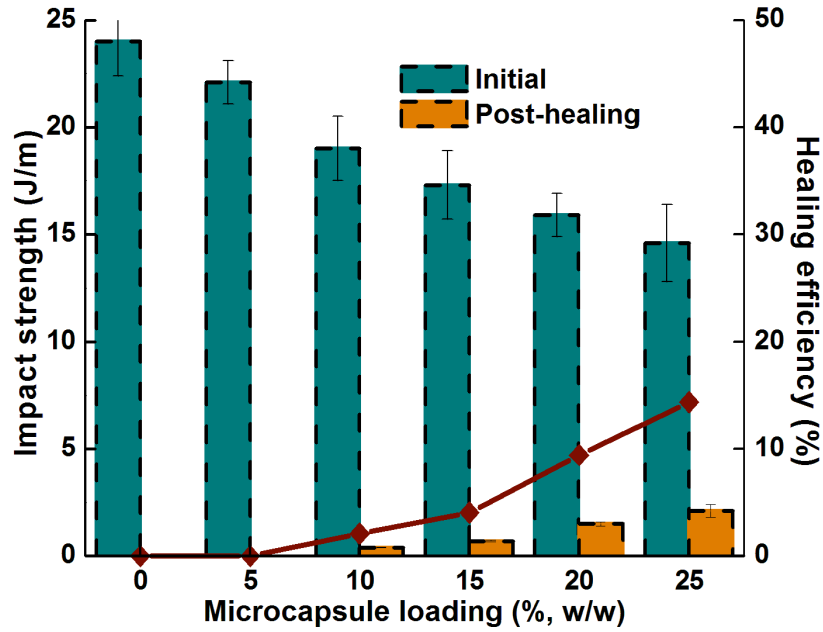
Figure A.13: Effect of increasing microcapsule loading "monolithic" type morphology on the impact strength (primary axis) and healing efficiency (secondary axis) of epoxy composite

SUPPLEMENTARY CONTENT

B1. Calculation of stoichiometric amounts of epoxy and amine

B.1 Determination of epoxy equivalent

For the purpose of quantification of epoxy equivalent, a known amount of epoxy resin (~ 0.5 g) was refluxed with 25 ml of pyridine hydrochloride solution (6.25 ml of conc. HCl (12 M) in 250 mL freshly distilled pyridine) for a period of 20 min, which led to the formation of a transparent solution. Post-cooling, the contents were titrated against previously standardized potassium hydroxide solution (0.2 M). Phenolphthalein was used as an indicator and the end point was observed as the appearance of pink colour. A blank experiment was performed in the absence of epoxy resin and the difference between the two sets was used to quantify the epoxy content. The epoxy equivalent was calculated to be 200 g/eq

B.2 Determination of Amine Hydrogen Equivalent Weight (AHEW g/eq) of TETA

AHEW is more commonly referred to as equivalent weight per active hydrogen, and is defined as the amount (g) of hardener that contains one equivalent of N-H groups. This is calculated as Mw of the hardener divided by the number of active hydrogen per molecule. The structure of TETA is shown in Figure B1.
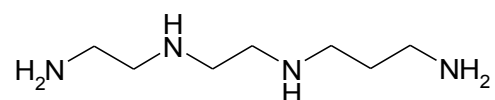
Figure B.1: Structure of triethylenetetramine (TETA)

Molecular weight of TETA = 146

No of active hydrogen per TETA molecule = 6

Amine hydrogen equivalent weight (AHEW) = 146/6= 24 g/eq

B3. Stoichiometric amounts of epoxy and amine (Parts per Hundred Resin (phr): It is defined as the grams of hardener needed per hundred grams of epoxy resin

$$phr = \frac{AHEW * 100}{EEW}$$

where, Epoxy equivalent weight (EEW) = 200 g/eq

For TETA hardener, AHEW = 24 g/eq

$$phr = \frac{24 * 100}{200} = 12$$

B4. Estimation of Hoy Solubility parameter

Solubility parameter is commonly symbolised as δ. As a first estimation, in the absence of strong interactions such as hydrogen bonding, solubility between two materials (1 and 2) is expected if $\delta 1 - \delta 2$ is less than 1.7-2.0 and not if this difference is appreciably larger. The easiest way to determine δ of a known structure is by using the molar attraction constants,E.

$$\delta = \frac{\rho \sum E}{M}$$

Where E values are summed over the structural configuration, with molecular weight, M and density ρ. The molar attraction constants of different groups are presented in Table B1.

Table B1: Molar attraction constants E, (cal cm³)^(1/2) mole^(-1 160)

Group	E	Group	E
-CH₃	148	-NH-	180
-CH₂.	131.5	-N-	61
-CH= aromatic	117	-O- epoxide	176
-C= aromatic	98	-O- ether, acetal	115
-COO-	326.5	Ortho	9.5
6- membered ring	-23.5	Meta	6.5
NH₂	226.5		

The calculations for Hoy solubility parameters of paraffin, cycloaliphatic epoxy and triethylenetetramine is presented below

Liquid Paraffin (Heavy)

Mol. Formula C_nH_{2n+2} where n=16~24

Density=0.860-0.890 g ml^{-1}

Molecular weight=226 g mole^{-1}

$E = 2137$ (cal cm^3)$^{1/2}$ mole^{-1}

$\delta = \mathbf{8.2737}$ **cal**$^{1/2}$**cm**$^{3/2}$ **mL**$^{-1}$

Cycloaliphatic Epoxy
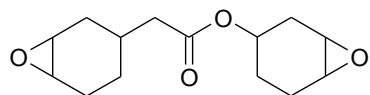
Density =1.1 g/mL

Molecular weight= 252 g mole^{-1}

E= 2068 (cal cm^3)$^{1/2}$ mole^{-1}

$\delta = 9.0269 \, \text{cal}^{1/2} \text{cm}^{3/2} \, \text{mL}^{-1}$

Triethylenetetramine
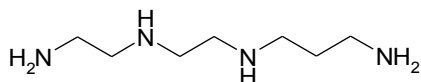
Density=982 mg/mL

Molecular weight=146.23g mole^{-1}

E=1602 (cal cm^3)$^{1/2}$ mole^{-1}

$\delta = 10.8 \, \text{cal}^{1/2} \text{cm}^{3/2} \, \text{mL}^{-1}$

REFERENCES

REFERENCES

(1)   Wool, R. P.; O'Connor, K. M. *Journal of Applied Physics***1981**, *52*, 5953.

(2)   Prager, S.; Tirrell, M. *The Journal of Chemical Physics***1981**, *75*, 5194.

(3)   Kim, Y. H.; Wool, R. P. *Macromolecules***1983**, *16*, 1115.

(4)   Jud, K.; Kausch, H. H. *Polymer Bulletin***1979**, *1*, 697.

(5)   Lin, C. B.; Lee, S.; Liu, K. S. *Polymer Engineering & Science***1990**, *30*, 1399.

(6)   Wang, P.P.; Lee, S.; Harmon, J. P. *Journal of Polymer Science Part B: Polymer Physics***1994**, *32*, 1217.

(7)   Hsieh, H. C.; Yang, T. J.; Lee, S. *Polymer***2001**, *42*, 1227.

(8)   Lin, C. B.; Lee, S.; Liu, K. S. *The Journal of Adhesion***1991**, *34*, 221.

(9)   White, S. R.; Sottos, N. R.; Geubelle, P. H.; Moore, J. S.; Kessler, M. R.; Sriram, S. R.; Brown, E. N.; Viswanathan, S. *Nature***2001**, *409*, 794.

(10)   Chen, X.; Wudl, F.; Mal, A. K.; Shen, H.; Nutt, S. R. *Macromolecules***2003**, *36*, 1802.

(11)   Chen, X.; Dam, M. A.; Ono, K.; Mal, A.; Shen, H.; Nutt, S. R.; Sheran, K.; Wudl, F. *Science***2002**, *295*, 1698.

(12)   Liu, Y. L.; Hsieh, C. Y. *Journal of Polymer Science Part A: Polymer Chemistry***2006**, *44*, 905.

(13)   Liu, Y. L.; Chen, Y. W. *Macromolecular Chemistry and Physics***2007**, *208*, 224.

(14)   Chung, C. M.; Roh, Y. S.; Cho, S. Y.; Kim, J. G. *Chemistry of Materials***2004**, *16*, 3982.

(15)   Takano, N.; Zako, M. *Journal of Intelligent Material Systems and Structures* **1999**, *10*, 836.

(16)   Hayes, S. A.; Zhang, W.; Branthwaite, M.; Jones, F. R. *Journal of The Royal Society Interface* **2007**, *4*, 381.

(17)   Hayes, S. A.; Jones, F. R.; Marshiya, K.; Zhang, W. *Composites Part A: Applied Science and Manufacturing* **2007**, *38*, 1116.

(18)   Outwater, J. O.; Gerry, D. J. *The Journal of Adhesion* **1969**, *1*, 290.

(19)   Yamaguchi, M.; Ono, S.; Terano, M. *Materials Letters* **2007**, *61*, 1396.

(20)   Larin, G. E.; Bernklau, N.; Kessler, M. R.; DiCesare, J. C. *Polymer Engineering & Science* **2006**, *46*, 1804.

(21)   Murphy, E. B.; Wudl, F. *Progress in Polymer Science* **2010**, *35*, 223.

(22)   Rule, J. D.; Moore, J. S. *Macromolecules* **2002**, *35*, 7878.

(23)   Mauldin, T. C.; Rule, J. D.; Sottos, N. R.; White, S. R.; Moore, J. S. *Journal of The Royal Society Interface* **2007**, *4*, 389.

(24)   Liu, X.; Lee, J. K.; Yoon, S. H.; Kessler, M. R. *Journal of Applied Polymer Science* **2006**, *101*, 1266.

(25)   Jones, A. S.; Rule, J. D.; Moore, J. S.; White, S. R.; Sottos, N. R. *Chemistry of materials* **2006**, *18*, 1312.

(26)   Rule, J. D.; Brown, E. N.; Sottos, N. R.; White, S. R.; Moore, J. S. *Advanced Materials* **2005**, *17*, 205.

(27)   Wilson, G. O.; Moore, J. S.; White, S. R.; Sottos, N. R.; Andersson, H. M. *Advanced Functional Materials* **2008**, *18*, 44.

(28)   Wilson, G. O.; Caruso, M. M.; Reimer, N. T.; White, S. R.; Sottos, N. R.;

Moore, J. S. *Chemistry of Materials* **2008**, *20*, 3288.

(29)   Rule, J. D.; Sottos, N. R.; White, S. R. *Polymer* **2007**, *48*, 3520.

(30)   Caruso, M. M.; Blaiszik, B. J.; White, S. R.; Sottos, N. R.; Moore, J. S. *Advanced Functional Materials* **2008**, *18*, 1898.

(31)   Keller MK, W. S., Sottos NR. *Advanced Functional Materials* **2007**, *17*, 2399.

(32)   Keller, M. W.; White, S. R.; Sottos, N. R. *Polymer* **2008**, *49*, 3136.

(33)   Cho, S. H.; Andersson, H. M.; White, S. R.; Sottos, N. R.; Braun, P. V. *Advanced Materials* **2006**, *18*, 997.

(34)   van Der Weij, F. W. *Macromolecular Chemistry and Physics* **1980**, *181*, 2541.

(35)   Tao Yin *Composites Science and Technology* **2007**, *67,,* 201.

(36)   Yan Chao Yuan, , *Macromolecules* **2008**, *41, ,* 5197.

(37)   Yan Chao Yuan *Polymer* **2008**, *49, ,* 2531.

(38)   Yuan, L.; Gu, A.; Liang, G. *Materials Chemistry and Physics* **2008**, *110*, 417.

(39)   Menei, P.; Benoit, J.-P.; Boisdron-Celle, M.; Fournier, D.; Mercier, P.; Guy, G. *Neurosurgery* **1994**, *34*, 1058.

(40)   Camarata, P. J.; Suryanarayanan, R.; Turner, D. A.; Parker, R. G.; Ebner, T. J. *Neurosurgery* **1992**, *30*, 313.

(41)   Boury, F.; Marchais, H.; Proust, J.; Benoit, J. *Journal of controlled release* **1997**, *45*, 75.

(42)   Baran, E.; Özer, N.; Hasirci, V. *Journal of microencapsulation* **2002**, *19*,

363.

(43) Das, M.; Rao, K. R. *Indian Journal of Pharmaceutical Sciences***2007**, *69*, 244.

(44) Suttiruengwong, S.; Rolker, J.; Smirnova, I.; Arlt, W.; Seiler, M.; Lüderitz, L.; Perez de Diego, Y.; Jansens, P. *Pharmaceutical development and technology***2006**, *11*, 55.

(45) Chowdary, K.; Mohapatra, P.; Krishna, M. M. *Indian Journal of Pharmaceutical Sciences***2006**, *68*.

(46) Naha, P. C.; Kanchan, V.; Manna, P.; Panda, A. K. *Journal of microencapsulation***2008**, *25*, 248.

(47) Langer, R. *Science***1990**, *249*, 1527.

(48) Kirby, C.; Whittle, C.; Rigby, N.; Coxon, D.; Law, B. *International Journal of Food Science & Technology***1991**, *26*, 437.

(49) Pothakamury, U. R.; Barbosa-Cánovas, G. V. *Trends in Food Science & Technology***1995**, *6*, 397.

(50) Wagner, L. A.; Warthesen, J. J. *Journal of food Science***1995**, *60*, 1048.

(51) Schrooyen, P. M.; van der Meer, R.; De Kruif, C. *Proceedings of the Nutrition Society***2001**, *60*, 475.

(52) F. Gibbs, S. K., Inteaz Alli, Catherine N. Mulligan, Bernard *International Journal of Food Sciences and Nutrition***1999**, *50*, 213.

(53) Chiu, Y.; Chiu, C.; Chien, J.; Ho, G.; Yang, J.; Chen, B. *Journal of Agricultural and Food Chemistry***2007**, *55*, 5123.

(54) Scher, H. B.; Rodson, M.; Lee, K. S. *Pest Management Science***1998**, *54*,

394.

(55)   Groenwold, B.; Pereiro, F.; Purnell, T.; Scher, H. In *Proceedings 1980 British Crop Protection Conference-Weeds.* 1980, p 185.

(56)   Bingham, G.; Gunning, R. V.; Gorman, K.; Field, L. M.; Moores, G. D. *Pest Management Science***2007**, *63*, 276.

(57)   Il'Ichev, A.; Stelinski, L.; Williams, D.; Gut, L. *Journal of Economic Entomology***2006**, *99*, 2048.

(58)   Mihou, A.; Michaelakis, A.; Krokos, F.; Mazomenos, B.; Couladouros, E. *Journal of Applied Entomology***2007**, *131*, 128.

(59)   Chen, Z.; Fang, Y.; Zhang, Z. *Chinese Science Bulletin***2007**, *52*, 1365.

(60)   Brown, E. N.; White, S. R.; Sottos, N. R. *Journal of Materials Science***2004**, *39*, 1703.

(61)   Toohey, K. S.; Sottos, N. R.; Lewis, J. A.; Moore, J. S.; White, S. R. *Nat Mater***2007**, *6*, 581.

(62)   Yuan, L.; Liang, G.-Z.; Xie, J.-Q.; Li, L.; Guo, J. *Journal of Materials Science***2007**, *42*, 4390.

(63)   Yuan, L.; Liang, G.; Xie, J.; Li, L.; Guo, J. *polymer***2006**, *47*, 5338.

(64)   Yuan, L.; Liang, G.-z.; Xie, J.-q.; He, S.-B. *Colloid and Polymer Science***2007**, *285*, 781.

(65)   Carolyn, D. *Smart Materials and Structures***1994**, *3*, 118.

(66)   Dry, C. *Composite Structures***1996**, *35*, 263.

(67)   Williams, G.; Trask, R.; Bond, I. *Composites Part A Applied Science and Manufacturing***2007**, *38*, 1525.

(68)   Hucker, M.; Bond, I.; Foreman, A.; Hudd, J. *Advanced Composites Letters***1999**, *8*, 181.

(69)   Hucker, M.; Bond, I.; Bleay, S.; Haq, S. *Composites Part A: Applied Science and Manufacturing***2003**, *34*, 927.

(70)   Pang, J. W. C.; Bond, I. P. *Composites Science and Technology***2005**, *65*, 1791.

(71)   Pang, J.; Bond, I. *Composites Part A: Applied Science and Manufacturing***2005**, *36*, 183.

(72)   Bleay, S. M.; Loader, C. B.; Hawyes, V. J.; Humberstone, L.; Curtis, P. T. *Composites Part A Applied Science and Manufacturing***2001**, *32*, 1767.

(73)   Motuku, M.; Vaidya, U.; Janowski, G. *Smart Materials and Structures***1999**, *8*, 623.

(74)   Li, V. C.; Lim, Y. M.; Chan, Y.-W. *Composites Part B: Engineering***1998**, *29*, 819.

(75)   Dry, C. *International Journal of Modern Physics B***1992**, *6*, 2763.

(76)   Toohey, K. S.; Hansen, C. J.; Lewis, J. A.; White, S. R.; Sottos, N. R. *Advanced Functional Materials***2009**, *19*, 1399.

(77)   Brown, E. N.; Sottos, N. R.; White, S. R. *Experimental Mechanics***2002**, *42*, 372.

(78)   Brown, E. N.; White, S. R.; Sottos, N. R. *Composites Science and Technology***2005**, *65*, 2474.

(79)   Yuan, C. e.; Zhang, M. Q.; Rong, M. Z. *Journal of Materials Chemistry A***2014**, *2*, 6558.

(80)   Barbero, E. J.; Ford, K. J. *Journal of Advanced Materials***2007**, *39,* 20.

(81)   Jackson, A. C.; Bartelt, J. A.; Marczewski, K.; Sottos, N. R.; Braun, P. V. *Macromolecular Rapid Communications***2011**, *32*, 82.

(82)   Yang, G.; Mauldin, T. C.; Lee, J. K. *RSC Advances***2015**, *5*, 59120.

(83)   Guadagno, L.; Raimondo, M.; Naddeo, C.; Longo, P.; Mariconda, A. *Polymer Engineering & Science***2014**, *54*, 777.

(84)   Kamphaus, J. M.; Rule, J. D.; Moore, J. S.; Sottos, N. R.; White, S. R. *Journal of The Royal Society Interface***2008**, *5*, 95.

(85)   Wang, H.; Liu, Y.; Li, Z.; Zhang, X.; Zhang, S.; Zhang, Y. *European Polymer Journal***2009**, *45*, 1535.

(86)   Cosco, S.; Ambrogi, V.; Musto, P.; Carfagna, C. *Macromolecular Symposia***2006**, *234*, 184.

(87)   Blaiszik, B. J. *Polymer***2009**, *50,* 990.

(88)   Cosco, S.; Ambrogi, V.; Musto, P.; Carfagna, C. *Journal of Applied Polymer Science***2007**, *105*, 1400.

(89)   Wang, H.-p.; Hu, S.-q.; Cai, S.-j.; Yu, F. *Polymer Bulletin***2014**, *71*, 2407.

(90)   Tripathi, M.; Rahamtullah; Kumar, D.; Rajagopal, C.; Kumar Roy, P. *Journal of Applied Polymer Science***2014**, *131*, 40572.

(91)   Tripathi, M.; Dwivedi, R.; Kumar, D.; Roy, P. K. *Polymer-Plastics Technology and Engineering***2016**, *55*, 129.

(92)   Choudhury I.; Khan N. I.; Mathur A.; Nath W.; Phukan A. *Advanced Materials Letters***2016**, *7*, 836.

(93)   Brown, E. N. *Journal of Microencapsulation***2003**, *20*, 719.

(94)   Li, Q.; Siddaramaiah; Kim, N. H.; Hui, D.; Lee, J. H. *Composites Part B: Engineering***2013**, *55*, 79.

(95)   Zorba, T.; Papadopoulou, E.; Hatjiissaak, A.; Paraskevopoulos, K. M.; Chrissafis, K. *Journal of Thermal Analysis and Calorimetry***2008**, *92*, 29.

(96)   Sharma, P.; Shukla, S.; Lochab, B.; Kumar, D.; Kumar Roy, P. *Materials Letters***2014**, *133*, 266.

(97)   Sharma, P.; Shukla, S.; Lochab, B.; Kumar, D.; Roy, P. K. *Materials Letters***2014**, *10.1016/j.matlet.2014.07.048*.

(98)   *Epoxy Resins Chemistry and Technology*; 2nd ed.; May, C. A., Ed.; Marcel Dekker: New York, 1988.

(99)   Sandler, S. R.; Karo, W.; Bonesteel, J.-A.; Pearce, E. M. In *Polymer Synthesis and Characterization*; Academic Press: San Diego, 1998, p 61.

(100)   Hodd, K. In *Comprehensive Polymer Science and Supplements*; Editor-in Chief: Sir Geoffrey, A., Ed.; Pergamon: Amsterdam, 1989, p 667.

(101)   Hodgkin, J. In *Encyclopedia of Materials: Science and Technology (Second Edition)*; Editors-in-Chief: , K. H. J. B., Robert, W. C., Merton, C. F., Bernard, I.,Edward, J. K., Subhash, M., Patrick, V., Eds.; Elsevier: Oxford, 2001, p 9215.

(102)   Takeichi, T.; Furukawa, N. In *Polymer Science: A Comprehensive Reference*; Editors-in-Chief: Krzysztof, M., Martin, M., Eds.; Elsevier: Amsterdam, 2012, p 723.

(103)   Goswami, T. H.; Nandan, B.; Alam, S.; Mathur, G. N. *Polymer***2003**, *44*, 3209.

(104) Roy, P. K.; Rawat, A. S.; Choudhary, V.; Rai, P. K. *Indian Journal of Chemical Technology***2004**, *11*, 51.

(105) McIlroy, D. A. *Macromolecules ,***2010**, *43, ,* 1855.

(106) Blaiszik, B. J.; Caruso, M. M.; McIlroy, D. A.; Moore, J. S.; White, S. R.; Sottos, N. R. *Polymer***2009**, *50,* 990.

(107) Yuan, L.; Liang, G.-Z.; Xie, J.-Q.; Guo, J.; Li, L. *Polymer Degradation and Stability***2006**, *91*, 2300.

(108) Rallison, J. M. *Annual Review of Fluid Mechanics***1984**, *16*, 45.

(109) Chaudhary, S.; Parthasarathy, S.; Kumar, D.; Rajagopal, C.; Roy, P. K. *Polymer Composites***2014**, *DOI: 10.1002/pc.22927*.

(110) Thies, C. In *Encyclopedia of Polymer Science and Engineering*; 2nd ed.; H. F. Mark, N. B., C. G. Overberger, G. Menges and, Kroschwitz, J. I., Eds.; Wiley: New York, Chichester, 1987; Vol. 9, p 724.

(111) Dunker, A. K.; John, W. E.; Rammon, R.; Farmer, B.; Johns, S. J. *The Journal of Adhesion***1986**, *19*, 153.

(112) Brown, E. N.; Kessler, M. R.; Sottos, N. R.; White, S. R. *Journal of Microencapsulation***2003**, *20*, 719.

(113) Finken, R.; Seifert, U. *Journal of Physics: Condensed Matter***2006**, *18*, L185.

(114) Salaün, F.; Vroman, I. *European Polymer Journal***2008**, *44*, 849.

(115) Joseph D. Rule *Polymer***2007**, *48*.

(116) Yin, T.; Rong, M. Z.; Zhang, M. Q.; Yang, G. C. *Composites Science and Technology***2007**, *67*, 201.

(117) McIlroy, D. A.; Blaiszik, B. J.; Caruso, M. M.; White, S. R.; Moore, J. S.; Sottos, N. R. *Macromolecules* **2010**, *43*, 1855.

(118) Poe, S. L.; Kobašlija, M.; McQuade, D. T. *Journal of the American Chemical Society* **2006**, *128*, 15586.

(119) Jin, H.; Mangun, C. L.; Stradley, D. S.; Moore, J. S.; Sottos, N. R.; White, S. R. *Polymer* **2012**, *53*, 581.

(120) Zhang, H.; Wang, P.; Yang, J. *Composites Science and Technology* **2014**, *94*, 23.

(121) Hudson, S.; Magner, E.; Cooney, J.; Hodnett, B. K. *The Journal of Physical Chemistry B* **2005**, *109*, 19496.

(122) Karimi, B.; Emadi, S.; Safari, A. A.; Kermanian, M. *RSC Advances* **2014**, *4*, 4387.

(123) Yiu, H. H. P.; Wright, P. A.; Botting, N. P. *Journal of Molecular Catalysis B:Enzymatic* **2001**, *15*, 81.

(124) Meynen, V.; Cool, P.; Vansant, E. F. *Microporous and Mesoporous Materials* **2009**, *125*, 170.

(125) Naskar, M. K.; Eswaramoorthy, M. *Journal of Chemical Sciences* **2008**, *120*, 181.

(126) Ramanathan, L. S.; Baskaran, D.; Shukla, P. G.; Sivaram, S. *Macromolecular Chemistry and Physics* **2002**, *203*, 998.

(127) Budrugeac, P.; Segal, E. *Journal of Thermal Analysis and Calorimetry* **2007**, *88*,703.

(128) Tripathi, M.; Kumar, D.; Rajagopal, C.; Kumar Roy, P. *Journal of*

*Thermal Analysis and Calorimetry***2015**, 119, 547.

(129) Fiedler, B.; Gojny, F. H.; Wichmann, M. H. G.; Nolte, M. C. M.; Schulte, K. *Compos. Sci. Technol.***2006**, *66*, 3115.

(130) Tripathi, M.; Kumar, D.; Roy, P. K. *Composites Communications***2017**, *3*, 38.

(131) Ramírez, C.; Rico, M.; Torres, A.; Barral, L.; López, J.; Montero, B. *European Polymer Journal***2008**, *44*, 3035.

(132) Chaudhary, S.; Parthasarathy, S.; Kumar, D.; Rajagopal, C.; Roy, P. K. *Journal Appied Polymer Science***2014**, 10.1002/app.40490.

(133) Chaudhary, S.; Parthasarathy, S.; Kumar, D.; Rajagopal, C.; Roy, P. K. *Journal Appied Polymer Science* **2013**, 10.1002/app.39941.

(134) Ramírez, C.; Abad, M. J.; Barral, L.; Cano, J.; Díez, F. J.; López, J.; Montes, R.; Polo, J. *Journal of Thermal Analysis and Calorimetry***2003**, *72*, 421.

(135) Yin, T.; Rong, M.; Zhang, L. M. *Advanced Materials Research***2013**, *716*.

(136) Tong, X. M.; Zhang, M.; Yang, M. Z. *Advanced Materials Research***2011**, *306-307*, 658.

(137) Ghaemy, M.; Yaghoob, S.; Karimi, M. *Iranian Polymer Journal***2010**, *19*, 661.

(138) Rosso, P.; Ye, L. *Macromolecular Rapid Communications***2007**, *28*, 121.

(139) Wang, J.; Laborie, M.-P. G.; Wolcott, M. P. *Thermochimica Acta***2005**, *439*, 68.

(140) Doyle, C. D. *Journal of Applied Polymer Science***1961**, *5*, 285.

(141)   Ghumara, R.; Adroja, P.; Parsania, P. H. *Journal of Thermal Analysis and Calorimetry***2013**, *114*, 873.

(142)   Prime, R. B. *Thermal Characterization of Polymeric Materials* Academic: New York 1997.

(143)   Blaiszik, B. J.; Sottos, N. R.; White, S. R. *Composites Science and Technology***2008**, *68*, 978.

(144)   Atria, A. M.; Cortes, P.; Garland, M. T.; Baggio, R. *Acta Crystallographica Section E***2003**, *59*, m1075.

(145)   Knott, J. F. *Fundamentals of Fracture Mechanics*; Butterworths: London,, 1976.

(146)   Kinloch, A. J. *Adhesion and adhesives: science and technology.*; Chapman & Hall:London, 1987.

(147)   Xiao, D. S.; Yuan, Y. C.; Rong, M. Z.; Zhang, M. Q. *Polymer***2009**, *50*, 2967.

(148)   Chaudhary, S.; Parthasarathy, S.; Kumar, D.; Rajagopal, C.; Roy, P. K. *Journal of Applied Polymer Science***2013**, 10.1002/app.39941.

(149)   Roy, P.; Iqbal, N.; Kumar, D.; Rajagopal, C. *Journal of Polymer Research***2014**, *21*,1.

(150)   Williams, J. G. *Composites Science and Technology***2010**, *70*, 885.

(151)   Voo, R.; Mariatti, M.; Sim, L. C. *Composites Part B: Engineering***2012**, *43*, 3037.

(152)   Roy, P. K.; Ullas, A. V.; Chaudhary, S.; Mangla, V.; Sharma, P.; Kumar, D.; Rajagopal, C. *Iranian Polymer Journal.***2013**, *22*, 709.

(153)   Pearson, R. A.; Yee, A. F. *Polymer***1993**, *34*, 3658.

(154)   Yuan, Y. C.; Rong, M. Z.; Zhang, M. Q.; Yang, G. C.; Zhao, J. Q. *Express Polymer Letters***2011**, *5*, 47.

(155)   Lee, J.; Bhattacharyya, D.; Zhang, M. Q.; Yuan, Y. C. *Express Polymer Letters***2011**, *5* 246.

(156)   Moll, J. L.; Jin, H.; Mangun, C. L.; White, S. R.; Sottos, N. R. *Composites Science and Technology***2013**, *79*, 15.

(157)   Dholakiya, B. *Polyester,*; (Ed.), Saleh, H. E.-D., Ed. **2012,**190.

(158)   *Handbook of free radical intiators*; Deniisov, E. T.; Deniisov, T. G.; Podikiova, T.S., Eds.; John Wiley and Sons: Hoboken, New Jersey 2003.

(159)   *Polymer Handbook*; 4th ed.; Brandrup, J. I., E.H.; Grulke, E.A., Ed.; John Wiley, :New York, 1999; Vol. II/2-69.

(160)   Koenhen, D. M.; Smoulders, C. A. *Journal of Applied Polymer Science***1975**, *19*,1163.

LIST OF PUBLICATIONS

Published

[1]**M. Tripathi**, Rahamtullah, D. Kumar, C. Rajagopal, P. K. Roy, Influence of microcapsule shell material on the mechanical behavior of epoxy composites for self-healing applications. Journal of Applied Polymer Science, 131 (2014) 40572.

[2]**M. Tripathi**, D. Kumar, C. Rajagopal, P.K. Roy, Curing kinetics of self-healing epoxy thermosets. Journal of Thermal Analysis and Calorimetry, 119 (2015) 547-555.

[3] **M. Tripathi**, R. Dwivedi, D. Kumar, P.K. Roy, Application of microencapsulated unsaturated polyester toward temperature-triggered healing in epoxy composites. Journal of Intelligent Material Systems and Structures, 27 (2016) 1650-1657.

[4] **M. Tripathi**, R. Dwivedi, D. Kumar, P.K. Roy, Thermal Activation of Mendable Epoxy through Inclusion of Microcapsules and Imidazole Complexes. Polymer-Plastics Technology and Engineering, 55 (2016) 129-137.

[5] **M. Tripathi**, D. Kumar, P. K. Roy, Healant release from microcapsules with varied internal microstructure.Composites Communications, 3 (2017) 38-41

Conference proceedings

[1]**M. Tripathi**, Rahamtullah, D. Kumar, C. Rajagopal, P. K. Roy, Mechanical behaviour of composites prepared using epoxy encapsulated urea-formaldehyde and melamine formaldehyde microcapsules for self healing applications. Asian Workshop on Polymer Processing (AWPP), Goa, 2013

[2] **M. Tripathi**, R. Dwivedi, D. Kumar, P. K. Roy, Microencapsulation of healing agents for self-healing applications. MACRO-2015, Kolkata, 2015.

[3] M. Tripathi, D. Kumar, P. K. Roy, Mesoporous Silica containers with reactive amine for self-healing application. Functional and Engineering Materials (FEM) 2016, DMSRDE, Kanpur.

Communicated

 [1] **M. Tripathi**, D. Kumar, P. K. Roy, Microencapsulation of reactive amine in interfacially engineered epoxy microcapsules for smart applications.Iranian Polymer Journal

[2] **M. Tripathi**, D. Kumar, P. K. Roy, Mesoporous silica as amine immobiliser for endowing healing functionality to epoxy resin. Composites Communications

[3] **M. Tripathi**, D. Kumar, P. K. Roy, Understanding the role of internal microstructure in capsule based healing of polymeric composites. Journal of Applied Polymer Science

BIO-DATA

MANORAMA TRIPATHI
Scientist 'D'
Centre for Fire, Explosive and Environment Safety
Defence Research and Development Organisation
Delhi-110054
Email id.- manorama@cfees.drdo.in

PERSONAL DETAILS   Female, Married

Date of Birth:14 January 1982

Languages known: Hindi & English

EDUCATION   M.Sc. (Chemistry), 2003

Department of Chemistry

Banaras Hindu University,Varanasi

HONOURS   UGC JRF-NET qualified

GATE qualified

JOB EXPERIENCE   Scientist 'B', DMSRDE, DRDO, 2004-2009

Scientist 'C', CFEES, DRDO, 2009-2014

Scientist 'D', CFEES, DRDO, 2014 till date